AN ANALYSIS OF THREE MODEL-BASED ESTIMATION METHODS FOR DIESEL ENGINE CONDITION MONITORING

By

Raluca F. Constantinescu

B. Eng. (Control Engineering) Bucharest Polytechnic Institute

A THESIS SUBMITTED IN PARTIAL FULFILLMENT OF

THE REQUIREMENTS FOR THE DEGREE OF

MASTER OF APPLIED SCIENCES

in

THE FACULTY OF GRADUATE STUDIES

ELECTRICAL ENGINEERING

We accept this thesis as conforming

to the required standard

THE UNIVERSITY OF BRITISH COLUMBIA

April 1995

In presenting this thesis in partial fulfilment of the requirements for an advanced degree at the University of British Columbia, I agree that the Library shall make it freely available for reference and study. I further agree that permission for extensive copying of this thesis for scholarly purposes may be granted by the head of my department or by his or her representatives. It is understood that copying or publication of this thesis for financial gain shall not be allowed without my written permission.

Department of Electrical Engineering

The University of British Columbia
Vancouver, Canada

Date April 24, 1995

DE-6 (2/88)

Abstract

In the context of engine fault detection and isolation, we focus on three main aspects: engine modeling and validation, engine parameter identification, and cylinder pressure waveform reconstruction. The problem of diesel engine modeling is solved using Euler's equation, under the assumption that the crankshaft is perfectly rigid. The model inputs are represented by the cylinder pressures and the output is the flywheel angular velocity fluctuation.

Simulation results obtained with MATLAB show a root mean square (RMS) error of 0.0891 rad/sec between the estimated and the actual crankshaft angular velocity fluctuation for the normal operating condition. The elimination of a strong sinusoidal trend for the faulty condition results in a RMS error range of 0.0973 rad/sec to 0.1836 rad/sec.

The identification methods involved the off-line standard least-squares technique, the recursive gradient estimator and the on-line least-squares estimators with exponential forgetting. The parameters of interest are engine inertia, and torque fluctuation. The RMS velocity error for the normal operation has a value of 0.0559 rad/sec, which represents approximately 30% improvement over the initial result, before identification.

The issue of cylinder pressure waveform reconstruction is addressed. The inverse dynamics are solved by redefining the system input as the torque due to gas pressure.

The cylinder pressure waveform is approximated by an impulse-like periodic function. We considered the problem of fault detection and isolation. The procedure uses 6 pressure templates. The estimated pressure variations are obtained using a standard least-squares technique. An under-fueling fault in the i-th firing cylinder can be determined exactly by the minimum value of the estimated pressure variation.

Using the pressure correction we are able to improve the estimation of the gas pressure torque. The RMS torque error for the normal operation reduces to 99.24 Nm. The case of an under-fueling fault is characterized by a reduced RMS torque error range of 85.7 Nm to 198.1 Nm.

The pressure waveform reconstruction is characterized by a RMS pressure error range of 0.155 MPa to 0.277 MPa for the normal operating condition.

For each of the six under-fueling faults, the pressure waveform corresponding to the faulty cylinder is reconstructed. The RMS error range is of 0.155 MPa to 0.386 MPa.

Table of Contents

List of Tables

List of Figures

Acknowledgements

The opportunity to pursue a study of diesel engine rotational dynamics was provided by a research assistantship in the Department of Electrical Engineering, University of British Columbia, a short time after my arrival in Canada. This project started as a collaboration between the Robotics and Control Laboratory and the Institute for Machinery Research, National Research Council of Canada. Given my initial background in control engineering, the transition to the new, for me, field of condition monitoring and fault diagnosis of internal combustion engines was challenging and sometimes full of difficulties. Without the help and insight of my research supervisor, Dr. Peter D. Lawrence this accommodation might have been impossible to achieve. During our multiple discussions, concepts like fault detection and isolation, engine inverse dynamics, and parametric identification were linked to each other, thus providing me with the necessary tools to approach this project.

In the spring of 1994, I had the opportunity to meet Dr. Phillip G. Hill, who, through many helpful disscusions, put my work into the mechanical engineering perspective. He also offered me the possibility to develop the pressure measurement experiments using the test cell in the Engine Test Laboratory. In the same laboratory, I was welcomed and helped by K. Bruce Hodgins, and Peter Mtui.

Dr. Terrence S. Brown and Devin Ostrom from the Institute for Machinery Research showed an active interest in this project. We discussed together many of the possible engine modeling approaches, and they helped me obtain the experimental data for model testing and validation.

My final acknowledgement, to my husband, Matthew Palmer is of another nature.

His patience in proofreading the manuscript, constant encouragement, and interest in my work, were invaluable and deeply appreciated.

Chapter 1

Introduction

dust and diesel

rise like incense from the road—

Bruce Cockburn, Dust and Diesel

The reciprocating internal-combustion engine is one of the most common power production systems. The diesel engine plays an essential role in commercial automotive applications. Engine condition monitoring systems have the potential to improve reliability, lower maintenance costs, and improve safety by early detection of operational faults. Model-based condition monitoring permits the localization of faults within the engine and therefore aids in fault diagnosis. Our research is directed at developing and validating an effective diesel engine model for condition monitoring applications. In this project we analyze 6 different actuator faults and the normal operating condition. The actuator fault is defined as the phenomenon of cylinder under-fueling which has as a direct consequence, the reduction of cylinder peak pressure. We use both pressure and flywheel angular velocity measurements. Data correspond to a two-stroke diesel engine, DDC 6V 92TA, manufactured by the Detroit Diesel Corporation. The engine specifications and much of the test data were furnished by the Institute for Machinery Research, National Research Council. Some measurements were done using the test cell in the Engine Test Laboratory in the Department of Mechanical Enginering at the University of British Columbia.

The concept of analytical redundancy emphasizes the use of accurate dynamic and static models for data processing and analysis. The major benefit is realized in the low cost and flexibility of a software versus a hardware implementation. A combination of analytical and physical redundancy is almost always necessary for a fault-tolerant system to maintain its function in the presence of certain failures. On the other hand, the paradigm of analytical redundancy has the advantage of fully exploiting the engine model and thus extracting information that otherwise might be difficult to obtain. This is the motivation for pursuing three directions of investigation: engine modeling and validation, parameter identification, and pressure waveform reconstruction.

Thus, the second chapter of this thesis outlines the theory behind modeling techniques and estimation procedures to be applied in our study and relates them to the field of fault detection and isolation. The analytical model-based approach is compared to knowledge-based methods and to neural network-based techniques. Parameter identification techniques can be employed in the detection and isolation of incipient faults. The literature review provides the basis for our investigations by emphasizing the importance of preserving a physical relationship to the engine throughout the modeling and identification processes. In this context, we also present the basic terms and specifications of the DDC 6V 92TA diesel engine and the DDEC II electronic engine controller, manufactured by Detroit Diesel Corporation.

The third chapter of this thesis aims to present the model for the dynamics of an N-cylinder diesel engine, emphasizing its features and properties from a system theory point of view. The system inputs are given by cylinder combustion pressures, $P_i(\theta)$, $i = 1, \ldots N$. Its output is represented by the flywheel angular velocity fluctuation, $\delta\omega(\theta)$. Both are expressed as functions of the crank angle, θ. The model is then verified using the MATLAB simulation package. The model effectiveness is assessed by measuring the standard deviation of the residual (root mean square error) and the ratio between the standard deviation of the residual and the standard deviation of the measured signal (residual to signal ratio). In each of the 6 under-fueling faults, the velocity fluctuation residual is found to exhibit a strong sinusoidal trend which accounts for unmodeled torques. We attributed this harmonic torque fluctuation, ΔT, to the crankshaft vibration and the oscillatory behaviour of the dynamometer loading.

The main goal of the fourth chapter is to describe a meaningful procedure for identification of engine parameters. Identification methods attempt to determine values for the unknown or uncertain system parameters using measurements of input and output signals. This concept is transferred to the field of engine fault detection and isolation through the assumption that the occurrence of a fault has as a direct consequence, changes of process parameters, which modify the system output. Therefore, parameter estimation techniques can be employed to detect incipient process faults. If the residual generator is implemented as a parametric identification procedure, then the residuals are represented by the output prediction errors. The decision making stage employs statistical comparisons between residuals and known fault signatures. Changes in parameter means and variances can be used as decision criteria. The identification problem is solved using the recursive gradient estimator and least-squares estimator with exponential forgetting. The results are presented in comparison with those obtained from the off-line standard least-squares estimator. The model parameters are functions of the crank-angle θ. The harmonic torque fluctuation, $\Delta T(\theta)$, and the total engine inertia, J_E, are estimated.

In the fifth chapter we analyze the model properties and the potential for solving the inverse problem of reconstructing the cylinder pressure waveform from noisy measurements of crankshaft/flywheel angular velocity. Because our model implements a multi-input single output (MISO) system, it is not possible to explicitly decouple the inverse dynamics. We have therefore considered two approaches. First, we redefine the system input and we rewrite the engine model as a single input single output (SISO) system. If the input pressure waveforms did not overlap, then one could imagine that the system is SISO with sharp discontinuities at the end of each input period. The new input is then the torque due to gas pressure, $T_p(\theta)$. Secondly, we approximate the pressure waveform with a periodic impulse-like continuous function. Using this latter template-based approach we are able to explicitly identify the condition of each cylinder and improve the torque estimation procedure.

The sixth chapter summarizes the results and outlines the use of these three methods in a model-based engine condition monitoring system.

Chapter 2

Background

Again, nothing, and again the machine
asked me politely: "Do you have the password?"
Umberto Eco, Foucault's Pendulum

Several methods of verifying the correct functioning of the diesel engine have been used by engineers from the early stages of the engine's development. The majority of those techniques relied on experience and close observation of some important engine operating factors such as: temperatures, pressures, flows, noise and vibration. Deviations from the normal operating characteristics were then recognized and classified.

Advances in transducers technologies and, in particular, the availability of low-cost embedded computer hardware has rendered feasible, the application of much more sophisticated condition monitoring schemes.

In this chapter we introduce the definitions associated with fault diagnosis of systems and outline some methods applicable to diesel engines. The review of some recent engine condition monitoring applications puts the model-based approach into perspective by comparing it with knowledge-based methods and neural network-based techniques. In this context, we also present the basic terms and specifications of the DDC 6V 92TA diesel engine and the DDEC II electronic engine controller. We conclude the chapter by specifying the objective of our research in the general framework of model-based design for diesel engine fault diagnosis.

2.1 Engine Modeling

The diesel engine is a complex device for which it is difficult to write a comprehensive mathematical model. For this reason, most models presented in the literature are application dependent. The laws of physics that govern a system represent an important modeling tool. Our modeling approach illustrates this aspect and is based on Euler's equations [1] applied to a generic internal combustion engine. These equations characterize the rotational dynamics of a diesel engine and can be subsequently used to derive the relationship between cylinder pressures and flywheel/crankshaft angular velocity fluctuation. The theory behind this approach is often applied to determine the equations of motions of any mechanical system [2]. Similar approaches dedicated to internal combustion engines can be found in references [3], [4] and [5]. The use of such a model in condition monitoring applications seems feasible as long as the correspondence between the model and the physical engine is transparent. We are interested in three main aspects. The first deals with validating the *direct* engine model, i.e. given the actual pressure inputs we are interested in measuring the error between the actual and the estimated crankshaft angular velocity. A second goal for our investigation aims at estimating some important engine parameters (inertia, and load torque) given input-output measurements. The third goal of this project is to present a method for pressure waveform reconstruction using the model and noisy measurements of the crankshaft angular velocity. This offers the possibility of replacing the direct measurement of cylinder pressures. The estimated pressures could then be used for a variety of calculations including heat-release analysis, net engine torque estimation, and cylinder power output calculation.

2.2 Diesel Engine Characteristics

The design of a model-based fault diagnosis system takes into account the nature of faults to consider, the complexity of implementation, the robustness with respect to model inaccuracies, and the diagnosis performance index (number of false alarms). The model design is a critical step in the development of such a system. In this section we introduce some general diesel engine definitions and present some features of the DDC 6V 92TA diesel engine and DDEC II electronic controller.

A diesel engine is a compression-ignition, reciprocating, internal-combustion engine. Four stroke diesel engines operate on a mechanical cycle [6, pp. 33–34] that has the idealized form shown in Figure 2.1. Each stroke is defined by the piston travel between top dead centre (TDC) and bottom dead centre (BDC). The induction stroke is characterized by constant pressure. The compression phase is followed by combustion at constant volume. The fuel is injected at the end of the compression stroke. Autoignition is made possible by a high compression ratio. After the expansion stroke the exhaust valve opens and the blow-down occurs at practically constant volume. The exhaust stroke takes place at constant pressure. Four-stroke diesel engines are used in many automotive applications. In a two-stroke engine the induction (entry of fresh air) and the exhaust (exit of burned gas) occur at the same time [6, pp. 274–323]. This phenomenon is called scavenging [7, pp. 213–215]. Some motorcycles, buses and locomotives are equipped with two-stroke diesel engines. The use of large two-stroke diesel engines is also common in marine applications. The advantages of two-stroke diesel engines are increased power output and high firing frequency. In our experiments we used the DDC 6V 92TA Detroit Diesel engine. Data were obtained from [3] and are illustrated in Table 2.1. This engine is turbocharged and uses in-cylinder fuel injection, therefore the scavenging is very efficient.

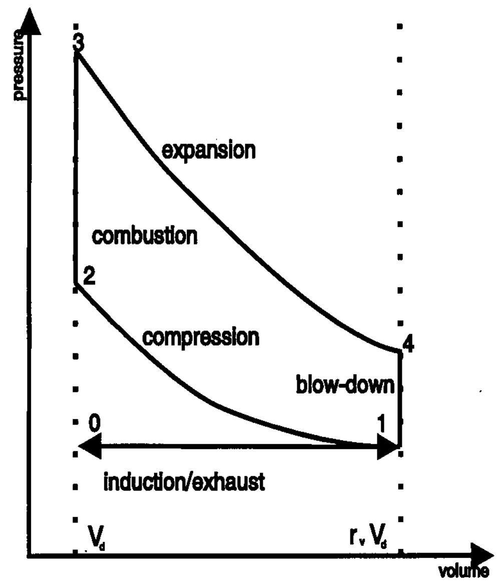

Figure 2.1: Illustrates a P-V diagram of an ideal four stroke Diesel cycle (from [6, pp. 34]). The strokes are: induction $(0-1)$, compression $(1-2)$ and combustion $(2-3)$, expansion $(3-4)$ and blow-down $(4-1)$, and exhaust $(1-0)$. V_d is the volume at top dead centre, and r_v is the compression ratio.

Table 2.1: General features of the turbocharged DDC 6V 92TA Detroit Diesel Engine.

Type:	two stroke
Number of cylinders:	6 (V)
Bore:	123 mm
Stroke:	127 mm
Displacement:	9.05 liters
Compression ratio:	17 : 1
Gross rated power output:	224 kW at 2100 rpm
Friction power loss:	44.073 kW at 1800 rpm
Overall mechanical efficiency:	84%

2.2.1 Data Acquisition

The test cell consists of a fully instrumented two-stroke diesel engine, DDC 6V 92TA, manufactured by Detroit Diesel Corporation (see Table 2.1). The engine is electronically controlled by two Detroit Diesel electronic controllers (DDEC II). Data used in our simulation were furnished by the Institute for Machinery Research (IMR), National Research Council (NRC) and consist of cylinder pressures and flywheel angular velocity waveforms recorded at 1,200 rpm. The dynamometer torque was 990 Nm. There are 7 data sets, each corresponding to a certain engine condition. One set was obtained under normal operating conditions (baseline) and the other 6 were from operation with one cylinder at a time under-fueled by 10%.

We also performed pressure measurements in the Engine Test Laboratory in the Department of Mechanical Engineering at UBC using a dedicated, completely instrumented test cell. This system was not equipped to measure the crankshaft speed fluctuations. The sensing system is very important for the accuracy of the condition monitoring system. Water-cooled piezoelectric pressure transducers were employed for measuring combustion pressure development [8]. For model validation purposes, both cylinder pressures and instantaneous crankshaft speed must be obtained simultaneously during the test. We measured the mean engine speed and the crank angle (CA) in the Engine Test Laboratory. An update of the test cell is proposed in [9] and its description is detailed in Appendix A.

2.2.2 Engine Control

A comprehensive description of the Detroit Diesel Electronic Control (DDEC) system was reported in [10]. The fuel volume flow and timing are controlled via a solenoid actuator. Each cylinder receives approximately equal quantities of fuel. The main control outputs are the beginning of injection (BOI) and the pulse-width (PW), i.e. duration of injection. Both depend on engine speed and torque. The top dead centre (TDC) corresponds to the minimum piston displacement, and the bottom dead centre (BDC) corresponds to the maximum piston displacement. The crank angle reference assumes 0 degrees at TDC and 180 degrees at BDC. The variables to be controlled are the engine speed and throttle position. Magnetic induction sensors are used to pick-up the time reference signal (TRSs), at 73.5 degrees BDC for each cylinder. The control action is not synchronized with changes in engine speed, and this can generate injection delays. The gain-scheduling (open-loop) solution is chosen for mid-range engine speeds. The engine controller functions in closed-loop for idle and rated speeds (when maximum output power is produced). The control time is 13 msec. The compressor boost pressure value is used to limit the allowable PW, and thus to compensate for smoke emissions caused by an inefficient scavenging process. A fast injection reduces the smoke production, while a torque increase has the opposite effect. Smoke control considerations require the acquisition of the following engine data: oil pressure and temperature, water flow and temperature, and air inlet temperature. Noise is caused mainly by the combustion process, and is reduced by delaying the BOI, which results in moving the combustion towards the end of the compression stroke.

2.3 Fault Detection and Isolation in Control Systems

Assume that the diesel engine can be described by a multi-input single output (MISO) model in the crank angle domain, θ. In this case, N defines the total number of cylinders, the model input is given by the N cylinder pressures, and the output is the crankshaft angular velocity fluctuation. We also assume that this dynamic system, $\mathcal{P}$ is characterized by the equations:

$$x'(\theta) = \frac{dx(\theta)}{d\theta} = A(p,\theta)x(\theta) + B(p,\theta)u(\theta),\ x(0) = x_0, \tag{2.1}$$

$$y(\theta) = c(p,x), \tag{2.2}$$

where $x, x' \in R^n$, are the state and its derivative, respectively. $p \in R^q$ describes the process parameters, $u \in R^N$ represents the input, and $y \in R$ the output.

The tracking, or servo problem, can be stated as follows: design a control law, $u_c(\theta)$ such that $\forall\ x_0 \in \mathcal{X} \subseteq R^n$, a measure of the tracking error, $\epsilon(\theta) = y_d(\theta) - y(\theta)$ is minimized, while x is maintained stable (bounded) [11, pp. 192–197]. The initial state is x_0, and $y_d(\theta)$ is the desired output trajectory.

The stabilization or regulation problem is equivalent to the tracking problem for constant $y_d(\theta)$. The control system refers, in general, to the following components: controller ($\mathcal{C}$), process to be controlled ($\mathcal{P}$), actuator ($\mathcal{A}$) and transducer ($\mathcal{T}$).

A fault-tolerant control system is designed to take into consideration modeling inaccuracies, measurement noise and possible sensor or actuator faults [12]. It incorporates a fault diagnosis (FD) module which has the ability to *detect*, *isolate* and *identify* component malfunctions from observed symptoms. From a systems theory point of view, an *abrupt fault* is defined as a sudden jump in system response or parameters that do not necessarily correspond to a physical failure [13]. Biases or drifts are included in the category of *incipient faults* [12]. The process of observing (supervising) certain variables for diagnosis is called condition monitoring (CM). Figure 2.2 illustrates a block-diagram of a fault-tolerant control system. It is hierarchically structured, and the top level performs the tasks of *condition monitoring*, *fault diagnosis* and *fault accommodation.* A fault-tolerant control system has to respond rapidly when a failure occurs. This design requirement has as a consequence, an increased sensitivity to measurement noise. *Fault detection and isolation* (FDI) are important steps in a fault diagnosis procedure. The

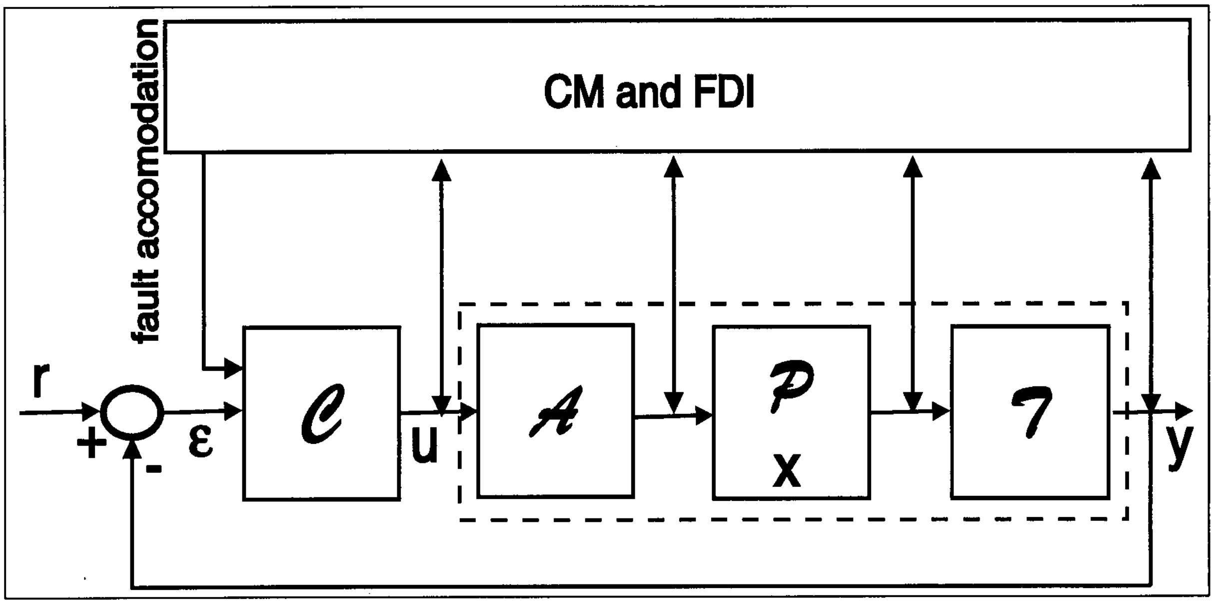

Figure 2.2: Illustrates a block-diagram of a supervised control system. The condition monitoring and fault diagnosis module allows the detection and isolation of component malfunctions. The controller is designed to exhibit robustness with respect to modeling inaccuracies and faulty sensors.

first implies the acknowledgement that a system component is defective (alarm) and the second locates the fault, i.e. differentiates between certain possible faults and determines the source of the failure [13]. The extent of the failure is evaluated as tolerable, conditionally tolerable or intolerable in the identification stage. System reorganization (fault accommodation) employs the substitution of the faulty component with a healthy one, if the fault is intolerable. Fault diagnosis and control could be carried out using a minimum set of measurements. In order to satisfy the requirements of high reliability and safety it is necessary to provide a degree of redundancy. The concept of physical (hardware) redundancy refers to the use of arrays (duplex, triplex, etc) of sensors for the measurement of the same variable. The concept of analytical redundancy refers to the use of process models and redundant functional relationships between plant variables of interest. The analytical (software) redundancy has the advantage of low cost and weight, flexibility and portability. Its reliability is strongly dependent on model accuracy. A combination of analytical and physical redundancy is almost always necessary for a fault-tolerant control system to maintain its function in the presence of certain system failures. There are model-based, knowledge-based and neural network-based fault detection and isolation schemes. Model-based fault detection and isolation algorithms make use of measurable process inputs and outputs, nonmeasurable state variables, nonmeasurable process parameters and nonmeasurable characteristic quantities [14]. The detection and isolation tasks are accomplished with the help of estimation algorithms developed from *a priori* knowledge of the system to be controlled. Thus, a central issue is the correct definition of the normal process. All these estimation techniques focus on the model accuracy.

There are two types of model uncertainties: structured or parametric and unstructured or unmodeled dynamics. An adaptive or a sliding-mode control scheme can compensate for the parametric uncertainties [11, pp. 276]. H^{∞} optimization takes into account a general perturbation model [15]. The principle of adaptive control (AC) is the continuous modification of the plant model and control law in response to parameter variation. The parameters can be identified explicitly (self-tuning AC) or implicitly (model reference AC).

2.4 Trends in Engine Condition Monitoring

The spread of electronic engine control modules (ECMs) in the 1980s, led mainly by the United States Clean Air Act, facilitated the incorporation of computers in cars and made possible the notion of up-integration (powertrain and vehicle control modules) and fault-diagnosis with the benefit of higher reliability [16]. In the U.S., the California Air Resource Board On-Board Diagnostic-II (CARB OBD-II) legislation had a powerful effect on new developments for automotive digital electronics. Thus, "zero emission" vehicles, with sophisticated diagnosis tools and better human interfaces are expected by the end of this decade. The airline industry is a pioneer in the field and many ideas have now been transferred to portable commercial power machinery applications in fields such as naval, agriculture, mining, oil-well, road-building. The new trends are also encouraged by a more demanding consumer in the automotive market and by the increased degree of automation in manufacturing and process control.

Most recent engine fault detection and isolation applications use: model, knowledge or neural network-based techniques [17]. This classification isn't exhaustive but represents the methods with which we are most familiar. The model-based approach employs techniques for state and/or parameter identification. The state can be estimated using a Luenberger observer (the deterministic case) or a Kalman filter (the stochastic case). Parameter identification methods are suitable for early detection of incipient faults, while state estimation techniques are commonly used for detection of abrupt faults. The concepts of state and parameter estimation are interchangeable to a certain extent. In the field of fault detection and isolation the estimation errors define the process of residual generation. The phase of decision making is accomplished by statistical threshold tests. A review of the state of the art of model-based fault diagnosis methods for jet engine systems can be found in [18, 19]. The authors emphasize engine sensor failures as the most critical problem to deal with. In the aerospace industry, there is a lot of interest in replacing the hydro-mechanical controllers with fault-tolerant electronic ones for aerojet engine systems. An example is the so-called full authority digital electronic controller (FADEC) for gas turbines. It controls the fuel flow rate and the exhaust nozzle area. The measured variables include: pressures, flows, temperatures and compressor shaft speed. A model-based fault diagnosis scheme for this complex non-linear system has been tested at NASA. It uses a Kalman filter for residual generation and a generalized likelihood ratio for decision making. It is therefore capable of detecting abrupt faults, but not dealing with the issue of incipient faults. Research in the field of engine fault detection and isolation is currently connected under the auspices of an international Technical Cooperation Panel with the participation of the Commonwealth countries and the United States [18].

In [20], the authors focus on a robust solution to the fault detection and isolation problem using the "disturbance decoupling" principle. The residual generator is a Luenberger state observer and the weighted output estimation error represents the fault indicator. This approach doesn't take into consideration the presence of measurement noise, and assumes a measurable system state.

A combination of model and knowledge-based methods is used in [21] for the development of a condition monitoring system for a Spey SM1A marine gas turbine engine. There are three components that define the overall structure: the signal processing subsystem (SPS) which collects and processes the raw sensor data, the signal identification subsystem (SIS) which makes use of linear engine models and SPS information to calculate engine parameters and performance, and the monitoring and diagnosis system (MDS) which gives a symbolic interpretation of the SIS output. This approach doesn't exploit the possibility of using dynamic models and their ability to predict system behaviour. It focuses mainly on the issue of explicit fault classification by means of rule-based techniques.

The subject of engine sensor faults or failures in automotive applications is treated in [22]. The authors introduce a model-based fault detection and isolation method for internal combustion engines. Residuals are generated using the eigenstructure assignment method, which is equivalent to the unknown input observer technique. These detection filters are used to localize failures in the throttle position and in the manifold absolute pressure sensors.

An attempt at diagnosis of the supercharger of a diesel engine is reported in [23]. The expert-system is tested on board a French Navy ship. There are four variables to be monitored: atmospheric pressure, temperature, accelerator position and engine speed. A "qualitative state" is associated with each of these parameters. The observed and the expected qualitative states are compared and then a decision is made using forward chain inference rules.

A neural network-based method is used in [24] to develop the classification of mechanical faults in newly manufactured engines. Data acquisition includes the following measurements: intake and exhaust manifold pressures, the crankcase air pressure and the oil pressure. These five waveforms are monitored by a neural network-based supervisor. The 29 classes consist of 28 different faults and the normal operating condition. The training is performed by the error back-propagation algorithm [25]. The information concerning the different faults is embedded in the network weights, but there is no explicit way of translating these values into physically meaningful parameters.

Our approach to the problem of engine fault diagnosis is based on the concept of parameter estimation. We are interested in early detection of faults that manifest as parameter biases or drifts. The engine model is developed as a continuous-time dynamic system, with parameters that have a physical relevance.

2.5 Residual Generation and Decision Making

A model-based fault detection and isolation procedure consists of two phases: residual generation (RG) and decision making (DM) [12]. First, the effect of the fault is amplified in order to make it recognizable (determine a fault signature). This is obtained by processing the sensor signals. The processed measurements are called residuals or fault indicators [26]. If the residual generator is designed as a parametric identification procedure, then the residuals are represented by the output prediction errors. The decision can be accomplished by a simple threshold test or by statistical methods. Consider the system described by (2.1)–(2.2) and assume that $u(\theta)$ and $y(\theta)$ are measurable, zero-mean signals. We also assume that a fault has as a direct consequence, changes of process parameters, p and/or state, $x(\theta)$, which modify the system output $y(\theta)$ [17]. Therefore, either state or parameter estimation techniques respectively can be used to detect incipient or abrupt process faults.

2.5.1 State Estimation-Based Techniques

State estimation-based residual generators include: the parity space method, dedicated observer approach, and fault detection filter approach [12]. The problem of discerning between different faults or between faults and other disturbances can be solved using the disturbance decoupling principle. If we take into account the effect of perturbations, (2.1)–(2.2) can be rewritten:

$$x'(\theta) = A(p,\theta)x(\theta) + B(p,\theta)u(\theta) + d(\theta),\ x(0) = x_0, \tag{2.3}$$

$$y(\theta) = c(p,x) + \eta(\theta), \tag{2.4}$$

where $d \in R^n$ and $\eta \in R$ describe the process and measurement noise, respectively. Both are considered unknown. In the stochastic case, d, and η are assumed zero-mean, independent white Gaussian processes. The estimator of the system normal state (see (2.3)–(2.4)) has the following form:

$$\hat{x}'(\theta) = A(p,\theta)\hat{x}(\theta) + B(p,\theta)u(\theta) + H(\theta)(y - \hat{y}),\ \hat{x}(0) = x_0, \tag{2.5}$$

$$\hat{y}(\theta) = c(p,\hat{x}), \tag{2.6}$$

where $H(\theta) \in R^n$ is the feedback gain. The state and the output estimation errors are given by:

$$\tilde{x}' = A(p,\theta)\tilde{x} + d(\theta) - H(\theta)\tilde{y},$$

$$\tilde{y} = y - \hat{y} = c(p,x) - c(p,\hat{x}) + \eta(\theta).$$

The condition monitoring system supervises the evolution of the residual (innovation) $\tilde{y}$. The fault detection can be the result of certain statistical tests performed on the residual: chi-squared test, or generalized likelihood ratio test [13]. Another approach consists of designing the gain $H(\theta)$ with the objective of amplifying the effect of certain failures in $\tilde{y}$ rather than providing good state tracking. Such observers are called Beard-Jones failure sensitive filters. Assume $d(\theta) = d_i b_i$ with b_i the i-th column of b, i.e. the fault corresponds to a bias in the i-th actuator. The expression for the residual becomes $\tilde{y}' = (A(p,\theta) - H(\theta))\tilde{y} + d_i b_i$, if $y = x$. For $H(\theta) = A(p,\theta) + \alpha_0 I_n$, $\tilde{y}$ has the orientation of b_i and a magnitude proportional to d_i. The gain design procedure is similar to the disturbance decoupling problem [13].

2.5.2 Parameter Estimation-Based Techniques

Identification methods attempt to find suitable approximations to the parameters associated with real systems. Let $\hat{p}$ be an estimate of the process parameter vector p. The output prediction is $\hat{y} = c(\hat{p},x)$ and the prediction error is $\tilde{y} = y - \hat{y} = y - c(\hat{p},x)$. The parameter estimation problem can be formulated as the minimization of a generalized prediction error function, E [27]. The necessary zero gradient condition for the minimum is:

$$\nabla_p E|_{p=\hat{p}} = 0. \tag{2.7}$$

From (2.7) the parameter estimates, $\hat{p}$, have to be determined. An analytical solution is tractable if c is linear in p, i.e $y(\theta) = c(p,x) = \Phi(\theta)p$ with $\Phi \in R^{1\times q}$ [27]. In this case $\tilde{y} = \Phi(\theta)(p - \hat{p}) = \Phi(\theta)\tilde{p}$, where $\tilde{p}$ is the parameter estimation error. The gradient estimators and the least-squares estimators with exponential forgetting are characterized by good robustness with respect to noise and parameter variation [11, pp. 367–369, 380–381]. The simplest parameter estimator is the gradient estimator. In this case, the parameter adaptation law is given by:

$$\frac{d\hat{p}}{d\theta} = -\Psi_0 \nabla_{\hat{p}} E = -\Psi_0 \Phi^T \tilde{y}, \tag{2.8}$$

where $E = \frac{1}{2} \parallel \tilde{y} \parallel^2$ is the squared output prediction error, and $\Psi_0 \in R^{s \times s} > 0$ is the gain matrix. The signal matrix, Φ has to be persistently exciting in order to achieve exponential parameter convergence, i.e. $\exists \alpha_0, \Theta > 0$ such that $\forall \Theta \geq 0$

$$\int_\theta^{\theta+\Theta} \Phi^T \Phi \geq \alpha_0 I_q, \tag{2.9}$$

with $I_q \in R^{q \times q}$ the idendity matrix [11, pp. 366].

The cost function used in least-squares estimation with exponential forgetting is:

$$E = \frac{1}{2} \int_0^\theta e^{-\int_t^\theta \lambda(r)dr} \parallel y(t) - \Phi(t)\hat{p} \parallel^2 dt, \tag{2.10}$$

where λ represents the forgetting factor. The parameters are updated using:

$$\frac{d\hat{p}}{d\theta} = -\Psi(\theta)\Phi^T \tilde{y}, \tag{2.11}$$

where

$$\Psi^{-1}(\theta) = \Psi^{-1}(0) e^{-\int_0^\theta \lambda(t)dt} + \int_0^\theta e^{-\int_t^\theta \lambda(r)dr} \Phi^T(t)\Phi(t)dt\,.$$

The gain matrix, $\Psi(\theta)$ is calculated recursively using the formula:

$$\frac{d\Psi}{d\theta} = -\lambda(\theta)\Psi + \Psi\Phi^T(\theta)\Phi(\theta)\Psi\,.$$

The decision making stage employs statistical comparisons between actual residuals and known fault signatures. Changes in parameter means and variances can be used as decision criteria.

Our research is directed at developing and validating an effective diesel engine model for fault diagnosis applications. The model is used in a parametric identification procedure to detect incipient faults in the fueling of engine cylinders [14]. The early detection and isolation of engine faults is accomplished using the gradient estimator and the least-squares estimator with exponential forgetting. The choice of these two identification methods is based on their robustness with respect to measurement noise and parameter variation [11, pp. 367,380]. The same model is used to obtain the cylinder pressure waveform, reconstructed from noisy measurements of flywheel/crankshaft angular velocity fluctuations.

Chapter 3

Engine Modeling and Validation

No more friction, no more slowing.
The length of the Earth day will then be
more than fifty times as long as the present day;
and the more distant Moon will turn in its orbit
in twice the period it now turns.
Isaac Asimov, Asimov on Astronomy

The first step in designing a comprehensive diesel engine fault detection and isolation system is to develop and validate a mathematical model. The model we develop here is configured to correspond to the DDC 6V 92TA Detroit Diesel engine. The analytical methodology follows that of C. F. Taylor [28, pp. 240–305], and the testing was performed using data supplied by the Institute for Machinery Research, National Research Council.

Our modeling approach is based on Euler's equation [1] applied to a generic internal combustion engine. These equations of motion characterize the rotational dynamics of a diesel engine and can be subsequently used to derive the relationship between cylinder pressures and flywheel/crankshaft angular velocity fluctuation. We define the total engine torque, $T_E(\theta)$, as the sum of all torques acting on the crankshaft taking into consideration the phase shift determined by the cylinder arrangements:

$$T_E(\theta) = T_p(\theta) + T_t(\theta) + T_r(\theta) + T_f(\theta) + T_l(\theta), \tag{3.1}$$

where θ is the crank angle. $T_p(\theta)$ is the indicated torque due to the gas pressure forces,

$T_t(\theta)$ is the torque due to the inertia of the reciprocating parts, and $T_r(\theta)$ is the torque due to the rotation of the connecting rods. $T_f(\theta)$ refers to the total friction torque (assumed constant), and $T_l(\theta)$ is the dynamometer (brake) load torque. The model is developed under the assumption that the crankshaft is a purely rotating rigid body. Similar approaches dedicated to internal combustion engines can be found in references [4] and [5]. The novelty of our model relies on the fact that it incorporates the torque due to angular acceleration of the connecting rods. We compare the measured angular velocity with the calculated one. The testing set consists of 6 different actuator faults and the normal operating condition. The actuator fault is defined here as the phenomenon of cylinder under-fueling which has as a direct consequence the reduction of cylinder peak pressure. We use both pressure and flywheel angular velocity measurements.

3.1 Geometrical Consideration

The engine crankshaft is assumed perfectly rigid. The connecting rod is modeled by two masses: m_t which is included in the piston assembly and m_r which rotates with the crank pin. Consider the diagram for the crank and connecting rod mechanism illustrated in Figure 3.1. The piston instantaneous position with respect to the top dead centre (TDC) is:

$$s = l + r - (r\cos\theta + l\cos\alpha), \tag{3.2}$$

with

$$\cos\alpha = \sqrt{1 - \frac{r^2}{l^2}\sin^2\theta}, \tag{3.3}$$

where r is the crank radius, l is the connecting rod length, θ is the crank angle, and α is the angle between the connecting rod axis and the cylinder axis. The piston instantaneous velocity is calculated by taking the time derivative of (3.2):

$$\dot{s} = r\omega c_1(\theta), \tag{3.4}$$

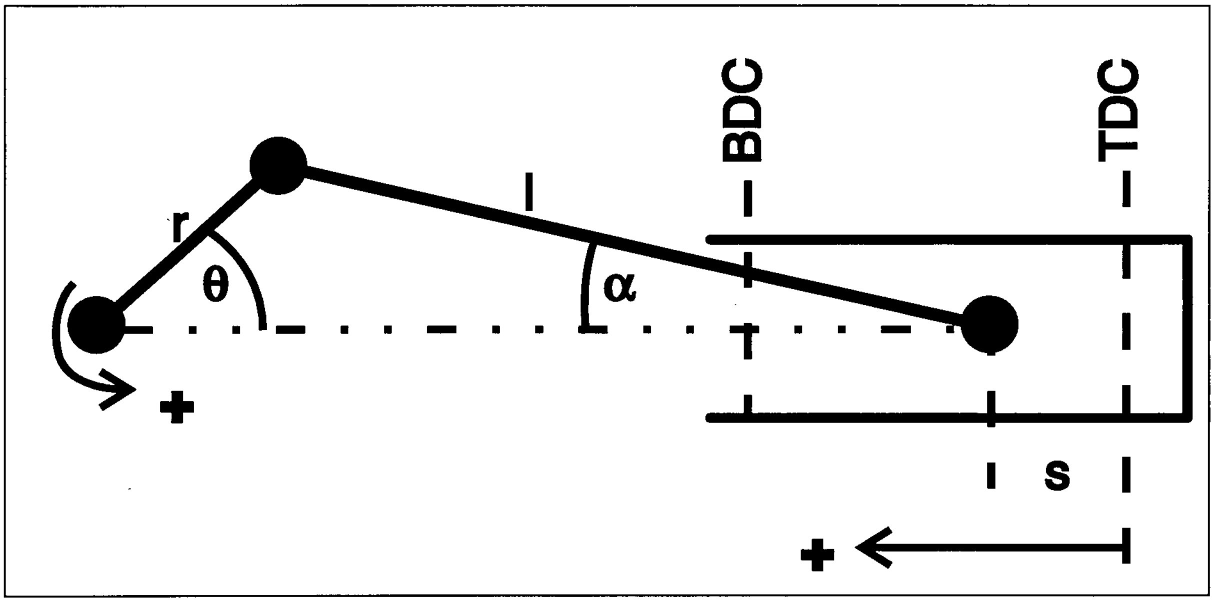

Figure 3.1: Crank arm and connecting rod mechanism: r is the crank radius, l is the connecting rod length, θ is the crank angle, and α is the angle between the connecting rod axis and the cylinder axis. The piston instantaneous position with respect to the top dead centre is $s = l + r - (r\cos\theta + l\cos\alpha)$.

where $\omega = \dot{\theta}$. The geometrical coeffcient $c_1(\theta)$ has the following expression:

$$c_1(\theta) = \left(1 + \frac{r}{l}\frac{\cos\theta}{\cos\alpha}\right)\sin\theta, \tag{3.5}$$

Similarly, the piston acceleration is given by:

$$\ddot{s} = r\left(c_1(\theta)\dot{\omega} + c_2(\theta)\omega^2\right), \tag{3.6}$$

The coefficient $c_2(\theta)$ is given by:

$$c_2(\theta) = \frac{dc_1(\theta)}{d\theta} = \left(1 + \frac{r}{l}\frac{\cos\theta}{\cos\alpha}\right)\left[\cos\theta + \frac{r}{l}\frac{\sin^2\theta}{\cos\alpha}\left(\frac{r}{l}\frac{\cos\theta}{\cos\alpha} - 1\right)\right]. \tag{3.7}$$

Figure 3.2 illustrates the variation of piston position (see (3.2)), speed (see (3.4)), and acceleration (see (3.6)) during one revolution, assuming a nominal rotational velocity of 1,200 rpm. The angular acceleration of the connecting rod is calculated from Figure 3.1

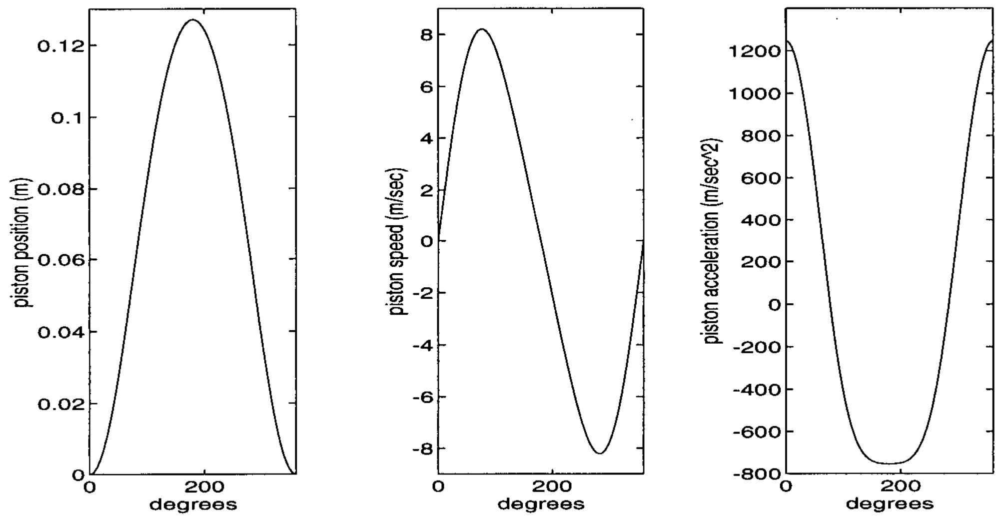

Figure 3.2: Instantaneous piston position, s (left), speed, $\dot{s}$ (middle) and acceleration, $\ddot{s}$ (right) during one revolution, assuming a nominal crankshaft angular velocity of 1,200 rpm.

as a function of $\dot{\omega}$ and ω^2:

$$\ddot{\alpha} = c_3(\theta)\dot{\omega} + c_4(\theta)\omega^2. \tag{3.8}$$

The coefficients $c_3(\theta)$ and $c_4(\theta)$ have the following form:

$$c_3(\theta) = \frac{r}{l}\frac{\cos\theta}{\cos\alpha}, \tag{3.9}$$

$$c_4(\theta) = \frac{dc_3(\theta)}{d\theta} = \frac{r}{l}\frac{\sin\theta}{\cos\alpha}\left(c_3^2(\theta) - 1\right). \tag{3.10}$$

Figure 3.3 illustrates the angular acceleration of the connecting rod (see (3.8)) during one revolution, assuming a nominal rotational velocity of 1,200 rpm.

3.2 Model Development

A modified engine model is developed in this thesis by finding explicit formulas for the torques involved in (3.1). $T_p(\theta)$ is defined under the assumption that the work done on

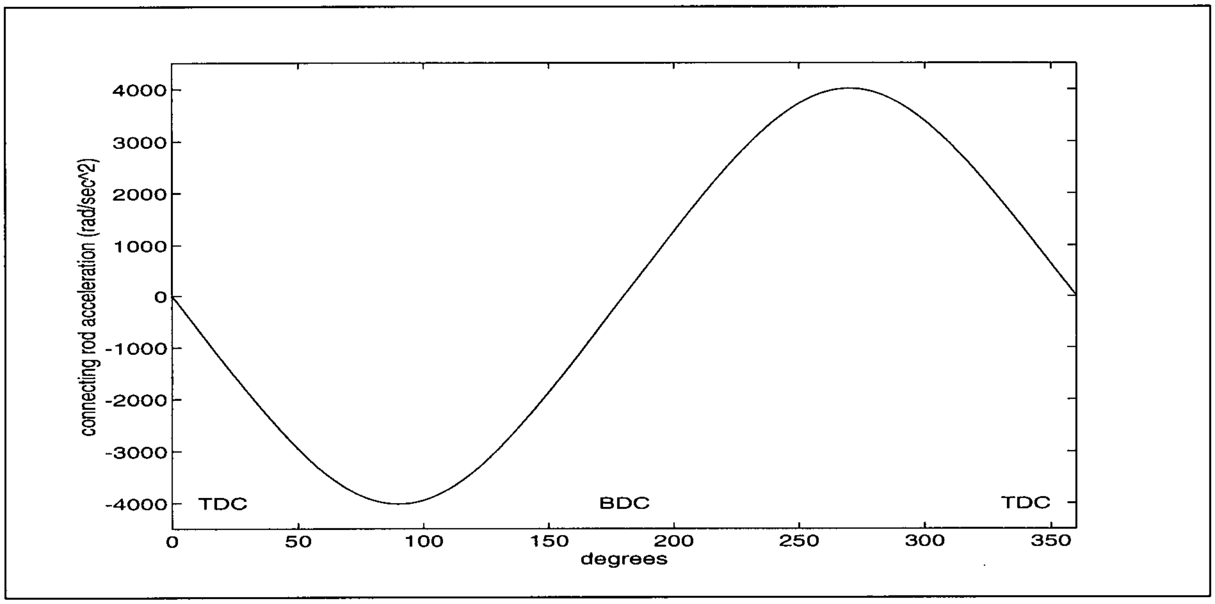

Figure 3.3: Angular acceleration of the connecting rod, $\ddot{\alpha}$, during one revolution, assuming a constant crankshaft angular velocity of 1,200 rpm.

the piston is equal to the work done on the crankshaft [28, pp. 268]. It depends directly on each cylinder pressure:

$$T_p(\theta) = A_p r \sum_{i=1}^{N} P_i(\theta) c_1(\theta - \phi_i) , \tag{3.11}$$

where N is the total number of cylinders, and A_p is the piston crown area. $P_i(\theta)$ refers to the pressure in the i-th cylinder and ϕ_i is the phase shift corresponding to the i-th firing cylinder. Figure 3.4 illustrates the measured torque due to gas pressure for the DDC 6V 92TA operating at 1,200 rpm. The phase angles ϕ_i are the angles of the crank arm relative to the crank angle when cylinder 1 is at top dead centre. For a two-stroke, even-firing, in-line, six-cylinder engine, $\phi_i = \frac{\pi}{3}(i-1), \quad i = 1 \ldots 6$ rad. In the case of the DDC 6V 92TA Detroit Diesel engine, the V-angle between cylinder banks is 63.5 degrees. The phase origin is the top dead centre of the first cylinder firing, and $\phi_1 = 0$, $\phi_2 = 56.5$, $\phi_3 = 120$, $\phi_4 = 176.5$, $\phi_5 = 240$, $\phi_6 = 296.5$ degrees.

The work done by the crankshaft on the connecting rod is equal to the change in

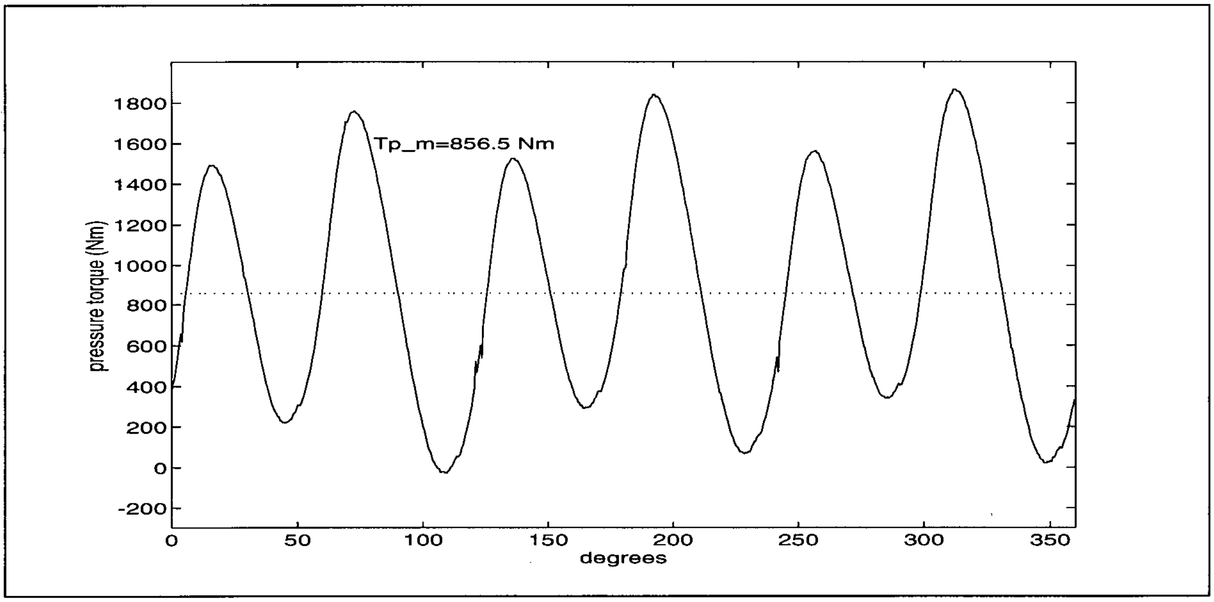

Figure 3.4: Torque due to gas pressure for the case of the six-cylinder DDC 6V 92TA Detroit Diesel Engine operating at 1, 200 rpm.

kinetic energy of the piston [28, pp. 264]. $T_t(\theta)$ is due to the inertia of the translating parts and depends on all piston accelerations (see (3.6) and Figure 3.2):

$$T_t(\theta) = -m_p r^2 \sum_{i=1}^{N} c_1(\theta - \phi_i)(c_1(\theta - \phi_i)\dot{\omega} + c_2(\theta - \phi_i)\omega^2) , \tag{3.12}$$

where m_p is the mass which is considered to reciprocate with the piston, i.e. piston, piston rings, piston pin and the upper end of the connecting rod.

The torque acting on the crankshaft due to the angular acceleration of all connecting rods is (see (3.8) and Figure 3.3):

$$T_r(\theta) = J_{cr} \sum_{i=1}^{N} c_3(\theta - \phi_i)(c_3(\theta - \phi_i)\dot{\omega} + c_4(\theta - \phi_i)\omega^2 , \tag{3.13}$$

where J_{cr} is the connecting rod moment of inertia.

We define the following variable parameters:

$$c_{11}(\theta) = \sum_{i=1}^{N} c_1^2(\theta - \phi_i) , \tag{3.14}$$

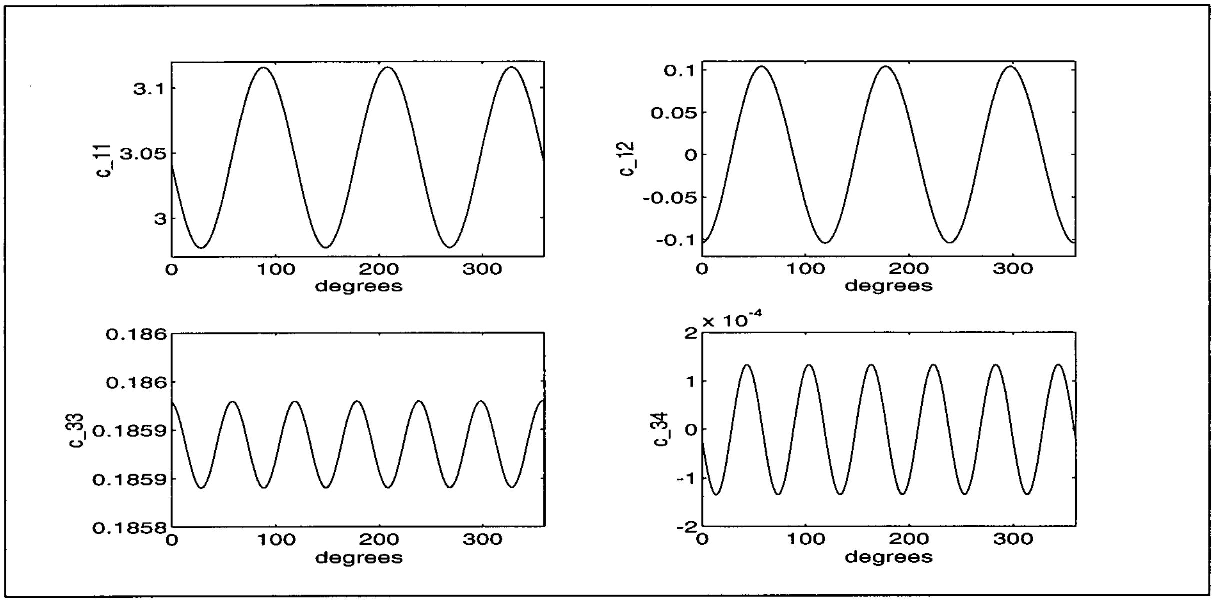

Figure 3.5: Variation of the torque coefficients: $c_{11}(\theta)$, $c_{12}(\theta)$, $c_{33}(\theta)$, and $c_{34}(\theta)$ with $\frac{r}{l} = 0.247$, during one crankshaft revolution.

$$c_{12}(\theta) = \sum_{i=1}^{N} c_1(\theta - \phi_i)c_2(\theta - \phi_i), \tag{3.15}$$

$$c_{33}(\theta) = \sum_{i=1}^{N} c_3^2(\theta - \phi_i)\,, \tag{3.16}$$

$$c_{34}(\theta) = \sum_{i=1}^{N} c_3(\theta - \phi_i)c_4(\theta - \phi_i)\,. \tag{3.17}$$

These parameters are illustrated in the graphs of Figure 3.5. We can rewrite (3.12) and (3.13) as:

$$T_t(\theta) = -m_p r^2 \left(c_{11}(\theta)\dot{\omega} + c_{12}(\theta)\omega^2\right), \tag{3.18}$$

$$T_r(\theta) = J_{cr} \left(c_{33}(\theta)\dot{\omega} + c_{34}(\theta)\omega^2\right). \tag{3.19}$$

Let J_E be the engine moment of inertia. The Euler equation for the diesel engine, viewed as a rotating rigid body is:

$$\frac{d(J_E\omega)}{dt} = T_E(\theta)\,, \tag{3.20}$$

or taking into consideration (3.1), (3.11), (3.18), (3.19):

$$\left(J_E - J_{cr}c_{33}(\theta) + m_p r^2 c_{11}(\theta)\right)\dot{\omega} = \left(J_{cr}c_{34}(\theta) - m_p r^2 c_{12}(\theta)\right)\omega^2 + T_f(\theta) + T_l(\theta) + A_p r \sum_{i=1}^{N} P_i(\theta - \phi_i)c_1(\theta - \phi_i)\,. \tag{3.21}$$

Let $x = \omega^2$, then,

$$\dot{\omega} = \frac{d\omega}{dt} = \frac{d\omega}{d\theta}\frac{d\theta}{dt} = \omega'\omega = \frac{1}{2}\frac{dx}{d\theta} = \frac{1}{2}x'\,. \tag{3.22}$$

Therefore, (3.21) becomes:

$$\frac{1}{2}\left(J_E - J_{cr}c_{33}(\theta) + m_p r^2 c_{11}(\theta)\right)x' = \left(J_{cr}c_{34}(\theta) - m_p r^2 c_{12}(\theta)\right)x + T_f(\theta) + T_l(\theta) + A_p r \sum_{i=1}^{N} P_i(\theta)c_1(\theta - \phi_i)\,. \tag{3.23}$$

Let $x_0 = \omega_0^2$ describe the engine operating point, with ω_0 the nominal engine speed. The engine speed fluctuation is $\delta\omega = \omega - \omega_0$, and this corresponds to a fluctuation of the variable x of the form:

$$\delta x = \delta\omega(2\omega_0 + \delta\omega) \approx 2\omega_0\delta\omega\,. \tag{3.24}$$

At the same time, the speed fluctuation can be determined from the variation δx using:

$$\delta\omega = \sqrt{\delta x + \omega_0^2} - \omega_0\,. \tag{3.25}$$

With these considerations, the state equation, given by (3.23), is rewritten in a form similar to (2.1):

$$\delta x' = A(\theta)\delta x + b^T(\theta)u(\theta) + d(\theta), \tag{3.26}$$

and (3.25) becomes the output equation similar to (2.2):

$$\delta\omega = c(\delta x)\,, \tag{3.27}$$

where

$$A(\theta) = \frac{J_{cr}c_{34}(\theta) - m_p r^2 c_{12}(\theta)}{\frac{1}{2}\left(J_E - J_{cr}c_{33}(\theta) + m_p r^2 c_{11}(\theta)\right)}\,, \tag{3.28}$$

$$b(\theta) = \frac{A_p r}{\frac{1}{2}\left(J_E - J_{cr}c_{33}(\theta) + m_p r^2 c_{11}(\theta)\right)} \begin{bmatrix} c_1(\theta - \phi_1) \\ \vdots \\ c_1(\theta - \phi_N) \end{bmatrix}, \quad u(\theta) = \begin{bmatrix} P_1(\theta) \\ \vdots \\ P_N(\theta) \end{bmatrix}, \tag{3.29}$$

$$d(\theta) = \frac{\left(J_{cr}c_{34}(\theta) - m_p r^2 c_{12}(\theta)\right) x_0 + T_f(\theta) + T_l(\theta)}{\frac{1}{2}\left(J_E - J_{cr}c_{33}(\theta) + m_p r^2 c_{11}(\theta)\right)},, \tag{3.30}$$

and

$$c(\delta x) = \sqrt{\delta x + \omega_0^2} - \omega_0 \,. \tag{3.31}$$

3.3 Simulation Results

The model described by (3.26) is validated using the MATLAB simulation package, and the code is listed in Appendix B. The most important M-files are:

- *c_1.m, c_2.m, c_3.m, c_4.m* which implement the coefficients described by (3.5), (3.7), (3.9), (3.10), respectively,
- *system.m* which implements the differential equation (3.26),
- *demo1.m* which calculates the residual and the estimation for a certain cylinder condition (faulty or not), and
- *rmse.m* which calculates the root mean square error (see (3.33)).

The model parameters, from [3] are: $N = 6$, $r = 0.0635$ m, $l = 0.2571$ m, $J_{cr} = 0.0745$ kgm^2, $m_p = 6.03$ kg, $A_p = 0.01188$ m^2. The engine effective moment of inertia includes the crankshaft and the flywheel moments of inertia and has the lumped value $J_E = 4.044$ kgm^2. The phase origin is the top dead centre of the first cylinder to fire, and $\phi_1 = 0$, $\phi_2 = 56.5$, $\phi_3 = 120$, $\phi_4 = 176.5$, $\phi_5 = 240$, $\phi_6 = 296.5$ degrees. The firing order is: 1L, 3R, 3L, 2R, 2L, 1R, where the letters "L" and "R" refer to the left and the right bank of cylinders, respectively. Data acquisition is performed for a nominal speed $\omega_0 = 125.7$

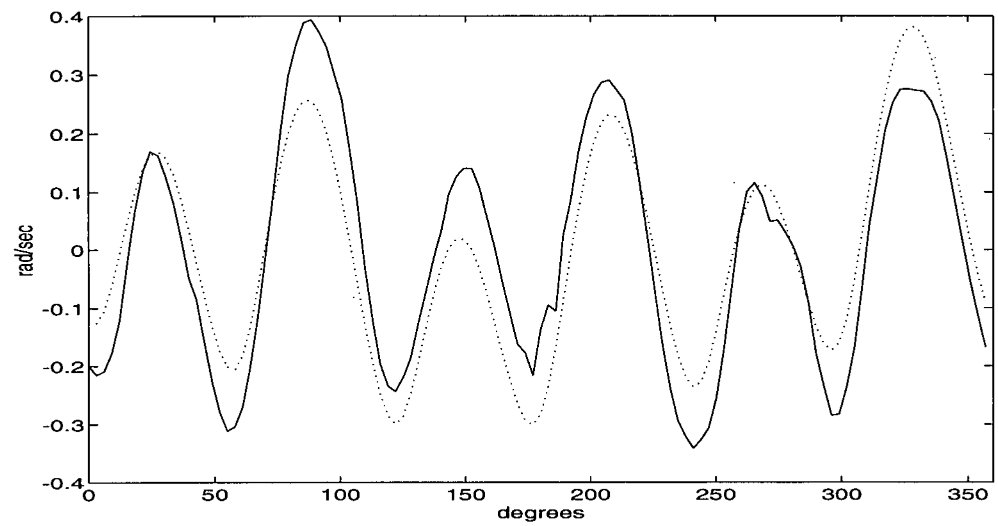

Figure 3.6: Presents the actual (solid line), $\delta\omega$, and the estimated (dashed line), $\delta\hat{\omega}$, flywheel angular velocity fluctuation for the normal operation of the diesel engine.

rad/sec (1,200 rpm) and a dynamometer torque, $T_l = 990$ Nm. This load represents 75% of the engine peak torque. $T_f = 156$ Nm is the value of the mechanical friction torque corresponding to a crankshaft angular velocity of $\omega_0 = 125.7$ rad/sec and an overall damping coefficient of 1.24 Nmsec.

The testing set consists of 6 different actuator faults and the normal operating condition. The actuator fault is represented by a 10% drop in cylinder fueling. In order to measure the modeling error we calculate the output residual:

$$\delta\tilde{\omega} = \delta\omega - \delta\hat{\omega}\,, \tag{3.32}$$

where $\delta\omega$ and $\delta\hat{\omega}$ are the actual and the estimated flywheel angular velocity fluctuation, respectively. Figure 3.6 illustrates the measured and estimated flywheel angular velocity fluctuation for the normal operating condition (baseline). The root mean square (RMS) error is defined as the standard deviation of the zero-mean residual:

$$\text{RMS velocity error} = \sqrt{\frac{\int_0^{2\pi} \left(\delta\tilde{\omega}(\theta)\right)^2 d\theta}{2\pi}}. \tag{3.33}$$

The ratio between the RMS error and the standard deviation of the measured fluctuation is the residual to signal ratio (RSR) and is used here to express the effectiveness of the model (3.26)–(3.27):

$$\text{RSR} = \frac{\text{RMS error}}{\sigma(\delta\omega)} 100\%, \tag{3.34}$$

where $\sigma(\delta\omega)$ is the standard deviation of $\delta\omega$.

The first step of the validation procedure is concerned with the analysis of the model behaviour in the case of engine normal operation. In the case of this experiment (see Figure 3.6), the RMS error is 0.0891 rad/sec. The standard deviation of the measured signal is 0.1956 rad/sec. This result yields an RSR value of 46%.

The model is then tested for the case of an under-fueling fault cylinder 1L. The difference between the actual and the estimated velocity waveforms for this situation is plotted in Figure 3.7.

In each of the 6 under-fueling faults (10% down condition for one cylinder at a time), this residual is found to exhibit a strong sinusoidal trend. A number of factors can explain this harmonic trend. The first is crankshaft vibration [29, pp. 64–74] which is not taken into consideration in our model since it assumes a perfectly rigid crankshaft. The amplitude of the vibration increases in the presence of cylinder under-fueling. Secondly, the dynamometer and the dynamometer controller form a feedback system which attempts to maintain a constant engine speed. This can induce an oscillatory behaviour in the dynamometer loading.

In order to eliminate this trend, the following technique is employed:

$$\delta\tilde{\omega}(\theta) = \delta\omega(\theta) - \delta\hat{\omega}(\theta) = \Omega_h \sin(\theta + \gamma) + \eta, \tag{3.35}$$

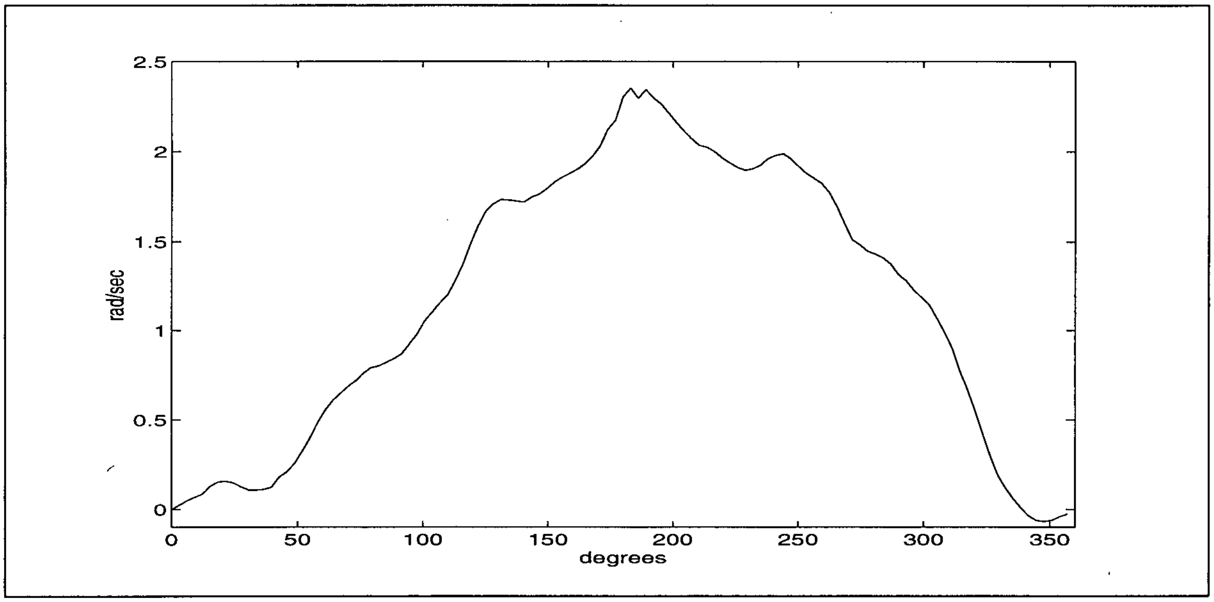

Figure 3.7: The difference between the estimated and measured velocity fluctuation, $\delta\tilde{\omega}$, in the case of 10% under-fueling in cylinder 1L.

with $\delta\tilde{\omega}$ the estimation error, Ω_h the unknown amplitude, γ the unknown phase, and η the measurement noise. We added the data to a version of itself shifted by 180 degrees. Since the estimation and the actual $\delta\omega$ are periodic with period 360 degrees, then the residual, $\delta\tilde{\omega}$, has the same property, and the shift becomes rotation:

$$\delta\tilde{\omega}(\theta) + \delta\tilde{\omega}(\theta + \pi) \approx 0. \tag{3.36}$$

The resulting estimate is shown in Figure 3.8 The RMS error reduces to 0.1368 rad/sec. This corresponds to a 38% RSR.

The RMS error for the six under-fueled conditions lies between 0.0973 and 0.1836 rad/sec. This corresponds to a RSR of 26% to 54%. The best results are obtained for an under-fueling fault in cylinder 1R, and the worst case corresponds to an under-fueling fault in cylinder 2L.

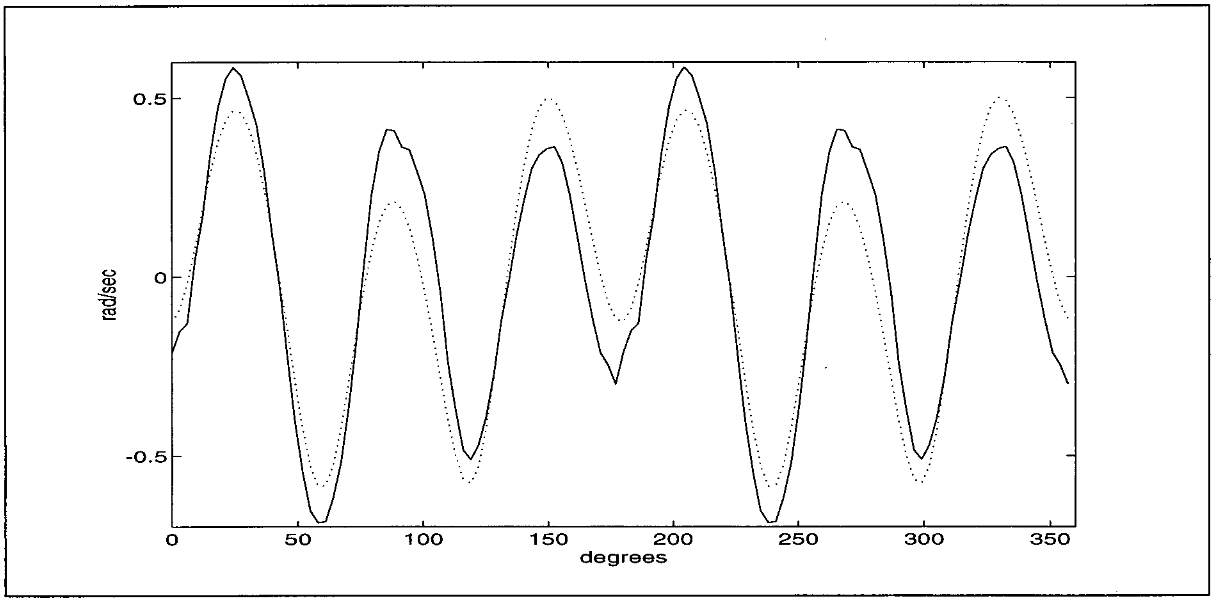

Figure 3.8: The actual (solid line) and the estimated (dashed line) flywheel angular velocity fluctuation for the faulty operation of the first cylinder on the left bank of the engine. These results are posterior to the elimination of a vibrational sine trend as per (3.36).

The results reported here can be improved via a parameter identification procedure. The uncertain system parameters are engine inertia, J_E and the unknown torque fluctuation, $\Delta T = T_h \sin(\theta + \gamma)$, where T_h is the torque amplitude, and γ the phase. This is the main objective of the following chapter.

Chapter 4

Parameter Identification

The one that has the most will be the greatest?
Now I understand, Sir, you are equating quality with quantity.
Eugène Ionesco, The Lesson

Identification methods attempt to determine values for the unknown or uncertain system parameters using measurements of input and output signals. This concept is transferred to the field of engine fault detection and isolation by assuming that the occurrence of a fault has as a direct consequence, changes of process parameters, which modify the system output. Therefore, parameter estimation techniques can be employed to detect incipient process faults. If the residual generator is implemented as a parametric identification procedure, then the residuals are represented by the output prediction errors. The decision making stage employs statistical comparisons between residuals and known fault signatures. Changes in parameter means and variances can be used as decision criteria.

The parameter identification procedure can be accomplished on-line or off-line. In this chapter we are focusing on two on-line identification methods: the gradient estimator and the least-squares estimator with exponential forgetting. The results are compared with those obtained from the off-line standard least-squares technique. The parameters of interest are the engine inertia, J_E, and the torque fluctuation, $\Delta T(\theta)$, which we attributed to unmodeled crankshaft vibration and oscillatory loading of the dynamometer. The reason for choosing these two estimators is found in their robustness with respect to measurement noise, and parameter variation [11, pp. 367, 380]. The analysis of the estimated parameters allows the classification of an engine cylinder as faulty or not.

4.1 Identification Model

There are a number of papers that attempt internal combustion engine parametric identification using least squares approaches. Many of them have as a final goal, the adaptive control of systems that have a diesel engine as the principal component [30, 31, 32]. Three such applications—adaptive speed control of a stationary diesel engine for power generation, self-adaptive idle speed control of an automotive diesel engine and adaptive performance optimization—are discussed in reference [30]. In that work the author uses the recursive least squares (RLS) method for parametric identification with engine models in the autoregressive (AR) form:

$$A(q^{-1})\omega(i) = B(q^{-1})u(i), \tag{4.1}$$

where $A(q^{-1})$ and $B(q^{-1})$ are polynomials in the shift operator q^{-1}, u is the fuel rack position, and ω is the engine speed.

The RLS identification of a diesel prime-mover with unknown dead-time is treated in references [31, 32]. Here the authors accelerate the algorithm convergence by imposing limits on model parameters.

The model used in [33] for gain scheduling control is a fifth order AR type (see (4.1)) and describes the dynamics relating the fuel rack to engine speed. The model parameters (the coefficients of polynomials $A(q^{-1})$ and $B(q^{-1})$) are nonlinear functions of engine speed and power output.

All models mentioned above are suitable for adaptive control applications, but they all have the disadvantage that they don't preserve any physical relationship to the engine throughout the identification process and therefore they are not ideally suited to condition monitoring applications.

A parametric identification approach to engine fault detection and isolation is reported in [4]. The authors assume that the influences of cylinder faults on the flywheel angular velocity can be decoupled from each other. This is a simplification that may lead to misclassification as faulty, a normal cylinder adjacent to the faulty cylinder. This problem is solved in [34], but the solution involves pattern recognition techniques. A combination of parameter estimation methods and expert-system interpretation techniques is used in [17]. This approach is applied to 4 case study experiments in [35]. The authors recommend the use of an analytical knowledge paradigm for well understood processes, followed by a heuristic analysis for aspects that cannot be fully explained by mathematical means.

Our identification model is obtained from the engine model developed in the previous chapter (see (3.26)–(3.27)):

$$\delta x' = A(\theta)\delta x + b^T(\theta)u(\theta) + d(\theta),$$

$$\delta\omega = c(\delta x),$$

where $A(\theta)$, $b(\theta)$, $d(\theta)$, $c(\delta x)$ are the system coefficients defined in (3.28)–(3.31), the variable δx is defined in (3.24), and $\delta\omega$ is the angular velocity fluctuation. The sinusoidal trend of the residual, depicted in Figure 3.7 which we attributed to the crankshaft vibration and oscillatory behaviour of the dynamometer loading is:

$$\Delta T(\theta) = T_h \sin(\theta + \gamma), \tag{4.2}$$

where T_h is the unknown torque amplitude, and γ the unknown phase. In order to obtain a linear parametrization model we rewrite (4.2) as:

$$\Delta T(\theta) = T_s \sin\theta + T_c \cos\theta, \tag{4.3}$$

where $T_s = T_h \cos\gamma$, and $T_c = T_h \sin\gamma$ are parameters to be identified, and θ is the crank angle. Taking into consideration (4.3), we can represent the system described by

(3.26)–(3.27) in the linear parametrization form:

$$Y(\theta) = \Phi(\theta)p, \tag{4.4}$$

where $\Phi(\theta)$ is the signal matrix:

$$\Phi(\theta) = \left[-\frac{1}{2}\delta x'(\theta) \quad \sin\theta \quad \cos\theta\right], \tag{4.5}$$

p is the vector of unknown parameters:

$$p = \left[J_E \;\; T_s \;\; T_c\right]^T, \tag{4.6}$$

and $Y(\theta)$ the modified torque output for the identification model:

$$\begin{aligned} Y(\theta) = {} & -m_p r^2 \left[\tfrac{1}{2}c_{11}(\theta)\delta x'(\theta) + c_{12}(\theta)\left(\delta x + x_0\right)\right] + \\ & J_{cr}\left[\tfrac{1}{2}c_{33}(\theta)\delta x'(\theta) + c_{34}(\theta)\left(\delta x + x_0\right)\right] + T_p(\theta) + T_f(\theta) + T_l(\theta), \end{aligned} \tag{4.7}$$

with m_p the mass of the reciprocating parts, r the crankshaft radius, J_{cr} the connecting rod mass moment of inertia, $T_p(\theta)$ the torque due to gas pressure forces (see (3.11)), $T_l(\theta)$ the nominal load torque, and $T_f(\theta)$ the friction torque. The torque coefficients, $c_{11}(\theta)$, $c_{12}(\theta)$, $c_{33}(\theta)$, $c_{34}(\theta)$ were defined in (3.14)–(3.17), and $x_0 = \omega_0^2$, with ω_0 the nominal engine speed. $Y(\theta)$ is a zero-mean variable and is plotted in Figure 4.1. Assume that the number of available measurements is equal to $N_m \geq 3$. Then, the objective of the identification procedure is to find the solution of the algebraic system of N_m equations of the form (4.4) with 3 unknowns: J_E, T_s, and T_c.

4.2 Performance Index

Assume that $\hat{p}$ is a solution of the following algebraic system:

$$Y(\theta_k) = \Phi(\theta_k)p, \quad k = 1, \ldots N_m, \tag{4.8}$$

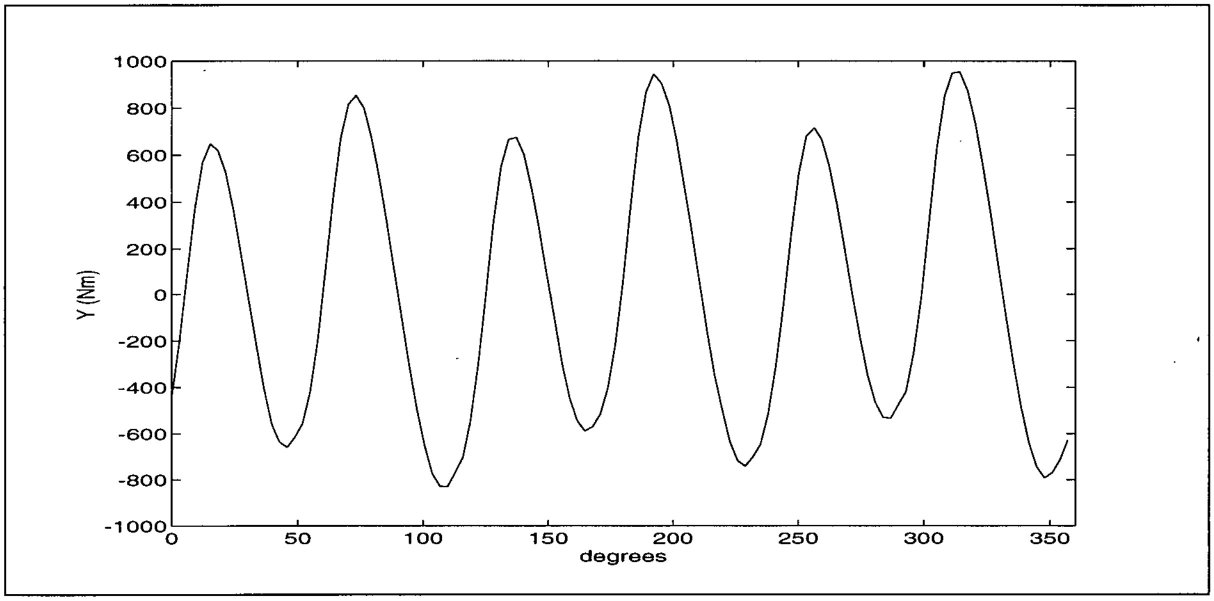

Figure 4.1: The variation of the corrected engine torque, $Y(\theta)$, during one crankshaft revolution for the normal operating condition.

where θ_k defines the k-th measurement (sampling instant). The output prediction is $\hat{Y}(\theta) = \Phi(\theta)\hat{p}$ and the output prediction error is $\tilde{Y}(\theta) = \Phi(\theta)\tilde{p}$, with $\tilde{p} = p - \hat{p}$. The parameter estimate, $\hat{p}$ is found by minimizing a measure of the output prediction error, $\tilde{Y}(\theta)$.

For standard least-squares estimation the cost function is given by:

$$E = \frac{1}{2}\int_0^\theta \| Y(t) - \Phi(t)\hat{p} \|^2 \, dt \tag{4.9}$$

Geometrically, this is equivalent to determining the projection of the unknown parameter vector p on the hyperplane defined by the columns of $\Phi(\theta)$. The off-line solution to the standard least-squares estimation problem is:

$$\hat{p} = \Phi^{+}(\theta)Y(\theta), \tag{4.10}$$

where $\Phi^{+}(\theta)$ is the pseudoinverse of $\Phi(\theta)$. The pseudoinverse exists if the matrix $\Phi^T(\theta)\Phi(\theta)$

is nonsingular:

$$\Phi^+(\theta) = \left(\Phi^T(\theta)\Phi(\theta)\right)^{-1} \Phi^T(\theta). \tag{4.11}$$

The cost function used for the least-squares estimator with exponential forgetting is (see (2.10)):

$$E = \frac{1}{2}\int_0^\theta e^{-\int_t^\theta \lambda(r)dr} \parallel Y(t) - \Phi(t)\hat{p} \parallel^2 dt, \tag{4.12}$$

where λ represents the forgetting factor. The on-line implementation of the least-squares estimator with exponential forgetting is described by the following equations:

$$\frac{d\hat{p}}{d\theta} = -\Psi(\theta_i)\Phi^T(\theta_i)\tilde{Y}(\theta_i), \tag{4.13}$$

$$\lambda(\theta_i) = \lambda_0\left(1 - \frac{\parallel \Psi(\theta_i) \parallel}{k_0}\right), \tag{4.14}$$

$$\frac{d\Psi}{d\theta} = -\lambda(\theta_i)\Psi(\theta_i) + \Psi(\theta_i)\Phi^T(\theta_i)\Phi(\theta_i)\Psi(\theta_i), \tag{4.15}$$

where $\Psi(\theta_i)$ represents the estimator gain at the i-th iteration, $\parallel \Psi(\theta_i) \parallel$ is the norm defined as the maximum singular value of the matrix $\Psi(\theta_i)$, λ_0 is the maximum allowable value for the forgetting factor, and $k_0 > 0$ [11, pp. 374–377].

The performance index used by the gradient estimator is the squared output prediction error:

$$E = \frac{1}{2} \parallel \tilde{Y} \parallel^2. \tag{4.16}$$

The parameters are estimated recursively following the law:

$$\frac{d\hat{p}}{d\theta} = -\Psi_0\Phi^T(\theta_i)\tilde{Y}(\theta_i), \tag{4.17}$$

where $\Psi_0 > 0$ is the descending step (estimator gain) [11, pp. 364–367].

4.3 Simulation Results

We analyzed the performance of the on-line gradient estimator and least-squares with exponential forgetting in comparison with the off-line standard least-squares estimator.

The simulation is performed using the MATLAB package and the code is listed in Appendix B. The main functions are:

- *sls.m* which implements the standard least-squares estimator,
- *itgr.m* which implements the on-line gradient estimator,
- *itls.m* which implements the recursive least-squares estimator with exponential forgetting, and
- *est.m* which calculates the velocity fluctuation using the parameter estimates.

The angular velocity is sampled at a period of $\pi/59$ rad. This sampling period corresponds to the total number of flywheel teeth, 118. The cylinder pressure data is characterized by a sampling period of $\pi/360$ rad. The model parameters are given the same numerical values as in Section 3.3. These are: $N = 6$, $r = 0.0635$ m, $l = 0.2571$ m, $J_{cr} = 0.0745$ kgm^2, $m_p = 6.03$ kg, $A_p = 0.01188$ m^2. The phase origin is the top dead center of the first cylinder to fire, and $\phi_1 = 0$, $\phi_2 = 56.5$, $\phi_3 = 120$, $\phi_4 = 176.5$, $\phi_5 = 240$, $\phi_6 = 296.5$ degrees. The firing order is again: 1L, 3R, 3L, 2R, 2L, 1R. Data acquisition is performed for a nominal speed $\omega_0 = 125.7$ rad/sec $(1,200$ rpm) and a dynamometer torque, $T_l = 990$ Nm. This load represents 75% of the engine peak torque. $T_f = 156$ Nm is the value of the mechanical friction torque corresponding to a crankshaft angular velocity of $\omega_0 = 125.7$ rad/sec and an overall damping coefficient of 1.24 Nmsec.

The parameters to be identified are the engine effective moment of inertia, J_E, which includes the crankshaft and the flywheel moments of inertia, and the torque fluctuation, ΔT. The testing set consists of 6 different actuator faults and the normal operating condition. The actuator fault consists of a 10% drop in cylinder fueling. The estimation is performed for $N_m = 118$ measurements. The effect of the parameter identification procedure is measured using the same criteria as in Section 3.3: the root mean square

Table 4.1: Engine inertia estimates, $\hat{J}_E$, depending on the number of measurements, $N_m = 118$, the engine operating condition (normal or faulty), the identification method: off-line standard least-squares (SLS), on-line gradient estimator (GE), and least-squares with exponential forgetting (LSEF).

Faulty Cylinder	$\hat{J}_E$ (kgm^2)		
	SLS	*GE*	*LSEF*
None	3.86	3.90	3.85
1	4.89	4.90	4.86
2	5.06	5.06	4.97
3	5.17	5.13	5.08
4	5.01	5.04	4.97
5	5.01	5.01	4.97
6	4.96	4.96	4.91

(RMS) error, defined as the standard deviation of the velocity residual and the residual to signal ratio (RSR), defined by the ratio between the standard deviation of the residual and the standard deviation of the actual angular velocity fluctuation. The different engine inertia estimates, $\hat{J}_E$, are illustrated in Table 4.1. Estimates for the other two parameters, $\hat{T}_s$ and $\hat{T}_c$, characterize the harmonic torque fluctuation (see (4.3)). Table 4.2 presents the values $\hat{T}_h$ and $\hat{\gamma}$ (see (4.2)) for different engine conditions.

Figures 4.2 and 4.3 present the estimation results for flywheel angular velocity fluctuation corresponding to two test cases—normal operating condition, and under-fueling fault in cylinder 1R. In the case of normal operation, we used the estimated parameters: $\hat{J}_E = 3.90$ kgm^2 and $\Delta\hat{T} = 60\sin(\theta + 210)$ Nm, obtained with the recursive gradient estimator. The RMS error has a value of 0.0559 rad/sec, which represents approximately 30% improvement over the result reported in Section 3.3. This identification procedure results in a RSR of 27%. This result is put in perspective by the fact that the occurrence of a 10% under-fueling fault in any of the six cylinders results in a RSR value between 55% and 159%. This RSR range is characteristic of a faulty condition. In addition,

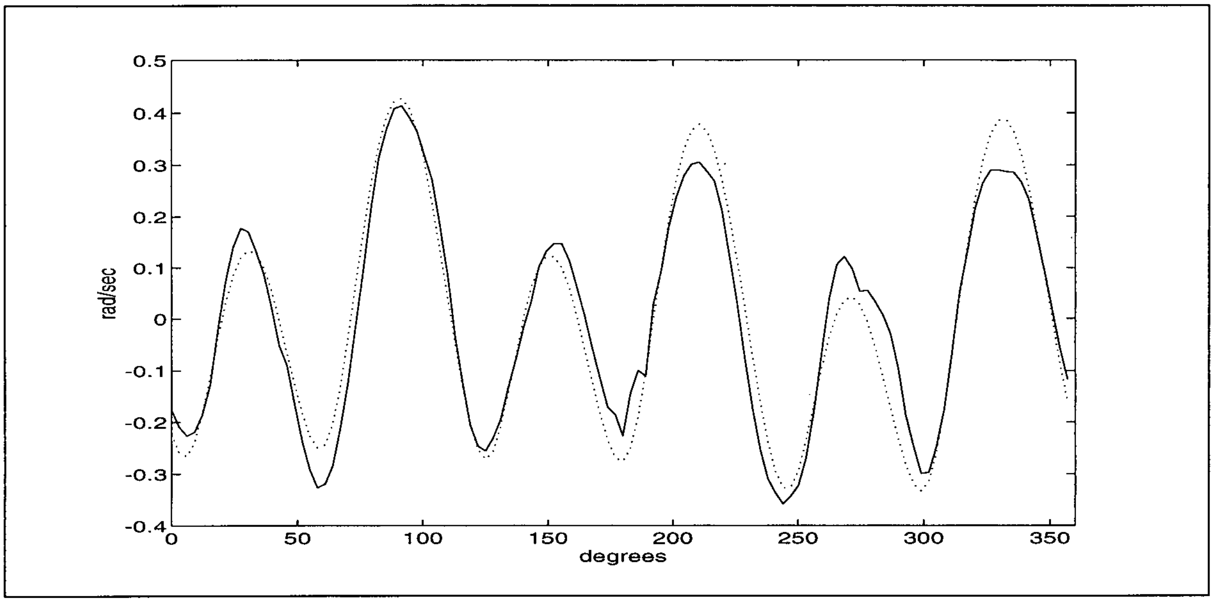

Figure 4.2: Actual (solid line), and the estimated (dashed line) velocity fluctuation during one crankshaft revolution for the normal operation condition. The results correspond to the gradient estimator.

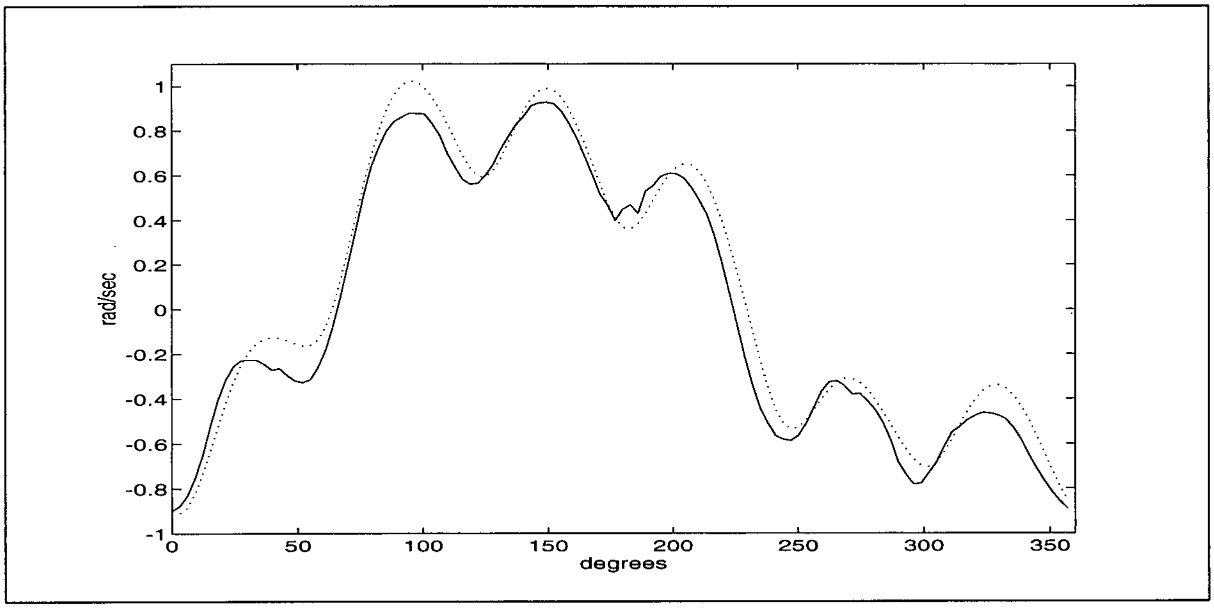

Figure 4.3: Actual (solid line), and estimated (dashed line) velocity fluctuation during one crankshaft revolution corresponding to an under-fueling fault in the first cylinder of the right bank (cylinder 6). The estimation is carried out by the on-line least-squares estimator with exponential forgetting.

Table 4.2: The parameter estimates, $\hat{T}_h$ and $\hat{\gamma}$ for $N_m = 118$. The estimates are obtained using the on-line gradient estimator.

Faulty Cylinder	$\hat{T}_h$ (Nm)	$\hat{\gamma}$ (degrees)
None	60	210
1	600	160
2	540	129
3	520	29
4	700	303
5	800	258
6	700	223

the detection of the faulty condition can be accomplished by observing the change in a parameter's mean and standard deviation. Our experiments show that the under-fueling of cylinder 1L causes a 6% change in the mean, and a 620% increase in the standard deviation of the estimated inertia. This result is obtained using the gradient estimator. For the same case, the least-squares estimator with exponential forgetting indicates a 16% change in the mean and a 327% change in the standard deviation of $\hat{J}_E$.

Table 4.3 illustrates the RSRs for all 6 actuator faults. The RMS error for the case presented in Figure 4.3 is 0.0829 rad/sec. This calculation is carried out using the estimated parameters: $\hat{J}_E = 4.91$ kgm^2 and $\Delta\hat{T} = 700\sin(\theta + 223)$ Nm, obtained from the on-line estimator with exponential forgetting. The prediction of this under-fueling fault is therefore characterized by a RSR of 14% (see Table 4.3). The overall RMS error range for the faulty condition is between 0.0804 and 0.1315 rad/sec. The best results are obtained for faulty conditions in cylinders 3L and 1R.

We considered the problem of fault isolation which deals with the correct classification of an engine cylinder as faulty or not. We considered the case when an under-fueling fault in cylinder 2 (3R) is misclassified as a fault in cylinder 1 (1L). This resulted in a RSR value of 36%, using the gradient estimator. Likewise, similar results were obtained

Table 4.3: Residual to signal ratio (RSR) for the 6 different under-fueling faults.

Faulty Cylinder	RSR (%)
1	20
2	24
3	20
4	13
5	16
6	14

for other misclassified cylinders. Alternatively, large changes in estimated parameter standard deviation can be used for the elimination of this misclassification. The gradient estimator shows a 227% change in the standard deviation of $\hat{J}_E$. The least-squares estimator with exponential forgetting records a 302% change for the same case.

On-line parameter identification methods are powerful tools for increasing the prediction ability of the engine model and, at the same time, can be employed in fault detection and isolation by monitoring parameter estimate changes.

The analytical redundancy provided by the engine model is enhanced further by the study of the inverse dynamics which allows the pressure waveform reconstruction from angular velocity fluctuation. This subject is treated in the next chapter.

Chapter 5

Pressure Waveform Reconstruction

It's here they got the range
and the machinery for change
and it's here they got the spiritual thirst.
Leonard Cohen, Democracy

In this chapter we investigate the procedure for pressure waveform reconstruction using the engine model and angular velocity measurements. This problem has multiple practical applications in engine control and diagnosis. It provides an indirect method for cylinder pressure measurement, and permits the implementation of a technique for estimating the torque due to gas pressure [36, 37, 38, 39] or the power contribution of each cylinder [40], and therefore allows the detection and identification of a variety of cylinder faults [41, 34].

The dynamics of a given system are represented by a collection of differential equations that permit the process output determination using the input history. The term "inverse dynamics" is used to characterize the calculation of the system input given the output history [11, pp. 263]. In our case, the diesel engine model is crank angle based and has N inputs, $u_i(\theta) = P_i(\theta), i = 1, \dots N$, represented by the cylinder pressures. The system output is given by the angular velocity fluctuation, $\delta\omega(\theta)$. Because our model implements a multi-input single output (MISO) system, it is not possible to explicitly decouple the inverse dynamics. We have therefore considered two approaches. First, we redefine the system input and we rewrite the engine model as a single input single output (SISO) system. The new input is then the torque due to gas pressure, $T_p(\theta)$, defined in (3.11) as:

$$T_p(\theta) = A_p r \sum_{i=1}^{N} P_i(\theta) c_1(\theta - \phi_i),$$

where N is the total number of cylinders, A_p is the piston crown area, $P_i(\theta)$ refers to the pressure in the i-th cylinder, ϕ_i is the phase shift corresponding to the i-th firing cylinder, and $c_1(\theta)$ is defined in (3.5) as:

$$c_1(\theta) = \left(1 + \frac{r}{l}\frac{\cos\theta}{\cos\alpha}\right)\sin\theta.$$

Secondly, we approximate the pressure waveform with a periodic impulse-like continuous function. Using this latter template-based approach we are able to explicitly identify the condition of each cylinder.

5.1 Gas Pressure Torque Estimation

The estimation of cylinder power from engine speed fluctuations is considered in [40]. The authors use a linear second order model to describe the relationship between engine speed and crankshaft torque. An inverse filtering technique is employed for pressure torque calculation. The power contribution is determined as the area under this torque curve, corresponding to the power stroke of each cylinder. Similarly, the approach taken in [37] involves a time-based 4 degree-of-freedom vibration model for the system composed by the vibration damper, engine, flywheel, and dynamometer. The authors assume a purely harmonic solution for the crank angle:

$$\theta = \Theta e^{j\omega t},$$

where Θ is the amplitude, and ω is the engine speed. The model is rewritten in the frequency domain as a matrix equation which is then solved for different harmonics of the engine fundamental frequency. The cylinder pressure is determined locally, in the vicinity of the pressure peak. This approach relies on the assumption that each cylinder contributes to the gas pressure torque only during its power stroke. In both these two papers, the engine model is developed in the time domain, and crankshaft/flywheel speed is sampled in the crank angle domain. The authors point out that this inadvertence represents a source of error.

The model used in [39] is written in the crank angle domain. The authors employ a deconvolution technique for the estimation of the pressure torque, $T_p(\theta)$ from noisy measurements of the crankshaft angular acceleration. Their analysis is based on the assumption that the torque fluctuation is concentrated at a frequency equal to the firing frequency. This results in the neglect of higher harmonics.

The solution adopted in [38] employs the design of an estimator in the crank angle domain. The authors use the following relationship to relate the crank angle and time bases: $t = \frac{\theta}{\omega_0}$, where θ is the crank angle, t is the time, and ω_0 is the nominal engine speed. In terms of the Laplace transform ($\mathcal{L}$) this relationship becomes: $s_\theta = \frac{s_t}{\omega_0}$, where s_t, and s_θ describe the Laplace transform variable in the time domain and the crank angle domain, respectively. This is correct under the assumption of constant speed.

A comprehensive analysis of the crank angle domain versus the time domain is reported in [42]. Here the authors model the engine rotational dynamics in the crank angle domain by a first order system characterized by the following transfer function:

$$H(s_\theta) = \frac{\omega(s_\theta)}{T_p(s_\theta)} = \frac{1}{J_E \omega_0 s_\theta + b}$$

where $\omega(s_\theta) = \mathcal{L}\{\omega(\theta)\}$, $T_p(s_\theta) = \mathcal{L}\{T_p(\theta)\}$, J_E is the engine mass moment of inertia, and b is the viscous friction coefficient. The authors point out that the assumption of constant speed introduces a fractional error of $\delta\omega/\omega_0$ due to this approximation for the pole of the transfer function.

A pattern recognition technique used for detection and isolation of faults due to cylinder under-fueling is reported in [34]. The authors constructed classes based on the fault signatures as observed in the flywheel angular velocity fluctuation data. A drawback of this approach is the assumption of reproducibility and linear scaling of the fault signatures with respect to the stored patterns. The method allows the estimation of the pressure peak, but doesn't allow the reconstruction of the actual pressure waveform.

Our diesel engine model was defined in (3.26)–(3.27). The equations are repeated here:

$$\delta x' = A(\theta)\delta x + b^T(\theta)u(\theta) + d(\theta),$$

$$\delta\omega = c(\delta x),$$

where the system coefficients $A(\theta)$, $b(\theta)$, $d(\theta)$, and $c(\delta x)$ were defined in (3.28)–(3.31). The system input is the vector of cylinder pressures:

$$u(\theta) = \begin{bmatrix} P_1(\theta) \\ \vdots \\ P_N(\theta) \end{bmatrix}.$$

By redefining the system input as $u(\theta) = T_p(\theta)$ we obtain the equivalent SISO system:

$$\delta x' = A(\theta)\delta x + b'(\theta)u(\theta) + d(\theta), \tag{5.1}$$

where $b'(\theta)$ is:

$$b'(\theta) = \frac{A_p r}{\frac{1}{2}\left(J_E - J_{cr}c_{33}(\theta) + m_p r^2 c_{11}(\theta)\right)}, \tag{5.2}$$

where A_p is the piston head area, r is the crank radius, m_p is the mass of the reciprocating parts, and J_E and J_{cr} are the mass moments of inertia of the engine and the connecting rod, respectively. The torque coefficient $c_{11}(\theta)$ was defined in (3.14). The system state, δx was defined in (3.24) as:

$$\delta x = \delta\omega(2\omega_0 + \delta\omega) \approx 2\omega_0\delta\omega.$$

Using the approximation we obtain:

$$\hat{u}(\theta) = \hat{T}_p(\theta) = \frac{2\omega_0 \left[\delta\omega'(\theta) + A(\theta)\delta\omega(\theta)\right] - d(\theta)}{b'(\theta)}, \tag{5.3}$$

which allows the estimation of the gas pressure torque using the measurement of angular velocity fluctuation.

5.2 Pressure Waveform Characteristics

Cylinder pressure is uniquely connected to the combustion process. Cycle-by-cycle and cylinder-by-cylinder pressure variations are correlated with the injection timing, the quantity of fuel injected, and the rate of mixing between the injected fuel and the air. The most important pressure-related parameters are: maximum cylinder pressure, the crank angle at which this maximum pressure occurs, the maximum rate of pressure rise, and the corresponding crank angle, and the indicated mean effective pressure (IMEP) [43, pp. 415]. A measure of the pressure cyclic variability is the coefficient of variability (COV) defined in [43, pp. 417]:

$$\mathrm{COV} = \frac{\sigma_{\mathrm{imep}}}{\mathrm{imep}} \times 100,$$

where σ_{imep} is the standard deviation in indicated mean effective pressure. The author asserts that vehicle driveability problems are characterized by a COV$>10\%$.

The cycle-by-cycle variation in cylinder pressure was modeled by a Gaussian probability distribution in [44]. A similar approach was taken in [5]. Here the authors modeled the cyclic pressure variation as a raised-cosine window amplitude-modulated by a white Bernoulli-Gaussian random sequence. The same authors reported their experimental results in [45]. The proposed stochastic model describes the gross pressure waveforms, but doesn't accurately characterize the instantaneous shape of the actual pressure waveforms.

Rather than trying to determine a stochastic description of the cycle-by-cycle and cylinder-by-cylinder pressure variation, our approach is to find a functional approximation for the cylinder pressure waveform, and subsequently relate the pressure variation to a minimum number of parameters. This approach is based on the observation that the cylinder pressure is an impulse-like periodic function. We consider a general description for a family of functions, related to the δ-function, given in [46, pp. 487–492]:

$$\delta(w, z) = \frac{w}{w^2 z^2 + 1} = \frac{d}{dz}\left[\tan^{-1}(wz)\right], \tag{5.4}$$

where $z \in R$, and w is a variable parameter. When $z = \sin\frac{\theta-\phi_i}{2}$, with θ the crank angle, and ϕ_i the phase of the i-th cylinder, the proposed impulse functional approximation for the pressure waveform is:

$$\hat{P}_i(\theta) = k_i\delta\left(w, \sin\frac{\theta-\phi_i}{2}\right) - P_0 = \frac{P_i^{\max}}{w^2\sin^2\frac{\theta-\phi_i}{2} + 1} - P_0\,, \tag{5.5}$$

where $P_i^{\max} = k_i w$ represents the maximum pressure value, $k_i > 0$ is a factor related to the pulse height, $w > 0$ is inversely proportional to the width of the pressure pulse, and P_0 is a pressure offset.

Taking into consideration (5.3), and (5.5), we can write the estimated gas pressure torque in a form similar to (3.11):

$$\hat{T}_p(\theta) = A_p r \sum_{i=1}^{N} \delta P_i \hat{P}_i(\theta) c_1(\theta - \phi_i), \tag{5.6}$$

where $\delta P_i, i = 1, \ldots N$ are parameters that describe the pressure variation with respect to the template given by $\hat{P}_i(\theta)$. The estimation of these parameters allows us to determine the condition of each cylinder (faulty or not). The standard least-squares estimator is:

$$\delta\hat{P} = (\Phi^T\Phi)^{-1}\Phi^T\hat{T}_p, \tag{5.7}$$

$$\hat{T}_p = \Phi\delta\hat{P}, \tag{5.8}$$

where

$$\delta\hat{P} = \begin{bmatrix} \delta\hat{P}_1 \\ \vdots \\ \delta\hat{P}_N \end{bmatrix},$$

and

$$\Phi = A_p r \left[\hat{P}_1(\theta)c_1(\theta - \phi_1), \quad \ldots, \quad \hat{P}_N(\theta)c_1(\theta - \phi_N)\right].$$

We analyzed the use of the engine model in solving the inverse dynamics, and thus providing an estimate for the torque due to gas pressure. We investigated a meaningful procedure for pressure waveform reconstruction based on the functional approximation introduced in (5.5). We are able to detect and isolate cylinder under-fueling faults using a standard least-squares identification method. The steps of our procedure can be summarized as follows:

1. Calculate the derivative $\delta\omega'$, using the measured angular velocity fluctuation, $\delta\omega$.

2. Calculate the initial estimated pressure torque, $\hat{T}_p$, using (5.3).

3. Obtain the least-squares estimates of the pressure variations, $\delta\hat{P}_i$, using (5.5) and (5.7).

4. Determine the new estimate of the gas pressure torque, $\hat{T}_p$, using (5.8).

5. Reconstruct the cylinder pressure waveforms using (5.5) and (5.7).

5.3 Simulation Methods

The simulation is performed with the MATLAB package and the programs are listed in Appendix B. The main functions are:

- *diffc.m* which implements a smooth differentiator,

- *tpe.m* which implements (5.3),
- *dlt.m* which implements (5.5), and
- *pwr.m* which calculates the pressure variation vector, $\delta\hat{P}$.

The angular velocity is sampled at a period of $\pi/59$ rad. This sampling period corresponds to the total number of flywheel teeth, 118. The cylinder pressure data is characterized by a sampling period of $\pi/360$ rad. The model parameters are given the same numerical values as in Sections 3.3 and 4.3. These are: $N = 6$, $r = 0.0635$ m, $l = 0.2571$ m, $J_{cr} = 0.0745$ kgm^2, $m_p = 6.03$ kg, $A_p = 0.01188$ m^2. The phase origin is the top dead center of the first cylinder to fire, and $\phi_1 = 0$, $\phi_2 = 56.5$, $\phi_3 = 120$, $\phi_4 = 176.5$, $\phi_5 = 240$, $\phi_6 = 296.5$ degrees. The firing order is again: 1L, 3R, 3L, 2R, 2L, 1R. Data acquisition is performed for a nominal speed $\omega_0 = 125.7$ rad/sec $(1,200$ rpm) and a dynamometer torque, $T_l = 990$ Nm. This load represents 75% of the engine peak torque. $T_f = 156$ Nm is the value of the mechanical friction torque corresponding to a crankshaft angular velocity of $\omega_0 = 125.7$ rad/sec and an overall damping coefficient of 1.24 Nmsec.

5.3.1 Torque Estimation and Pressure Approximation

The testing set consists of 6 different actuator faults and the normal operating condition. The actuator fault consists of a 10% drop in cylinder fueling. The root mean square (RMS) error is defined as the standard deviation of the torque residual, $\tilde{T}_p = T_p - \hat{T}_p$:

$$\text{RMS torque error} = \sqrt{\frac{\int_0^{2\pi} \left(\tilde{T}_p(\theta)\right)^2 d\theta}{2\pi}}. \tag{5.9}$$

The gas pressure torque is estimated from (5.3). The residual to signal ratio (RSR) is:

$$\text{RSR} = \frac{\text{RMS error}}{\sigma(T_p)} 100\%, \tag{5.10}$$

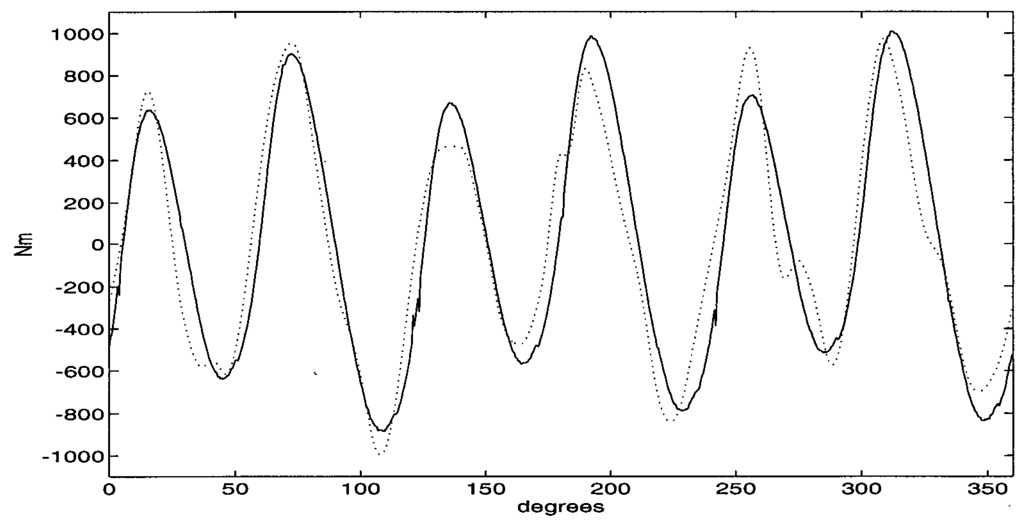

Figure 5.1: Actual (solid line), and the estimated (dashed line) gas pressure torque fluctuation during one crankshaft revolution for the normal operation condition.

where $\sigma(T_p)$ is the standard deviation of the actual gas pressure torque. The same performance indicators are used to assess the magnitude of the pressure residual, $\tilde{P} = P - \hat{P}$.

Figures 5.1 and 5.2 present the estimated gas pressure torque, $\hat{T}_p(\theta)$, corresponding to two test cases—normal operating condition, and an under-fueling fault in cylinder 1R. The results are obtained after the elimination of the harmonic torque fluctuation, $\Delta T = T_h \sin(\theta + \gamma)$, where T_h is the amplitude of the torque fluctuation, and γ is the phase (see Chapter 4). In the case of normal operation (see Figure 5.1), the engine moment of inertia is $J_E = 3.85$ kgm^2, and the mean value for the gas pressure torque is $\bar{T}_p = 856$ Nm. The resulting RMS error has a value of 196.2 Nm, which corresponds to a RSR of 35%. In the case of an under-fueling fault in cylinder 1R (see Figure 5.2), the engine moment of inertia is $J_E = 5$ kgm^2, and the mean value for the gas pressure torque is $\bar{T}_p = 1215$ Nm. The resulting RMS error has a value of 271.4 Nm, which corresponds

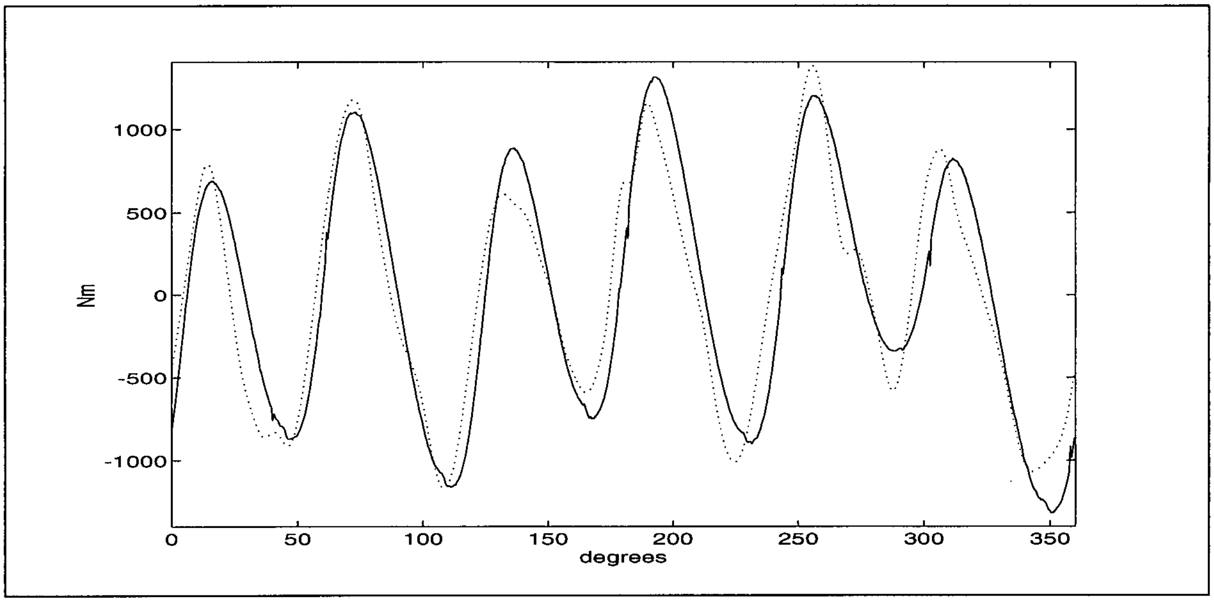

Figure 5.2: Actual (solid line), and estimated (dashed line) gas pressure torque fluctuation during one crankshaft revolution corresponding to an under-fueling fault in the first cylinder of the right bank (cylinder 6).

to a RSR of 38%. The gas pressure torque for the faulty operation is estimated by a RMS torque error range of 271.4 Nm to 308.7 Nm, which corresponds to a RSR range of 38% and 43%. The worst results are associated with a fault in cylinder 2L. The best results are obtained for an under-fueling fault in cylinder 1R.

Figure 5.3 illustrates the actual and the estimated pressure waveform for the normal operation of cylinder 3L. We used (5.5) and the following values: $P_3^{\max} = 11.8$ MPa, $w = 5.5$, and $P_0 = 0.5$ MPa for the approximation of $\hat{P}_3(\theta)$. The RMS pressure error is 0.149 MPa. This corresponds to a RSR of 5%. For the normal operating condition, this functional approximation is characterized by a RMS pressure error range of 0.145 MPa to 0.177 MPa, which corresponds to a RSR range of 5% to 6%. The smallest error is obtained for cylinder 1L.

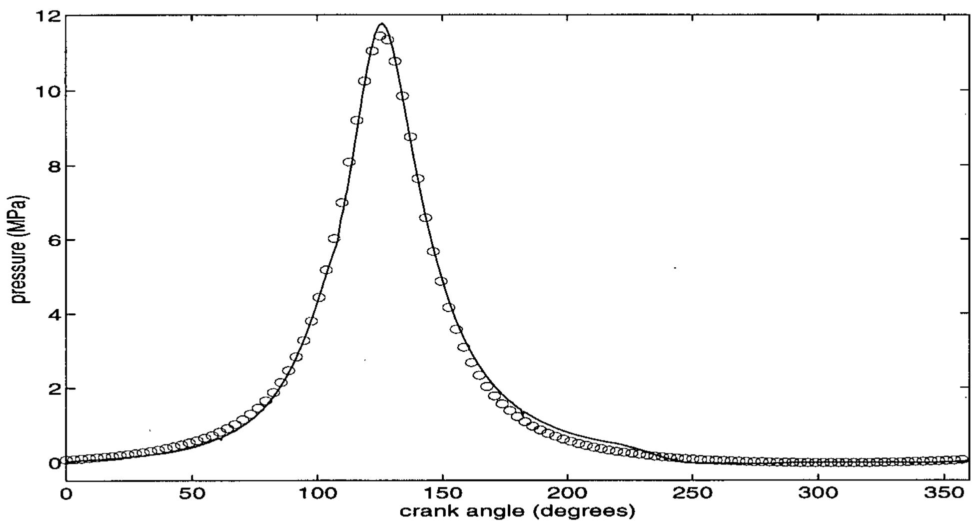

Figure 5.3: Illustrates a typical cylinder pressure waveform (solid line) and its approximation (circles) as per (5.5). The phase corresponds to the third firing cylinder.

5.3.2 Fault Detection and Isolation Results

We considered the problem of fault detection and isolation. The procedure uses 6 pressure templates determined by taking into consideration each cylinder firing phase, ϕ_i. All the 6 pressure waveforms are characterized by (5.5) with the same values $P_i^{\max} = P^{\max} = 11$ MPa, and $w_i = w = 5.5$, $i = 1, \ldots 6$. The estimated parameters, $\delta \hat{P}_i$ are obtained using a standard least-squares technique, and their values are presented in Table 5.1. An underfueling fault in the i-th firing cylinder can be determined exactly by the value of the estimated pressure variation, $\delta \hat{P}_i$ using the decision rule:

$$\delta \hat{P}_i = \min_{k=1,\ldots 6} \delta \hat{P}_k. \tag{5.11}$$

This detection problem can be formulated also from the perspective of the Bayes classifier [47, pp. 221–233].

The two classes are determined from the estimates presented in Table 5.1: *faulty cylinder*, which corresponds to a mean pressure variation, $\delta \bar{p}_f = 0.83$ MPa, and *healthy*

Table 5.1: Estimated pressure variation parameters, $\delta\hat{P}_i$ (MPa) for the normal condition, and the 6 different under-fueling faults using the impulse like template described by (5.5).

Faulty Cylinder	$\delta\hat{P}_1$	$\delta\hat{P}_2$	$\delta\hat{P}_3$	$\delta\hat{P}_4$	$\delta\hat{P}_5$	$\delta\hat{P}_6$
None	1.01	1.09	1.09	1.10	1.15	1.06
1	**0.78**	1.05	1.08	1.11	1.10	0.93
2	0.90	**0.79**	1.03	1.09	1.14	0.95
3	0.96	0.89	**0.80**	0.96	1.16	1.07
4	1.05	1.04	0.95	**0.87**	1.10	1.02
5	1.01	1.10	1.02	0.99	**0.93**	0.99
6	0.97	1.10	1.07	1.05	1.07	**0.78**

cylinder, which corresponds to a mean pressure variation, $\delta\bar{p}_h = 1.04$ MPa. The noise is assumed Gaussian with zero mean and a calculated standard deviation of $\sigma_n = 0.07$. If the data is assumed Gaussian, 95% of the estimated pressure variation samples, $\delta\hat{P}_i$ lie within $\pm 2\sigma_n$ of the mean estimate, $\delta\bar{p}_h$:

$$0.9 < \delta\hat{P}_i < 1.18.$$

Large changes in the value of the estimated parameter can be used for the detection and isolation of the faulty engine cylinder. For example, a fault in the first firing cylinder (1L) results in a 23% decrease in $\delta\hat{P}_1$, and a fault in the second firing cylinder (3R) results in a 28% decrease in $\delta\hat{P}_2$.

Under-fueling faults are thus uniquely determined by the values of the estimated pressure variation, $\delta\hat{P}_i, i = 1, \ldots 6$. The same parameter allows the reconstruction of the cylinder pressure waveform by correcting the value of $P_i^{\max}$ initially assigned in (5.5):

$$P_i^{\max} = \delta\hat{P}_i P^{\max}. \tag{5.12}$$

The pressure waveform reconstruction is characterized by a RMS pressure error range of 0.155 MPa to 0.277 MPa for the normal operating condition. This corresponds to a RSR range of 5% to 10%.

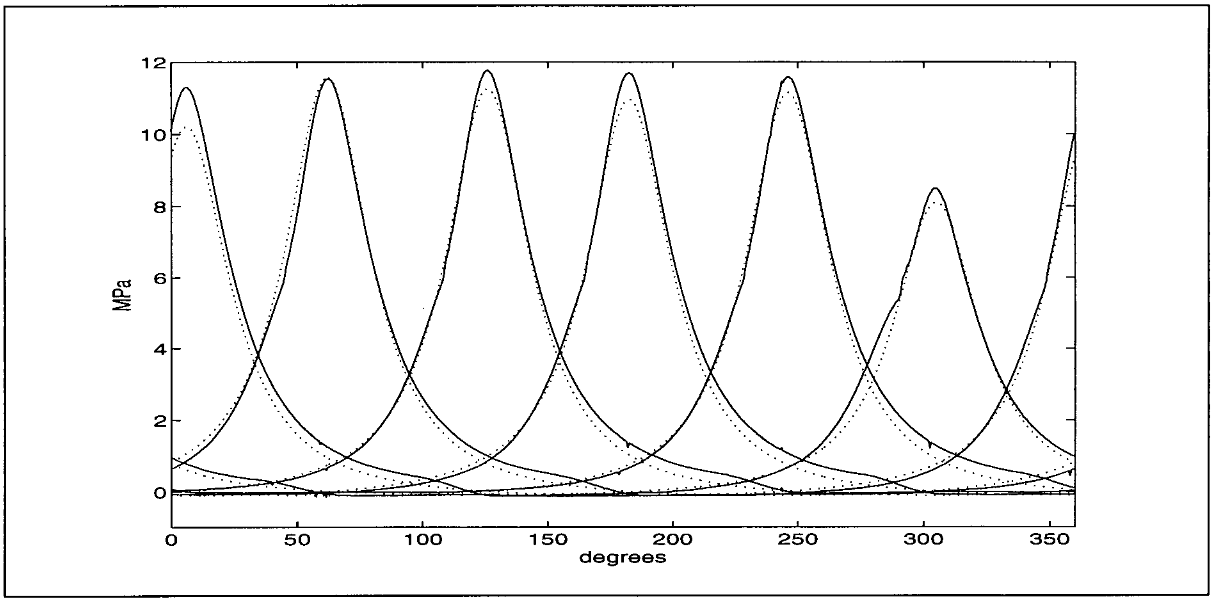

Figure 5.4: Actual (solid line), and estimated (dashed line) gas pressure waveform during one crankshaft revolution corresponding to an under-fueling fault in cylinder 1R.

For each of the six under-fueling faults, the pressure waveform corresponding to the faulty cylinder is reconstructed. The RMS error range is of 0.155 MPa to 0.386 MPa. The corresponding RSR range is 7% and 18%.

The best results (RSR from 5% to 9%) are obtained in the case of an under-fueling fault in the six firing cylinder (1R). This situation is illustrated in Figure 5.4. Using this correction (see (5.12)) we are also able to improve the estimation of the gas pressure torque, $\hat{T}_p(\theta)$. The new estimate is plotted in Figure 5.5, for the normal operation. The RMS torque error is reduced to 99.24 Nm, and this corresponds to a RSR of 14%.

The case of an under-fueling fault in cylinder 1R is illustrated in Figure 5.6. The RMS torque error reduces to 85.7 Nm, and the RSR is 12%.

These results are compatible with those reported in [34] for the calculation of only the peak cylinder pressure. Our procedure has the advantage that the overall pressure waveform can be reconstructed using (5.5) and the correction (5.12). This approach is

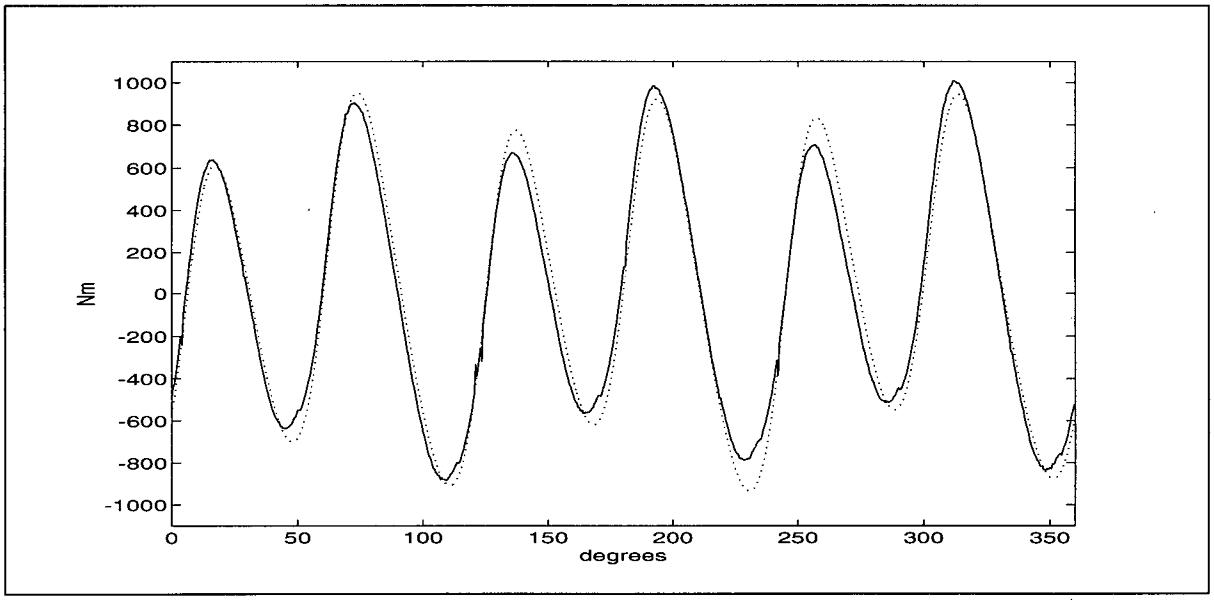

Figure 5.5: Actual (solid line), and the estimated (dashed line) gas pressure torque during one crankshaft revolution for the normal operating condition, using the correction described in (5.12).

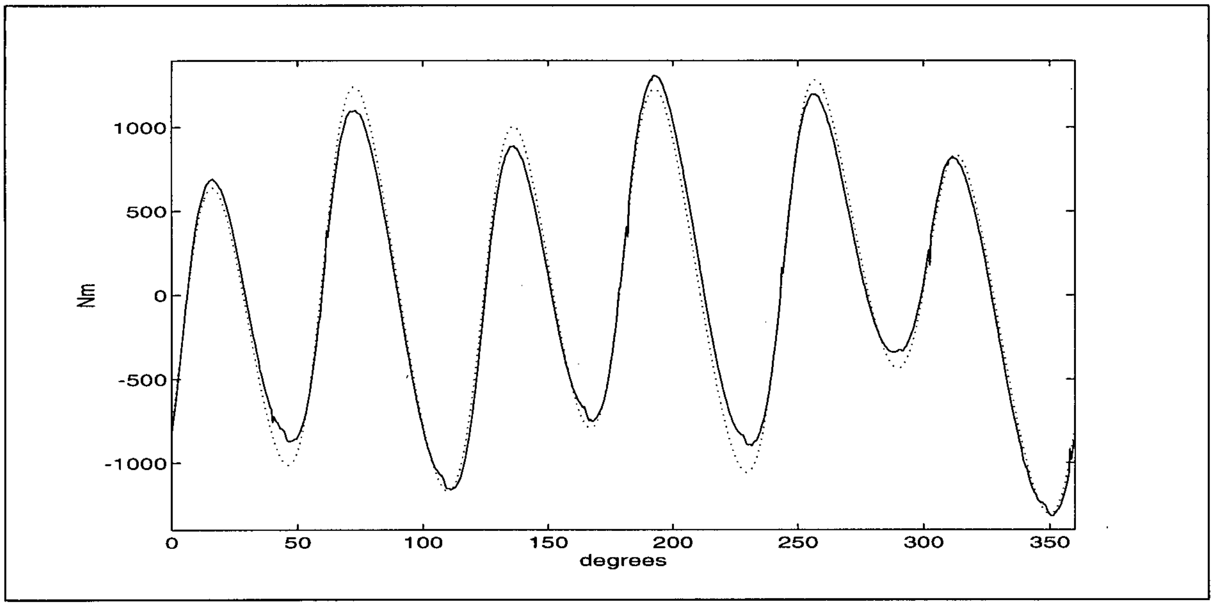

Figure 5.6: Actual (solid line), and estimated (dashed line) gas pressure torque during one crankshaft revolution corresponding to an under-fueling fault in cylinder 1R, taking into consideration (5.12)

simpler and less computationally demanding than the stochastic techniques reported in [5, 44].

Chapter 6

Summary, Discussion, and Conclusions

What we call the beginning is often the end
And to make an end is to make a beginning
The end is where we start from.
T. S. Eliot, Little Gidding

The concept of analytical redundancy emphasizes the use of accurate dynamic and static models for data processing and analysis. The major benefit is realized in the low cost and flexibility of a software implementation versus a hardware implementation. A combination of analytical and physical redundancy is almost always necessary for a fault-tolerant system to maintain its function in the presence of certain failures. On the other hand, the paradigm of analytical redundancy has the advantage of fully exploiting the engine model and thus extracting information that otherwise might be difficult to obtain. This was the motivation for pursuing three directions of investigation: engine modeling and validation, parameter identification, and pressure waveform reconstruction.

Chapter 2 established a global framework for our analysis. The field of model-based fault detection and isolation was linked to the problem of system state and parameter identification. The latter option, parametric identification, was pursued in our study because of its ability to detect early system faults.

where

$$\delta\hat{P} = \begin{bmatrix} \delta\hat{P}_1 \\ \vdots \\ \delta\hat{P}_N \end{bmatrix},$$

and

$$\Phi = A_p r \left[\hat{P}_1(\theta)c_1(\theta - \phi_1), \quad \ldots, \quad \hat{P}_N(\theta)c_1(\theta - \phi_N)\right].$$

We analyzed the use of the engine model in solving the inverse dynamics, and thus providing an estimate for the torque due to gas pressure. We investigated a meaningful procedure for pressure waveform reconstruction based on the functional approximation introduced in (5.5). We are able to detect and isolate cylinder under-fueling faults using a standard least-squares identification method. The steps of our procedure can be summarized as follows:

1. Calculate the derivative $\delta\omega'$, using the measured angular velocity fluctuation, $\delta\omega$.
2. Calculate the initial estimated pressure torque, $\hat{T}_p$, using (5.3).
3. Obtain the least-squares estimates of the pressure variations, $\delta\hat{P}_i$, using (5.5) and (5.7).
4. Determine the new estimate of the gas pressure torque, $\hat{T}_p$, using (5.8).
5. Reconstruct the cylinder pressure waveforms using (5.5) and (5.7).

5.3 Simulation Methods

The simulation is performed with the MATLAB package and the programs are listed in Appendix B. The main functions are:

- *diffc.m* which implements a smooth differentiator,

- *tpe.m* which implements (5.3),
- *dlt.m* which implements (5.5), and
- *pwr.m* which calculates the pressure variation vector, $\delta \hat{P}$.

The angular velocity is sampled at a period of $\pi/59$ rad. This sampling period corresponds to the total number of flywheel teeth, 118. The cylinder pressure data is characterized by a sampling period of $\pi/360$ rad. The model parameters are given the same numerical values as in Sections 3.3 and 4.3. These are: $N = 6$, $r = 0.0635$ m, $l = 0.2571$ m, $J_{cr} = 0.0745$ kgm^2, $m_p = 6.03$ kg, $A_p = 0.01188$ m^2. The phase origin is the top dead center of the first cylinder to fire, and $\phi_1 = 0$, $\phi_2 = 56.5$, $\phi_3 = 120$, $\phi_4 = 176.5$, $\phi_5 = 240$, $\phi_6 = 296.5$ degrees. The firing order is again: 1L, 3R, 3L, 2R, 2L, 1R. Data acquisition is performed for a nominal speed $\omega_0 = 125.7$ rad/sec (1,200 rpm) and a dynamometer torque, $T_l = 990$ Nm. This load represents 75% of the engine peak torque. $T_f = 156$ Nm is the value of the mechanical friction torque corresponding to a crankshaft angular velocity of $\omega_0 = 125.7$ rad/sec and an overall damping coefficient of 1.24 Nmsec.

5.3.1 Torque Estimation and Pressure Approximation

The testing set consists of 6 different actuator faults and the normal operating condition. The actuator fault consists of a 10% drop in cylinder fueling. The root mean square (RMS) error is defined as the standard deviation of the torque residual, $\tilde{T}_p = T_p - \hat{T}_p$:

$$\text{RMS torque error} = \sqrt{\frac{\int_0^{2\pi} \left(\tilde{T}_p(\theta)\right)^2 d\theta}{2\pi}}. \tag{5.9}$$

The gas pressure torque is estimated from (5.3). The residual to signal ratio (RSR) is:

$$\text{RSR} = \frac{\text{RMS error}}{\sigma(T_p)} 100\%, \tag{5.10}$$

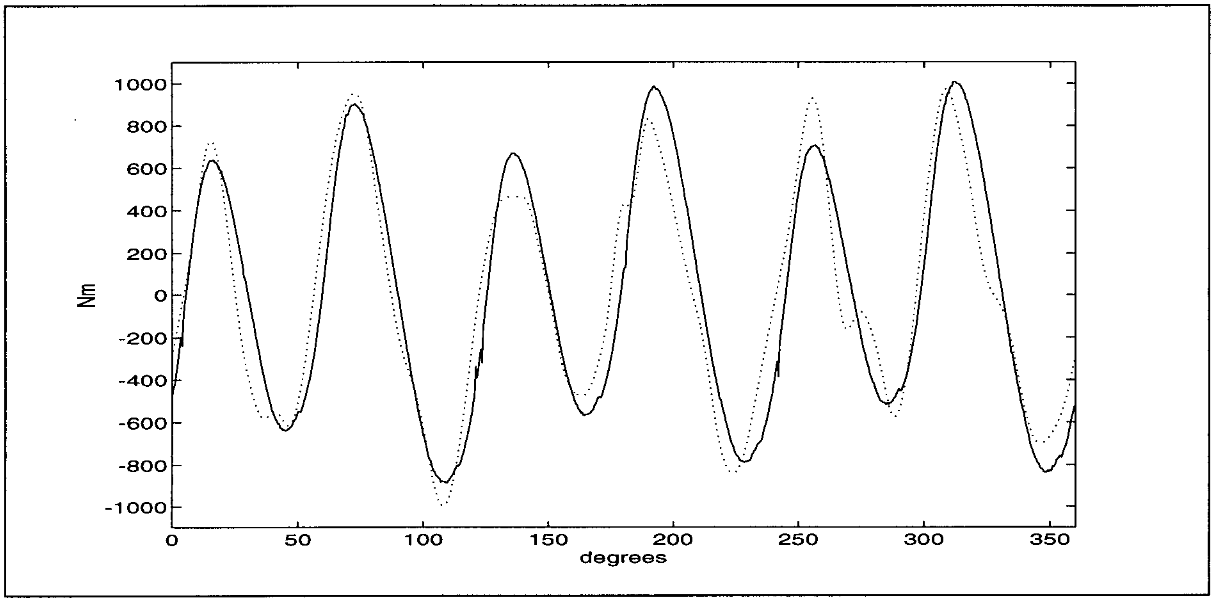

Figure 5.1: Actual (solid line), and the estimated (dashed line) gas pressure torque fluctuation during one crankshaft revolution for the normal operation condition.

where $\sigma(T_p)$ is the standard deviation of the actual gas pressure torque. The same performance indicators are used to assess the magnitude of the pressure residual, $\tilde{P} = P - \hat{P}$.

Figures 5.1 and 5.2 present the estimated gas pressure torque, $\hat{T}_p(\theta)$, corresponding to two test cases—normal operating condition, and an under-fueling fault in cylinder 1R. The results are obtained after the elimination of the harmonic torque fluctuation, $\Delta T = T_h \sin(\theta + \gamma)$, where T_h is the amplitude of the torque fluctuation, and γ is the phase (see Chapter 4). In the case of normal operation (see Figure 5.1), the engine moment of inertia is $J_E = 3.85$ kgm^2, and the mean value for the gas pressure torque is $\bar{T}_p = 856$ Nm. The resulting RMS error has a value of 196.2 Nm, which corresponds to a RSR of 35%. In the case of an under-fueling fault in cylinder 1R (see Figure 5.2), the engine moment of inertia is $J_E = 5$ kgm^2, and the mean value for the gas pressure torque is $\bar{T}_p = 1215$ Nm. The resulting RMS error has a value of 271.4 Nm, which corresponds

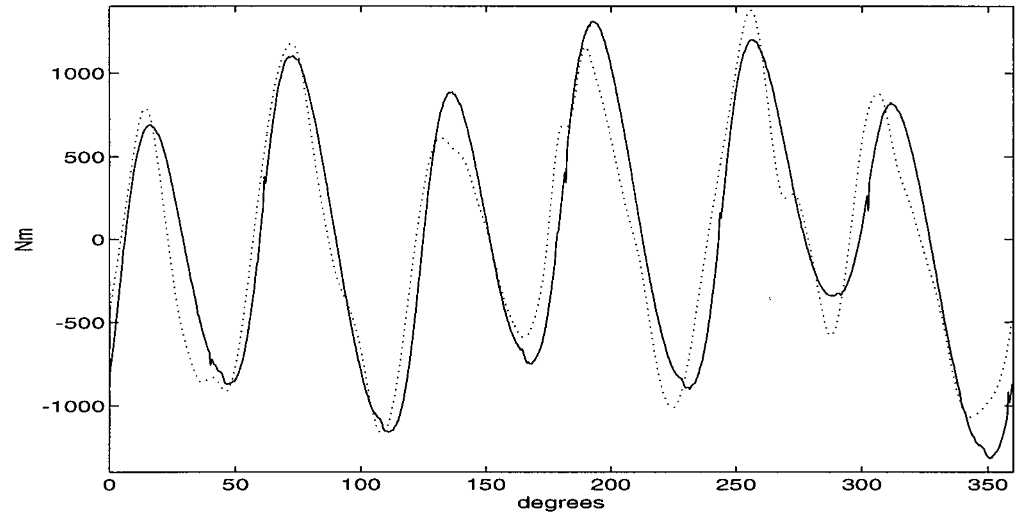

Figure 5.2: Actual (solid line), and estimated (dashed line) gas pressure torque fluctuation during one crankshaft revolution corresponding to an under-fueling fault in the first cylinder of the right bank (cylinder 6).

to a RSR of 38%. The gas pressure torque for the faulty operation is estimated by a RMS torque error range of 271.4 Nm to 308.7 Nm, which corresponds to a RSR range of 38% and 43%. The worst results are associated with a fault in cylinder 2L. The best results are obtained for an under-fueling fault in cylinder 1R.

Figure 5.3 illustrates the actual and the estimated pressure waveform for the normal operation of cylinder 3L. We used (5.5) and the following values: $P_3^{\max} = 11.8$ MPa, $w = 5.5$, and $P_0 = 0.5$ MPa for the approximation of $\hat{P}_3(\theta)$. The RMS pressure error is 0.149 MPa. This corresponds to a RSR of 5%. For the normal operating condition, this functional approximation is characterized by a RMS pressure error range of 0.145 MPa to 0.177 MPa, which corresponds to a RSR range of 5% to 6%. The smallest error is obtained for cylinder 1L.

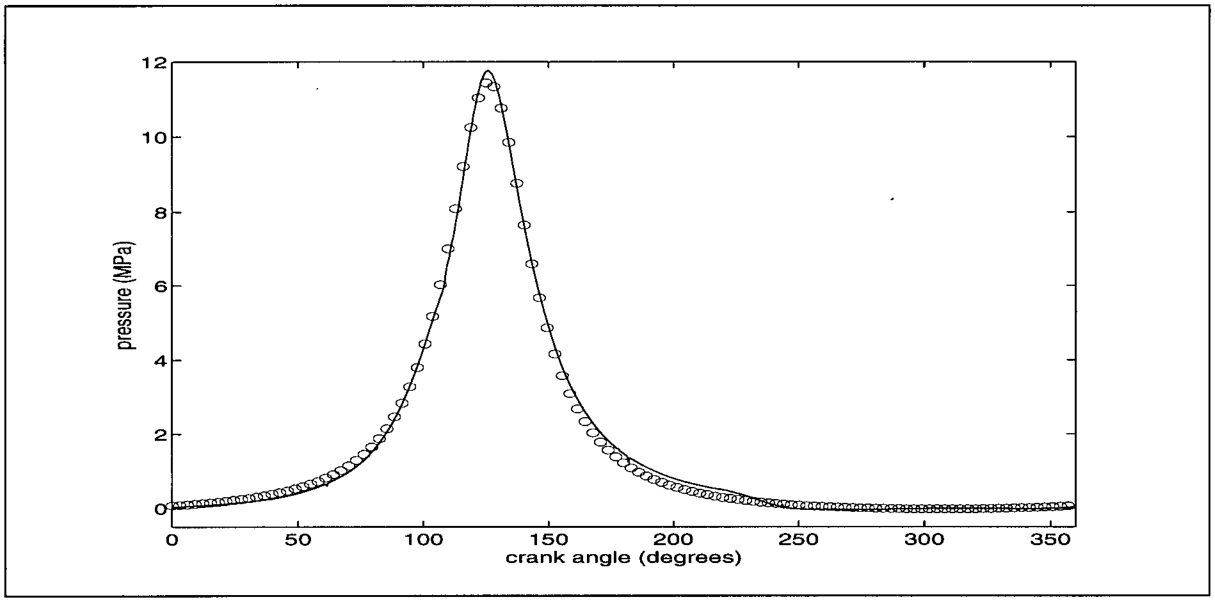

Figure 5.3: Illustrates a typical cylinder pressure waveform (solid line) and its approximation (circles) as per (5.5). The phase corresponds to the third firing cylinder.

5.3.2 Fault Detection and Isolation Results

We considered the problem of fault detection and isolation. The procedure uses 6 pressure templates determined by taking into consideration each cylinder firing phase, ϕ_i. All the 6 pressure waveforms are characterized by (5.5) with the same values $P_i^{\max} = P^{\max} = 11$ MPa, and $w_i = w = 5.5$, $i = 1, \dots 6$. The estimated parameters, $\delta\hat{P}_i$ are obtained using a standard least-squares technique, and their values are presented in Table 5.1. An under-fueling fault in the i-th firing cylinder can be determined exactly by the value of the estimated pressure variation, $\delta\hat{P}_i$ using the decision rule:

$$\delta\hat{P}_i = \min_{k=1,\dots 6} \delta\hat{P}_k. \tag{5.11}$$

This detection problem can be formulated also from the perspective of the Bayes classifier [47, pp. 221–233].

The two classes are determined from the estimates presented in Table 5.1: *faulty cylinder*, which corresponds to a mean pressure variation, $\delta\bar{p}_f = 0.83$ MPa, and *healthy*

Table 5.1: Estimated pressure variation parameters, $\delta\hat{P}_i$ (MPa) for the normal condition, and the 6 different under-fueling faults using the impulse like template described by (5.5).

Faulty Cylinder	$\delta\hat{P}_1$	$\delta\hat{P}_2$	$\delta\hat{P}_3$	$\delta\hat{P}_4$	$\delta\hat{P}_5$	$\delta\hat{P}_6$
None	1.01	1.09	1.09	1.10	1.15	1.06
1	**0.78**	1.05	1.08	1.11	1.10	0.93
2	0.90	**0.79**	1.03	1.09	1.14	0.95
3	0.96	0.89	**0.80**	0.96	1.16	1.07
4	1.05	1.04	0.95	**0.87**	1.10	1.02
5	1.01	1.10	1.02	0.99	**0.93**	0.99
6	0.97	1.10	1.07	1.05	1.07	**0.78**

cylinder, which corresponds to a mean pressure variation, $\delta\bar{p}_h = 1.04$ MPa. The noise is assumed Gaussian with zero mean and a calculated standard deviation of $\sigma_n = 0.07$. If the data is assumed Gaussian, 95% of the estimated pressure variation samples, $\delta\hat{P}_i$ lie within $\pm 2\sigma_n$ of the mean estimate, $\delta\bar{p}_h$:

$$0.9 < \delta\hat{P}_i < 1.18.$$

Large changes in the value of the estimated parameter can be used for the detection and isolation of the faulty engine cylinder. For example, a fault in the first firing cylinder (1L) results in a 23% decrease in $\delta\hat{P}_1$, and a fault in the second firing cylinder (3R) results in a 28% decrease in $\delta\hat{P}_2$.

Under-fueling faults are thus uniquely determined by the values of the estimated pressure variation, $\delta\hat{P}_i, i = 1, \ldots 6$. The same parameter allows the reconstruction of the cylinder pressure waveform by correcting the value of $P_i^{\max}$ initially assigned in (5.5):

$$P_i^{\max} = \delta\hat{P}_i P^{\max}. \tag{5.12}$$

The pressure waveform reconstruction is characterized by a RMS pressure error range of 0.155 MPa to 0.277 MPa for the normal operating condition. This corresponds to a RSR range of 5% to 10%.

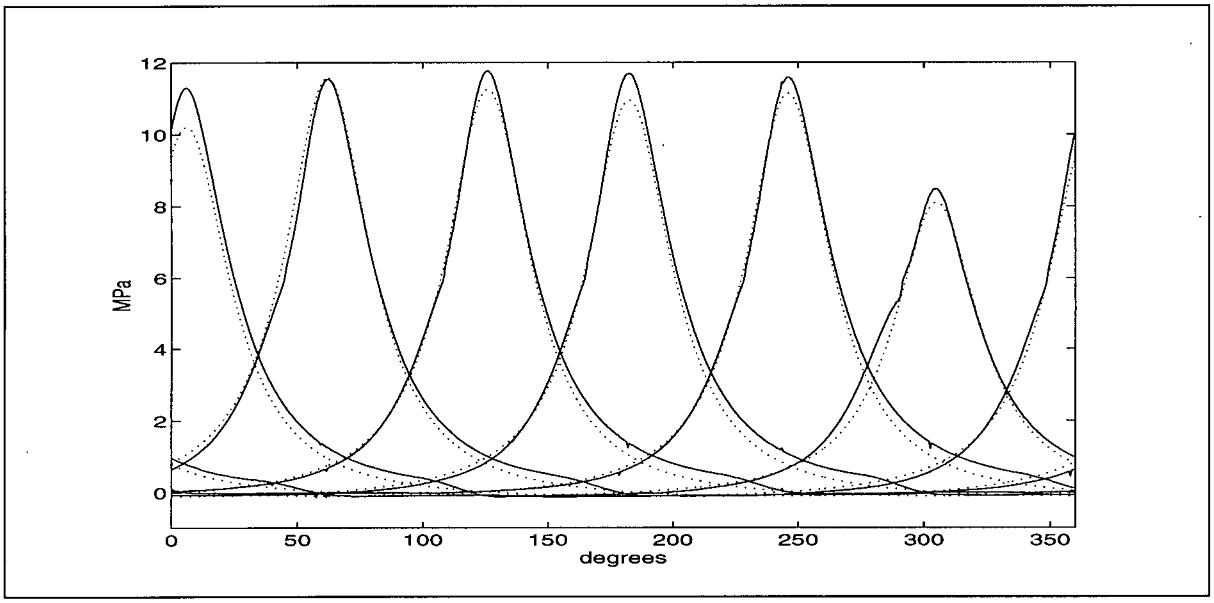

Figure 5.4: Actual (solid line), and estimated (dashed line) gas pressure waveform during one crankshaft revolution corresponding to an under-fueling fault in cylinder 1R.

For each of the six under-fueling faults, the pressure waveform corresponding to the faulty cylinder is reconstructed. The RMS error range is of 0.155 MPa to 0.386 MPa. The corresponding RSR range is 7% and 18%.

The best results (RSR from 5% to 9%) are obtained in the case of an under-fueling fault in the six firing cylinder (1R). This situation is illustrated in Figure 5.4. Using this correction (see (5.12)) we are also able to improve the estimation of the gas pressure torque, $\hat{T}_p(\theta)$. The new estimate is plotted in Figure 5.5, for the normal operation. The RMS torque error is reduced to 99.24 Nm, and this corresponds to a RSR of 14%.

The case of an under-fueling fault in cylinder 1R is illustrated in Figure 5.6. The RMS torque error reduces to 85.7 Nm, and the RSR is 12%.

These results are compatible with those reported in [34] for the calculation of only the peak cylinder pressure. Our procedure has the advantage that the overall pressure waveform can be reconstructed using (5.5) and the correction (5.12). This approach is

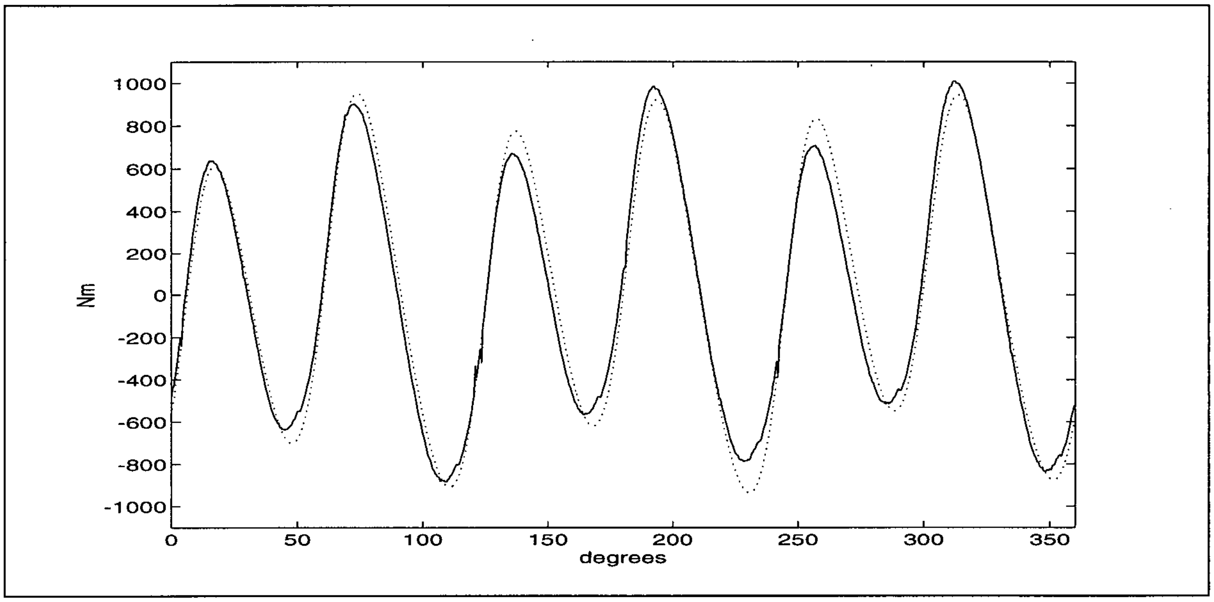

Figure 5.5: Actual (solid line), and the estimated (dashed line) gas pressure torque during one crankshaft revolution for the normal operating condition, using the correction described in (5.12).

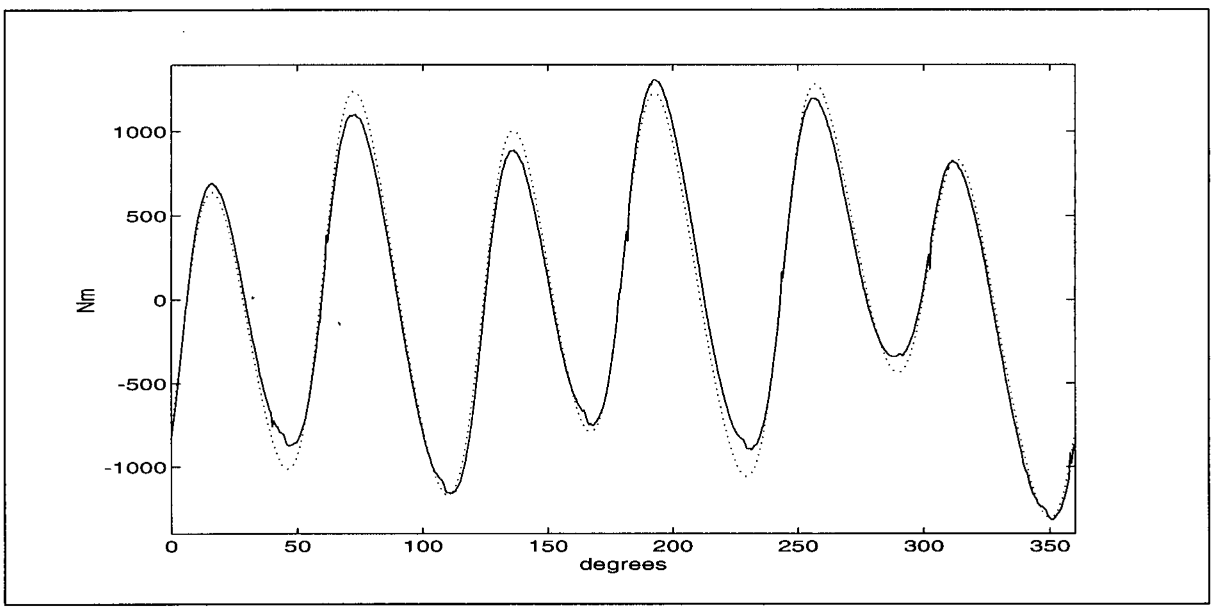

Figure 5.6: Actual (solid line), and estimated (dashed line) gas pressure torque during one crankshaft revolution corresponding to an under-fueling fault in cylinder 1R, taking into consideration (5.12)

simpler and less computationally demanding than the stochastic techniques reported in [5, 44].

Chapter 6

Summary, Discussion, and Conclusions

What we call the beginning is often the end
And to make an end is to make a beginning
The end is where we start from.
T. S. Eliot, Little Gidding

The concept of analytical redundancy emphasizes the use of accurate dynamic and static models for data processing and analysis. The major benefit is realized in the low cost and flexibility of a software implementation versus a hardware implementation. A combination of analytical and physical redundancy is almost always necessary for a fault-tolerant system to maintain its function in the presence of certain failures. On the other hand, the paradigm of analytical redundancy has the advantage of fully exploiting the engine model and thus extracting information that otherwise might be difficult to obtain. This was the motivation for pursuing three directions of investigation: engine modeling and validation, parameter identification, and pressure waveform reconstruction.

Chapter 2 established a global framework for our analysis. The field of model-based fault detection and isolation was linked to the problem of system state and parameter identification. The latter option, parametric identification, was pursued in our study because of its ability to detect early system faults.

6.1 Modeling and Validation

The model we developed in Chapter 3 was configured to correspond to the DDC 6V 92TA Detroit Diesel engine. The analytical methodology followed that of C. F. Taylor [28, pp. 240–305], and the testing was performed using data supplied by the Institute for Machinery Research, National Research Council. The system inputs were given by cylinder combustion pressures, and its output is represented by the flywheel angular velocity fluctuation. Both are expressed as functions of the crank angle. A drawback of our modeling technique derives from the assumptions that the crankshaft is perfectly rigid and the engine operates at steady state. This was compensated by the accuracy of the model which, after a change of state variable, is a first order linear θ-variant multi-input single output system.

The diesel engine model was validated using the MATLAB simulation package, and its effectiveness was measured by the root mean square (RMS) error, and the residual to signal ratio (RSR). The use of an unified performance index allowed us to assess each method using a similar scale, and thus provided the first step towards the integration of these three techniques in a condition monitoring system.

6.2 Parameter Identification

The prediction capability of the model was improved via a parametric identification procedure in Chapter 4. The estimated parameters were the engine mass moment of inertia, and the harmonic torque fluctuation, which we attributed to the crankshaft vibration and oscillatory behaviour of the dynamometer loading. The estimation of this unmodeled torque reduced the error created by those modeling assumptions.

We used three identification methods: off-line standard least-squares, on-line gradient estimator, and recursive least-squares with exponential forgetting. The results obtained were similar with these three methods. For the normal operation we obtained an estimated engine inertias between 3.85 kgm^2 and 3.90 kgm^2. For the six fault conditions, the estimated engine inertia had values between 4.88 kgm^2 and 5.17 kgm^2. In the case of cylinder under-fueling faults, the amplitude of the estimated torque fluctuation is approximately 10 times larger than in the case of normal operation.

The correct prediction of the six under-fueling faults was characterized by a RSR range of 13% to 24%. In addition, the detection of a cylinder under-fueling fault condition was accomplished by observing the change in a parameter's mean and standard deviation. For example, the under-fueling of cylinder 1L caused a 6% change in the mean, and a 620% increase in the standard deviation of the inertia estimated with the gradient estimator. For the same case, the least-squares estimator with exponential forgetting indicated a 16% change in the mean and a 327% change in the standard deviation of the estimated engine inertia.

Alternatively, large changes in estimated parameter standard deviation can be used for the elimination of fault misclassification. We considered the case when an under-fueling fault in cylinder 3R is misclassified as a fault in cylinder 1L. The gradient estimator showed a 227% change in the standard deviation of estimated inertia. The least-squares estimator with exponential forgetting recorded a 302% change for the same variable.

6.3 Pressure Waveform Reconstruction

In Chapter 5 we investigated the procedure for pressure waveform reconstruction using the engine model and angular velocity measurements. Because our model implements a multi-input single output system, it was not possible to explicitly decouple the inverse dynamics. We therefore considered two approaches. First, we redefined the system input and we rewrote the engine model as a single input single output system. The new input was then the torque due to gas pressure.

Secondly, we approximated the cylinder pressure waveforms with a periodic continuous impulse-like function. Using this template-based approach we were able to exactly identify the condition of each cylinder, and to improve the estimation procedure for the gas pressure torque. Initial simulation of normal operating condition resulted in a RMS error of 196.2 Nm, while the template-based approach resulted in a RMS torque error of only 99.24 Nm.

In the case of an under-fueling fault, the gas pressure torque was initially estimated with a RMS error between 271.4 Nm and 308.7 Nm, while the pressure-template approach reduce the final RMS torque error to the range of 85.7 Nm to 198.1 Nm.

6.3.1 Individual Cylinder Pressure Reconstruction

Cylinder pressure waveforms were approximated by an impulse-like periodic function. For the normal operating condition, this functional approximation was characterized by a RMS pressure error between 0.145 MPa and 0.177 MPa, which correspond to a RSR range of only 5% to 6%.

The torque due to gas pressure waveform reconstruction was obtained from the superposition of the six individual pressure waveform templates. All 6 pressure waveforms are initially characterized by the same maximum value and width. The estimated pressure variations were obtained using a standard least-squares technique. An under-fueling fault in the i-th cylinder could be determined exactly by the minimum value of the estimated pressure variation. The RMS pressure error was between 0.155 MPa and 0.277 MPa for the normal operating condition corresponding to a RSR between 5% and 10%.

For each of the six under-fueling faults, the pressure waveform corresponding to the faulty cylinder was reconstructed. The RMS error was between 0.155 MPa and 0.386 MPa. The RSR was between 7% and 18%.

6.4 Towards Condition Monitoring

In the foregoing work, we have laid the groundwork for a diesel engine condition monitoring system. In short, we have developed and validated a model, and shown its utility in detecting faults using two separate strategies—parameter estimation, and cylinder pressure reconstruction. In the latter strategy, we have introduced a new template-based scheme for estimating individual cylinder pressures. These results suggest a condition monitoring scheme which is highly sensitive to input variation due to fueling faults. Furthermore, reconstructed torque due to gas pressure by superposition of the templates results in very accurate estimates—RSR of about 5%—which are as good as the best results reported in the literature.

The integration of these three methods (modeling and validation, parametric identification, and pressure waveform reconstruction) exploits the use of the diesel engine model from the perspective of the analytical redundancy paradigm. Our simulation results suggest that parametric identification methods represent important tools for solving engine fault detection and isolation problems. Parameter means and standard deviations were used to differentiate between healthy and faulty conditions, and to eliminate misclassifications of faulty cylinders. Using a combination of functional approximation and parametric identification techniques we were able to determine the condition of each cylinder and to reconstruct close approximations to the cylinder pressure waveforms.

6.5 Conclusions

A new method for computing individual cylinder pressures from crankshaft velocity variation has been developed. The pressure template-based method provides estimates of pressure to an accuracy of 5% residual to signal ratio.

The single cylinder model of C. F. Taylor [28, pp. 240–305] has been transformed to a model based on engine speed fluctuation as a function of pressure input. The engine model was further modified to multiple cylinders, and was linearized in state and parameters. The resulting model was validated using recorded data to produce a RMS estimation error of 0.0559 rad/sec for the normal operating condition.

The above model, improved by parametric identification allowed the correction for harmonic torque fluctuation, and the identification of total engine inertia.

Nomenclature

We have used the following notation:

- J_E = engine mass moment of inertia (kgm^2);
- J_{cr} = connecting rod mass moment of inertia (kgm^2);
- $m_t + m_r$ = total connecting rod mass (kg);
- m_p = mass of the reciprocating parts (kg);
- A_p = piston crown area (m^2);
- r = crankshaft radius (m);
- l = connecting rod length (m);
- T_E = total engine torque (Nm);
- T_p = torque due to gas pressure (Nm) and thus, $\hat{T}_p$ = estimated gas pressure torque (Nm), $\tilde{T}_p$ = torque residual, and $\bar{T}_p$ = mean pressure torque (Nm);
- T_t = torque due to the inertia of the reciprocating masses (Nm);
- T_r = torque due to the angular acceleration of the connecting rod (Nm);
- T_f = friction torque (Nm);
- T_l = load torque (Nm);
- ΔT = unmodeled harmonic torque fluctuation (Nm) and thus, $\Delta\hat{T}$ = estimated torque fluctuation (Nm);

- T_h = torque fluctuation amplitude (Nm);
- γ = torque phase (degrees);
- N = number of cylinders, or number of system inputs;
- N_m = number of measurements (data points);
- θ = crank angle (degrees or rad), and thus, $\dot{\theta} = \omega$ angular velocity (rad/sec), and $\ddot{\theta} = \dot{\omega}$ angular acceleration (rad/sec^2);
- ω_0 = nominal engine speed (rpm or rad/sec);
- $\delta\omega$ = measured angular velocity fluctuation, and thus $\delta\hat{\omega}$ = estimated crankshaft angular velocity fluctuation, and $\delta\tilde{\omega}$ = angular velocity residual (rad/sec);
- Ω_h = velocity residual amplitude (rad/sec);
- α = angle between the connecting rod axis and the cylinder axis (degrees or rad), and thus, $\dot{\alpha}$ = connecting rod angular velocity (rad/sec), and $\ddot{\alpha}$ = connecting rod angular acceleration (rad/sec^2);
- s = piston position (m), and thus, $\dot{s}$ = piston velocity (m/sec), and $\ddot{s}$ = piston acceleration (m/sec^2);
- P_i = pressure in the i-th cylinder (MPa);
- δP_i = pressure variation and thus, $\delta\hat{P}_i$ = estimated pressure variation;
- ϕ_i = phase shift corresponding to the i-th cylinder (degrees);
- $x \in R^n$ system state with x_0 = initial condition, and thus, $\hat{x}$ = estimated state, and $\tilde{x}$ = state estimation error. In the case of the engine model, $x = \omega^2$, and the state is described by the variable $\delta x \in R$;

- $u \in R^N$ system input, $\hat{u}$ estimated system input, and u_c = control law. For the engine model the input is represented by $N = 6$ cylinder pressures;
- $y \in R$ system output, and thus, $\hat{y}$ = predicted output, and $\tilde{y}$ = prediction error. For the engine model, $y = \delta\omega$;
- Y = corrected engine torque, output of the identification model;
- y_d = desired trajectory, and ϵ = tracking error;
- $p \in R^q$ vector of system parameters and thus, $\hat{p}$ = parameter estimates, and $\tilde{p}$ = parameter estimation error;
- A, c, and B, b or b' = engine model coefficients;
- η = measurement noise;
- d = process disturbance;
- H = gain of the Beard-Jones filter;
- c_1, c_2, c_3, c_4 = geometrical coefficients;
- $c_{11}, c_{12}, c_{33}, c_{34}$ = torque coefficients;
- E = performance index;
- Φ = signal matrix;
- Ψ_0 = gain matrix for the gradient estimator;
- Ψ = variable gain matrix for the least-squares estimator with exponential forgetting;
- λ = forgetting factor;

- σ = standard deviation.

Bibliography

[1] S. E. Salcudean, *Introduction to Robotics (course notes).* Dept. of EE—UBC, 1993.

[2] P. E. Wellstead, *Physical System Modelling.* Academic Press, 1979.

[3] *Diesel Dynamic Model Mathematical Analysis, Technical Report # GTL-19-34-TR.1.* GasTOPS Ltd., March 1991.

[4] A. K. Sood, A. A. Fahs, and N. A Henein, "Engine fault analysis: Part II-Parameter estimation approach," *IEEE Trans. Automat. Contr.*, vol. 32, pp. 301–307, Nov. 1985.

[5] F. T. Connolly and A. F. Yagle, "Modeling and identification of the combustion pressure process in internal combustion engines using engine speed fluctuations," in *Transportation Systems-92: Winter Annual Meeting of the American Society of Mechanical Engineers*, pp. 191–206, Nov. 1992.

[6] R. Stone, *Introduction to Internal Combustion Engines.* Macmillan Press, 2nd ed., 1992.

[7] C. F. Taylor, *The Internal-Combustion Engine in Theory and Practice, Volume I: Thermodynamics, Fluid Flow, Performance.* The Technology Press of the MIT and John Willey & Sons, 1960.

[8] K. B. Hodgins and P. Mtui, *Evaluation of PCB Pressure Transducers, Internal Report.* Dept. of ME—UBC, June 1994.

[9] P. G. Hill and P. D. Lawrence, *Diesel Engine Advanced Condition Monitoring System (Research Proposal—DRAFT).* UBC, 1994.

[10] M. J. Jennings, P. N. Blumberg, and R. W. Amann, "A dynamic simulation of the Detroit Diesel electronic control system in heavy duty powertrains," *SAE Trans., J. Engines*, vol. 95, pp. 942–966, 1986. Section 3, Paper No. 861959.

[11] J. J. Slotine and W. Li, *Applied Nonlinear Control.* Prentice Hall, 1991.

[12] P. M. Frank, "Fault diagnosis in dynamic systems using analytical and knowledge-based redundancy–A survey and some new results," *Automatica*, vol. 26, pp. 459–474, Sep. 1990.

[13] A. S. Willsky, "A survey of design methods for failure detection in dynamic sytems," *Automatica*, vol. 12, pp. 601–611, Dec. 1976.

[14] R. Isermann, "Process fault detection based on modeling and estimation methods–A survey," *Automatica*, vol. 20, pp. 387–404, Dec. 1984.

[15] H. Kwakernaak, "Robust control and H^∞–optimization–Tutorial paper," *Automatica*, vol. 29, pp. 255–273, Apr. 1993.

[16] J. Auzins and R. V. Wilhelm, "Automotive electronics: Steering toward the next frontiers," *IEEE Potentials*, vol. 13, pp. 32–36, Oct. 1994.

[17] R. Isermann and B. Freyermuth, "Process fault diagnosis based on process model knowledge–Part I: principles for fault diagnosis with parameter estimation," *Trans. ASME, J. Dynamic Systems, Measurement and Control*, vol. 113, pp. 620–626, Dec. 1991.

[18] R. J. Patton and J. Chen, "Detection of faulty sensors in aero jet engine systems using robust model-based methods," in *IEE Colloquim No. 156: Condition Monitoring for Fault Diagnosis*, pp. 2/1–2/22, IEE, 1991.

[19] R. J. Patton, "Fault detection and diagnosis in aerospace systems using analytical redundancy," *Computing and Control Engineering Journal*, vol. 2, pp. 127–135, May 1991.

[20] R. J. Patton, J. Chen, and H. Y. Zhang, "Modeling methods for improving robustness in fault diagnosis of jet engine system," in *Proc. of the 31st Annual Conference on Decision and Control*, pp. 2330–2335, IEEE, 1992.

[21] M. N. Brown, R. W. Stewart, T. S. Durrani, and T. W. Buggy, "DSP subsystem for knowledge based health monitoring of gas turbine engines," in *ICASSP'92: Acoustics, Speech & Signal Processing Conference*, pp. 69–72, IEEE, 1992.

[22] G. Rizzoni and P. S. Min, "Detection of sensor failures in automotive engines," *IEEE Trans. Veh. Technol.*, vol. 40, pp. 487–500, May 1991.

[23] L. Dubost and J. N. Heude, "On-line diagnosis of a superchargher in a noisy environment," in *Proc. of the IEE Conference on Intelligent Systems Engineering*, pp. 65–70, 1992.

[24] K. A. Marko, B. Bryant, and N. Soderborg, "Neural network application to comprehensive engine diagnostics," in *Proc. of the International Conference on Systems, Man, and Cybernatics*, pp. 1016–1022, IEEE, 1992.

[25] K. S. Narendra and K. Parthasarathy, "Identification and control of dynamical systems using neural networks," *IEEE Trans. Neural Networks*, vol. 1, pp. 4–27, March 1990.

[26] R. J. Patton and J. Chen, "Advances in fault diagnosis using analytical redundancy," in *IEE Colloquim No. 019: Plant Optimisation for Profit*, pp. 6/1–6/12, IEE, 1993.

[27] P. Eykhoff, *System Identification: Parameter and State Estimation.* John Wiley & Sons, 1974.

[28] C. F. Taylor, *The Internal-Combustion Engine in Theory and Practice, Volume II: Combustion, Fuels, Materials, Design.* The Technology Press of the MIT and John Willey & Sons, 1968.

[29] J. S. Rao, *Advanced Theory of Vibration.* John Wiley & Sons, 1st ed., 1992.

[30] P. E. Wellstead, "Application of adaptive techniques to internal combustion engine control," in *The benefits of electronic control systems for internal combustion engines—Seminar Proceedings*, pp. 11–23, Inst. Mech. Engineers, Jan. 1989.

[31] S. Roy, O. P. Malik, and G. S. Hope, "Adaptive control of speed and equivalence ratio dynamics of a diesel driven power plant," *IEEE Trans. Energy Conversion*, vol. 8, pp. 13–19, March 1993.

[32] S. Roy, O. P. Malik, and G. S. Hope, "Real time test results with adaptive speed controllers for a diesel prime mover," *IEEE Trans. Energy Conversion*, vol. 8, pp. 499–505, Sep. 1993.

[33] J. Jiang, "Design and implementation of an optimal gain scheduling controller for a diesel engine," in *Proc. of the Second IEEE Conference on Control Applications*, pp. 667–672, 1993.

[34] T. Brown and W. Neill, "Determination of engine cylinder pressures from crankshaft speed fluctuations," *SAE Trans., J. Engines*, vol. 101, pp. 10–19, 1992. Section 3, Paper No. 920463.

[35] R. Isermann and B. Freyermuth, "Process fault diagnosis based on process model knowledge–Part II: case study experiments," *Trans. ASME, J. Dynamic Systems, Measurement and Control*, vol. 113, pp. 627–633, Dec. 1991.

[36] T. H. B. Jewitt and B. Lawton, "The use of speed sensing for monitoring the condition of military vehicles engines," in *International Conference on Vehicle Condition Monitoring and Fault Diagnosis*, pp. 67–72, Inst. Mech. Engineers, 1985.

[37] S. J. Citron, J. E. O'Higgins, and L. Y Chen, "Cylinder by cylinder engine pressure and pressure torque waveform determination utilizing speed fluctuations," *SAE Trans., J. Engines*, vol. 98, pp. 933–947, 1989. Section 3, Paper No. 890486.

[38] M. T. K Srinivasan, G Rizzoni and G. C. Luh, "On-line estimation of net engine torque from crankshaft angular velocity measurement using repetitive estimators," in *Proc. of 1992 American Control Conference*, pp. 516–520, 1992.

[39] W. B. Ribbens and G. Rizzoni, "Applications of precise crankshaft position measurements for engine testing, control and diagnosis," *SAE Trans., J. Engines*, vol. 98, pp. 1582–1596, 1989. Section 3, Paper No. 890885.

[40] J. W. Freestone and E. G. Jenkins, "The diagnosis of cylinder power faults in diesel engines by flywheel speed measurement," in *International Conference on Vehicle Condition Monitoring and Fault Diagnosis*, pp. 15–24, Inst. Mech. Engineers, 1985.

[41] G. Rizzoni, "Diagnosis of individual cylinder misfires by signature analysis of crankshaft speed fluctuations," *SAE Trans., J. Engines*, vol. 98, pp. 1572–1581, 1989. Section 3, Paper No. 890884.

[42] Y. K. Chin and F. E. Coats, "Engine dynamics: Time-based versus crank-angle based," *SAE Trans., J. Engines*, vol. 95, pp. 937–956, 1986. Section 3, Paper No. 860412.

[43] J. B. Heywood, *Internal Combustion Engine Fundamentals.* McGraw Hill, 1st ed., 1988.

[44] G. Rizzoni, "A stochastic model for the indicated pressure process and the dynamics of the internal combustion engine," *IEEE Trans. Veh. Technol.*, vol. 38, pp. 180–192, Aug. 1989.

[45] F. T. Connolly and A. E. Yagle, "Modeling and identification of the combustion process in internal combustion engines: II—Experimental results," *Trans. ASME, J. of Engineering for Gas Turbines and Power*, vol. 115, pp. 801–809, Oct. 1993.

[46] Y. Z. Tsypkin, *Relay Control systems.* Cambridge University Press, 1984.

[47] M. Schwartz and L. Shaw, *Signal Processing: Discrete Spectral Analysis, Detection, and Estimation.* McGraw-Hill, 1st ed., 1975.

Appendix A

Test Cell Description

An IBM-PC computer equipped with analog to digital (A/D) conversion board and a pulse-timer board is used for high speed data acquisition. In order to reduce equipment cost, only two cylinder pressure signals are acquired (one "healthy" cylinder and one under-fueled cylinder). Data from 2 channels (2 cylinder pressures) are sampled simultaneously by the sample and hold preamplifiers; a multiplexer directs each sample to the A/D converter. The A/D converter is triggered by an index signal, bottom dead centre (BDC) of the first left (1L) cylinder, from an optical shaft encoder connected to the crankshaft. The optical shaft encoder is used for measuring the crank angle. The resolution is 360 pulses per revolution. The flywheel proximity sensor is a sensing-transduction coil which uses the magnetic pick-up principle. The signal conditioning system includes charge amplifiers with very high input impedance suitable for use with piezoelectric cylinder pressure gauges. The signal from the crankshaft/flywheel proximity sensor is passed through a zero-crossing circuit to produce digital pulses which are then fed to the pulse-timer input of the data acquisition system. The variations of angular velocity are measured indirectly by recording the number of clock cycles (absolute time) between two successive crank angle sampling intervals. Each measurement is repeated for different brake (dynamometer load) torque values and with several levels of fuel starvation. The proposed data acquisition system is very similar to the one used by the Institute for Machinery Research (IMR).

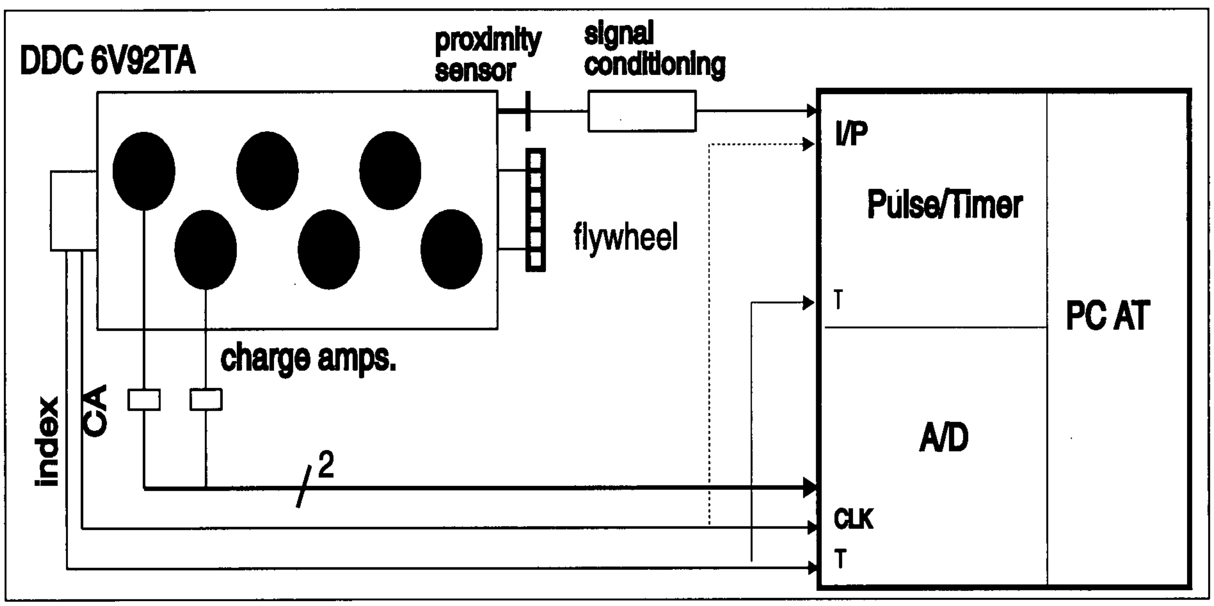

Figure A.1: Illustrates a data acquisition system for measuring cylinder pressures and crankshaft/flywheel speed variations.

Appendix B

Program Listings

c1.m

```
function y = c_1(theta,r,l)
   %FUNCTION        C_1.M
   %ARGUMENTS:      r        = crankshaft radius (m);
   %                l        = connecting rod length (m);
   %                theta    = crank angle (rad);
   %RETURNS:        y        = the ratio v/(r.w).
   x=r/l;
   f11=sin(theta).^2;
   f12=sqrt(ones(size(theta))-(x^2)*f11);
   y=sin(theta)+x*sin(theta).*cos(theta)./f12;
```

c2.m

```
function y = c_2(theta,r,l)
   %FUNCTION        C_2.M
   %ARGUMENTS:      r        = crankshaft radius (m);
   %                l        = connecting rod length (m);
   %                theta    = crank angle (rad);
   %RETURNS:        y        = acceleration coefficient.
   x=r/l;
   calpha=sqrt(ones(size(theta))-(x^2)*sin(theta).^2);
   xx=x*cos(theta)./calpha;
   y=(ones(size(theta))+xx).*(cos(theta)+...
   x.*(xx-ones(size(theta))).*(sin(theta).^2)./calpha);
```

c3.m

```
function y = c_3(theta,r,l)
   %FUNCTION        C_3.M
   %ARGUMENTS:      r = crankshaft radius;
   %                l = connecting rod length;
   %                theta    = crank angle;
   %RETURNS:        y        = c3 acceleration coefficient.
   x=r/l;
   calpha=sqrt(ones(size(theta))-...
   (x^2)*sin(theta).^2);
   y=x*cos(theta)./calpha;
```

<u>c4.m</u>

```
function y = c_4(theta,r,l)
   %FUNCTION        C_4.M
   %ARGUMENTS:      r        = crankshaft radius;
   %                l        = connecting rod length;
   %                theta    = crank angle;
   %RETURNS:        y        = c4 acceleration coefficient.
   x=r/l;
   calpha=sqrt(ones(size(theta))-...
   (x^2)*sin(theta).^2);
   xx=x*cos(theta)./calpha;
   y=x*(sin(theta)).*(xx.^2-...
   ones(size(theta)))./(calpha);
```

<u>cmpall.m</u>

```
%CMPALL.M
   %Calls: demo1.m, rmse.m, rot.m
   disp('NORMAL OPERATING CONDITION')
   w0hat=demo1(0,w0);
   disp('ROOT MEAN SQUARE velocity error (rad/sec):')
   e0=rmse(w0-0.8325*w0hat)
   disp('RESIDUAL TO SIGNAL RATIO (%):')
   RSR0=e0/rmse(w0)*100
   figure(1)
   plot(ca0*180/pi,w0,ca0*180/pi,.8325*w0hat,':')
   xlabel('degrees')
   ylabel('rad/sec')
   title('Estimated (..) and  Actual (--) Velocity Fluctuation')
   disp('Press any key to continue...')
   pause
   disp('TESTING 6 ACTUATOR FAULTS')
   disp('The actuator fault is defined as')
   disp('10% under-fueling of each cylinder at a time.')
   w1hat=demo1(1,w1l);
   w2hat=demo1(2,w2l);
   w3hat=demo1(3,w1r);
   w4hat=demo1(4,w1l);
   w5hat=demo1(5,w3r);
   w6hat=demo1(6,w3l);
   w1x = w1hat + rot(w1hat,59);
   w2x = w2hat + rot(w2hat,59);
   w3x = w3hat + rot(w3hat,59);
   w4x = w4hat + rot(w4hat,59);
   w5x = w5hat + rot(w5hat,59);
   w6x = w6hat + rot(w6hat,59);
   w1lx=w1l+rot(w1l,59);
   w3rx=w3r+rot(w3r,59);
   w3lx=w3l+rot(w3l,59);
   w2rx=w2r+rot(w2r,59);
   w2lx=w2l+rot(w2l,59);
```

```
w1rx=w1r+rot(w1r,59);
w1x=w1x-mean(w1x);
w2x=w2x-mean(w2x);
w3x=w3x-mean(w3x);
w4x=w4x-mean(w4x);
w5x=w5x-mean(w5x);
w6x=w6x-mean(w6x);
w1lx=w1lx-mean(w1lx);
w2lx=w2lx-mean(w2lx);
w3lx=w3lx-mean(w3lx);
w1rx=w1rx-mean(w1rx);
w2rx=w2rx-mean(w2rx);
w3rx=w3rx-mean(w3rx);
disp('Elimination of the Sinusoidal Trend')
disp('The RMS velocity errors (rad/sec) and')
disp('the corresponding RSRs (%)')
disp('are displayed in the cylinder order:')
e1=rmse(w1lx-.6647*w1x)
RSR1=e1/rmse(w1lx)*100
e2=rmse(w3rx-.6154*w2x)
RSR2=e2/rmse(w3rx)*100
e3=rmse(w3lx-.5599*w3x)
RSR3=e3/rmse(w3lx)*100
e4=rmse(w2rx-.5897*w4x)
RSR4=e4/rmse(w2rx)*100
e5=rmse(w2lx-.5820*w5x)
RSR5=e5/rmse(w2lx)*100
e6=rmse(w1rx-.7686*w6x)
RSR6=e6/rmse(w1rx)*100
disp('The average RMS error (rad/sec) is:')
e_m=(e1+e2+e3+e4+e5+e6)/6
disp('The average RSR (%) is:')
RSR_m=(RSR1+RSR2+RSR3+RSR4+RSR5+RSR6)/6
figure(2)
subplot(3,2,1)
plot(ca0*180/pi,w1lx,ca0*180/pi,.6*w1x,':')
xlabel('degrees')
ylabel('rad/sec')
subplot(3,2,2)
plot(ca0*180/pi,w3rx,ca0*180/pi,.6*w2x,':')
xlabel('degrees')
ylabel('rad/sec')
subplot(3,2,3)
plot(ca0*180/pi,w3lx,ca0*180/pi,.6*w3x,':')
xlabel('degrees')
ylabel('rad/sec')
subplot(3,2,4)
plot(ca0*180/pi,w2rx,ca0*180/pi,.6*w4x,':')
xlabel('degrees')
ylabel('rad/sec')
subplot(3,2,5)
plot(ca0*180/pi,w2lx,ca0*180/pi,.6*w5x,':')
```

```
   xlabel('degrees')
   ylabel('rad/sec')
   subplot(3,2,6)
   plot(ca0*180/pi,w1rx,ca0*180/pi,.6*w6x,':')
   xlabel('degrees')
   ylabel('rad/sec')
   disp('Press any key to continue... ')
   pause
```

demo1.m

```
function dwhat = demo1(n,dw)
   %FUNCTION        DEMO1.M
   %ARGUMENTS:      n        = integer corresponding to
   %                           the down cylinder;
   %                dw       = actual angular velocity;
   %RETURNS:        dwhat    = estimated angular velocity.
   %Calls: geom.m, ldown.m
   global ca ca0 x0 w_0
   [p1 p2 p3 p4 p5 p6] = ldown(n);
   [u,q,m] = geom(ca,p1,p2,p3,p4,p5,p6);
   uu = (x0*q + u);
   d =  -mean(uu);
   dT = ca(2)-ca(1);
   dxhat = dw(1)*(2*w_0+dw(1)) +...
   igr((uu + d)./m,dT);
   dwhat = sqrt(x0 + dxhat) - w_0;
   dwhat=dwhat-mean(dwhat);
   dwhat=rot(interp1(ca,dwhat,ca0),1);
```

demo2.m

```
function [JEhat01,JEhat02,JEhat03,TLhat01,...
   TLhat02,TLhat03,dwhat01,dwhat02,...
   dwhat03,rms,rsr]=demo2(n,dw,PAR0)
   %FUNCTION        DEMO2.M
   %ARGUMENTS:      n       = cylinder number;
   %                dw      = angular velocity waveform;
   %                PAR0    = parameter initialization;
   %RETURNS:        JEhat01 = estimated engine inertia using
   %                          standard least-squares;
   %                JEhat02 = estimated engine inertia using
   %                          the recursive gradient estimator;
   %                JEhat03 = estimated engine inertia using
   %                          least-squares with exponential forgetting;
   %                TLhat01 = estimated torque fluctuation using SLS;
   %                TLhat02 = estimated torque fluctuation using GE;
   %                TLhat03 = estimated torque fluctuation using LSEF;
   %                dwhat01 = estimated speed fluctuation using SLS;
   %                dwhat02 = estimated speed fluctuation using GE;
   %                dwhat03 = estimated speed fluctuation using LSEF;
```

```
%                 rms     = vector of root mean square velocity errors;
%                 rsr     = vector of residual to signal ratios.
%Calls: ldown.m, diffc.m, sls.m, itgr.m, est.m, itls.m, rmse.m.
p0=0.3;
P0=diag([1 1 1]);
lambda=15;
%crank angle for pressure sampling
ca = [0:719]' /720 * 2 * pi;
%crank angle for velocity sampling
ca0 = [0:117]'/118 * 2 * pi;
[p1,p2,p3,p4,p5,p6]=ldown(n);
p1=interp1(ca,p1,ca0);
p2=interp1(ca,p2,ca0);
p3=interp1(ca,p3,ca0);
p4=interp1(ca,p4,ca0);
p5=interp1(ca,p5,ca0);
p6=interp1(ca,p6,ca0);
dca0=ca0(2)-ca0(1);
dwp=diffc(dw,dca0);
[Y01,PHI01,PAR01,ERR01,JEhat01,TLhat01,ep01,dwhat01]=...
sls(ca0,p1,p2,p3,p4,p5,p6,dw,dwp);
[ERR02,PAR02]=itgr(Y01,PHI01,p0,PAR0);
[JEhat02,TLhat02,ep02,dwhat02]=...
est(PAR02,ca0,p1,p2,p3,p4,p5,p6,dw,dwp);
[ERR03,PAR03]=itls(Y01,PHI01,lambda,P0,PAR0);
[JEhat03,TLhat03,ep03,dwhat03]=...
est(PAR03,ca0,p1,p2,p3,p4,p5,p6,dw,dwp);
rms=[rmse(ep01) rmse(ep02) rmse(ep03)];
rsr=[rmse(ep01) rmse(ep02) rmse(ep03)]/rmse(dw)*100;
```

diffc.m

```
function y = diffc(x,dT)
   %FUNCTION       DIFFC.M
   %ARGUMENTS:     x       = vector of samples;
   %               dT      = crank angle interval;
   %RETURNS:       y       = smooth derivative.
   ll=length(x);
   for i=3:ll-2
   y(i)=(x(i+2)/4 + x(i+1)/2-...
   x(i-1)/2-x(i-2)/4)/2;
   end
   y(1)=(x(3)/4+x(2)/2-x(ll)/2 -...
   x(ll-1)/4)/2;
   y(2)=(x(4)/4+x(3)/2-x(1)/2-...
   x(ll)/4)/2;
   y(ll)=(x(2)/4+x(1)/2-x(ll-1)/2 -...
   x(ll-2)/4)/2;
   y(ll-1)=(x(1)/4+x(ll)/2-x(ll-2)/2 -...
   x(ll-3)/4)/2;
   y=y'/dT;
```

dlt.m

```
function y=dlt(alpha,beta,gamma,x)
   %FUNCTION        DLT.M
   %ARGUMRNTS:      alpha    = impulse gain;
   %                beta     = impulse width;
   %                gamma    = offset;
   %                x        = crank angle vector;
   %RETURNS:        y        = periodic impulse.
   y=beta./(beta^2*sin(x/2).^2+1);
   y=y*alpha-gamma;
```

est.m

```
function [JEhat,TLhat,ep,dwhat]=...
   est(PAR,ca0,p1,p2,p3,p4,p5,p6,dw,dwp)
   %FUNCTION        EST.M
   %ARGUMENTS:      PAR    = vector of estimated parameters;
   %                ca0    = crank angle vector;
   %                pi     = cylinder pressure, i=1,..., 6;
   %                dw     = angular velocity waveform;
   %                dwp    = angular acceleration waveform;
   %RETURNS:        JEhat = vector of estimated inertias;
   %                TLhat = estimated torque fluctuation;
   %                ep     = velocity residuals;
   %                dwhat = estiamted angular velocity;
   %Calls: c_1.m, c_2.m, c_3.m, c_4.m, igr.m.
   %Engine data correspond to DDC 6V 92TA:
   w_0=125.5;    %engine speed (rad/sec)
   b_c=1.24;     %damping (Nm/(rad/sec))
   m_p=6.03;     %piston mass (kg)
   r=0.0635;     %crankshaft radius (m)
   l=0.2571;     %connecting rod length (m)
   Ap=0.01188;   %piston area (m^2)
   J_C=0.1544;   %crankshaft inertia (kg m^2)
   J_CR=0.0745; %connecting rod inertia (kg m^2)
   J_F=3.85;     %flywheel inertia (kg m^2)
   x0=w_0^2;
   %Pressure inputs: p1 p2 p3 p4 p5 p6
   %Firing order (right hand rotation):
   %1L 3R 3L 2R 2L 1R
   %1  2  3  4  5  6
   dca0=ca0(2)-ca0(1);
   ca1=ca0;
   c_11=c_1(ca1,r,l);
   c_21=c_2(ca1,r,l);
   c_31=c_3(ca1,r,l);
   c_41=c_4(ca1,r,l);
   ca2=ca1-(60-3.5)*pi/180;
   c_12=c_1(ca2,r,l);
   c_22=c_2(ca2,r,l);
```

```
c_32=c_3(ca2,r,l);
c_42=c_4(ca2,r,l);
ca3=ca2-(60+3.5)*pi/180;
c_13=c_1(ca3,r,l);
c_23=c_2(ca3,r,l);
c_33=c_3(ca3,r,l);
c_43=c_4(ca3,r,l);
ca4=ca3-(60-3.5)*pi/180;
c_14=c_1(ca4,r,l);
c_24=c_2(ca4,r,l);
c_34=c_3(ca4,r,l);
c_44=c_4(ca4,r,l);
ca5=ca4-(60+3.5)*pi/180;
c_15=c_1(ca5,r,l);
c_25=c_2(ca5,r,l);
c_35=c_3(ca5,r,l);
c_45=c_4(ca5,r,l);
ca6=ca5-(60-3.5)*pi/180;
c_16=c_1(ca6,r,l);
c_26=c_2(ca6,r,l);
c_36=c_3(ca6,r,l);
c_46=c_4(ca6,r,l);
s11=c_11.*c_11 + c_12.*c_12 + c_13.*c_13 +...
c_14.*c_14 + c_15.*c_15 + c_16.*c_16;
s12=c_11.*c_21 + c_12.*c_22 + c_13.*c_23 +...
c_14.*c_24 + c_15.*c_25 + c_16.*c_26;
s33=c_31.*c_31 + c_32.*c_32 + c_33.*c_33 +...
c_34.*c_34 + c_35.*c_35 + c_36.*c_36;
s34=c_31.*c_41 + c_32.*c_42 + c_33.*c_43 +...
c_34.*c_44 + c_35.*c_45 + c_36.*c_46;
sp=(1e+6)*(c_11.*p1 + c_12.*p2 + c_13.*p3 +...
c_14.*p4 + c_15.*p5 + c_16.*p6);
dx=2*w_0*dw;
dxp=2*w_0*dwp;
phi1=0.5*dxp;
fact=max(phi1);
lhat=length(PAR);
th=(0:lhat-1)/lhat*2*pi;
JEhat=PAR(1,:)./fact;
TLhat=PAR(2,:).*sin(th)+PAR(3,:).*cos(th);
JE=PAR(1,lhat)./fact;
TL=PAR(2,lhat).*sin(ca0)+PAR(3,lhat).*cos(ca0);
y3=Ap*r*sp;
m=(JE+m_p*r^2*s11-J_CR*s33)/2;
inp=y3-TL; %TLhat(1:lhat-1)';
inp=inp-mean(inp);
dxhat = dw(1)*(2*w_0+dw(1)) + igr(inp./m,dca0);
dwhat = sqrt(x0 + dxhat) - w_0;
dwhat=dwhat-mean(dwhat);
%dwhat=0.9*rot(dwhat,1);
ep=dw-dwhat;
```

geom.m

```
function [u,q,m]=geom(ca,p1,p2,p3,p4,p5,p6)
   %FUNCTION:       GEOM.M
   %ARGUMENTS:      ca       = crank angle (rad);
   %                pi       = pressure in the i-th cylinder (MPa);
   %RETURNS:        [u,q,m] = model coefficients.
   %Calls: c_1.m, c_2.m, c_3.m, c_4.m
   %Engine data correspond to DDC 6V 92TA:
   %w_0=125.5;  %nominal engine speed (rad/sec)
   b_c=1.24; %damping (Nm/(rad/sec))
   m_p=6.03; %piston mass (kg)
   r=0.0635; %crankshaft radius (m)
   l=0.2571; %connecting rod length (m)
   Ap=0.01188; %piston area (m^2)
   J_C=0.1544; %crankshaft inertia (kg m^2)
   J_CR=0.0745; %connecting rod inertia (kg m^2)
   J_F=3.85; %flywheel inertia (kg m^2)
   %Pressure inputs: p1 p2 p3 p4 p5 p6
   %Firing order (right hand rotation)
   %1L 3R 3L 2R 2L 1R
   %1  2  3  4  5  6
   ca1=ca;
   c_11=c_1(ca1,r,l);
   c_21=c_2(ca1,r,l);
   c_31=c_3(ca1,r,l);
   c_41=c_4(ca1,r,l);
   ca2=ca1-(60-3.5)*pi/180;
   c_12=c_1(ca2,r,l);
   c_22=c_2(ca2,r,l);
   c_32=c_3(ca2,r,l);
   c_42=c_4(ca2,r,l);
   ca3=ca2-(60+3.5)*pi/180;
   c_13=c_1(ca3,r,l);
   c_23=c_2(ca3,r,l);
   c_33=c_3(ca3,r,l);
   c_43=c_4(ca3,r,l);
   ca4=ca3-(60-3.5)*pi/180;
   c_14=c_1(ca4,r,l);
   c_24=c_2(ca4,r,l);
   c_34=c_3(ca4,r,l);
   c_44=c_4(ca4,r,l);
   ca5=ca4-(60+3.5)*pi/180;
   c_15=c_1(ca5,r,l);
   c_25=c_2(ca5,r,l);
   c_35=c_3(ca5,r,l);
   c_45=c_4(ca5,r,l);
   ca6=ca5-(60-3.5)*pi/180;
   c_16=c_1(ca6,r,l);
   c_26=c_2(ca6,r,l);
   c_36=c_3(ca6,r,l);
```

```
c_46=c_4(ca6,r,l);
s11=c_11.*c_11 + c_12.*c_12 + c_13.*c_13 +...
c_14.*c_14 + c_15.*c_15 + c_16.*c_16;
s12=c_11.*c_21 + c_12.*c_22 + c_13.*c_23 +...
c_14.*c_24 + c_15.*c_25 + c_16.*c_26;
s33=c_31.*c_31 + c_32.*c_32 + c_33.*c_33 +...
c_34.*c_34 + c_35.*c_35 + c_36.*c_36;
s34=c_31.*c_41 + c_32.*c_42 + c_33.*c_43 +...
c_34.*c_44 + c_35.*c_45 + c_36.*c_46;
sp=(1e+6)*(c_11.*p1 + c_12.*p2 + c_13.*p3 +...
c_14.*p4 + c_15.*p5 + c_16.*p6);
q = J_CR*s34-m_p*r^2*s12;
u = Ap*r*sp;
m = 0.5*(J_C+J_F-J_CR*s33+m_p*r^2*s11);
```

igr.m

```
function II=igr(y,dT)
   %FUNCTION        IGR.M
   %ARGUMENTS:      y        = vector of samples;
   %                dT       = crank angle interval;
   %RETURNS:        II       = numerical integration.
   II(1)=0;
   cs=cumsum(y)-y(1);
   for i=2:length(y)
   II(i)=y(1)/2+cs(i-1)+y(i)/2;
   end
   II=dT*II';
```

itgr.m

```
function [err,PAR]=itgr(y,phi,p0,PAR0)
   %FUNCTION        ITGR.M
   %ARGUMENTS:      y        = output vector;
   %                phi      = signal matrix;
   %                p0       = gain for the gradient estimator;
   %                PAR0     = initialization;
   %RETURNS:        err      = vector of residuals;
   %                PAR      = estiamted parameters.
   Nit=length(y);
   h=2*pi/118;
   PAR(:,1)=PAR0;
   for i=1:Nit
   err(i)=phi(i,:)*PAR(:,i)-y(i);
   E(i)=0.5*err(i)'*err(i);
   PAR(:,i+1)=PAR(:,i)-h*p0*phi(i,:)'*err(i);
   end
   err=err';
```

<u>itls.m</u>

```
function [err,PAR]=itls(y,phi,lambda,P0,PAR0)
   %FUNCTION        ITLS.M
   %ARGUMENTS:      y        = output vector;
   %                phi      = signal matrix;
   %                lambda   = forgetting factor;
   %                P0       = gain initialization;
   %                PAR0     = parameter initialization;
   %RETURNS:        err      = vector of residuals;
   %                PAR      = estimated parameters.
   Nit=length(y);
   h=2*pi/118;
   P=P0;
   PAR(:,1)=PAR0;
   for i=1:Nit
   err(i)=phi(i,:)*PAR(:,i)-y(i);
   PAR(:,i+1)=PAR(:,i)-h*P*phi(i,:)'*err(i);
   lambda=lambda*(1-norm(P)/70);
   P=P-h*P*(lambda+phi(i,:)'*phi(i,:)*P);
   end
   err=err';
```

<u>ldown.m</u>

```
function [y1, y2, y3, y4, y5, y6] = ldown(n)
   global p1col p5col pres0
   %FUNCTION:       LDOWN.M
   %ARGUMENTS:      n                     = integer;
   %RETURNS:        [Y1,Y2,Y3,Y4,Y5,Y6] = six cylinder
   %                                        pressure waveforms.
   %Load 5 pressures from healthy cylinders
   %originating from PRES.DAT, first 6*720
   %values and a single 'down' cylinder corresponding
   %to number n. If n is not in the range 0 through 6
   %then all healthy cyls are loaded. If n is zero then
   %the pres0 waveforms are loaded.
   %Note variable p1col should be loaded (healthy cyls),
   %and p5col (down cyls), and pres0 (baseline).
   %Calls: separate.m
   [y1 y2 y3 y4 y5 y6] = separate(p1col);
   [d1 d2 d3 d4 d5 d6] = separate(p5col);
   if n==0
   [y1 y2 y3 y4 y5 y6] = separate(pres0);
   elseif n==1
   y1 = d1;
   elseif n==2
   y2 = d2;
   elseif n==3
   y3 = d3;
   elseif n==4
   y4 = d4;
   elseif n==5
```

```
y5 = d5;
elseif n==6
y6 = d6;
end
```

piall.m

```
%PIALL.M
   %Calls: demo2.m, rmse.m
   input('Enter option number: ');
   n=ans;
   %initialization for the normal condition
   PAR0=[970 -50 -30]';
   %initialization for 1L down
   PAR01l=[1510 -580 204]';
   %initialization for 3R down
   PAR03r=[1380 -350 400]';
   %initialization for 3L down
   PAR03l=[1650 450 250]';
   %initialization for 2R down
   PAR02r=[1780 400 -615]';
   %initialization for 2L down
   PAR02l=[1700 -170 -790]';
   %initialization for 1R down
   PAR01r=[1730 -510 -480]';
   if n==0
   PAR0 = PAR0;
   dw=1.05*rot(w0,117);
   disp('NORMAL OPERATING CONDITION')
   elseif n==1
   PAR0 = PAR01l;
   dw=w1l;
   disp('FAULT 1L')
   elseif n==2
   PAR0 = PAR03r;
   dw=w3r;
   disp('FAULT 3R')
   elseif n==3
   PAR0 = PAR03l;
   dw=w3l;
   disp('FAULT 3L')
   elseif n==4
   PAR0 = PAR02r;
   dw=w2r;
   disp('FAULT 2R')
   elseif n==5
   PAR0 = PAR02l;
   dw=w2l;
   disp('FAULT 2L')
   elseif n==6
   PAR0 = PAR01r;
   dw=w1r;
   disp('FAULT 1R')
   elseif n==10
   PAR0 = PAR0;
   dw=w0;
   n=1;
```

```
disp('FAULT 1L vs. NORMAL OPERATING CONDITION')
elseif n==20
PAR0 = PAR0;
dw=w0;
n=2;
disp('FAULT 3R vs. NORMAL OPERATING CONDITION')
elseif n==30
PAR0 = PAR0;
dw=w0;
n=3;
disp('FAULT 3L vs. NORMAL OPERATING CONDITION')
elseif n==40
PAR0 = PAR0;
dw=w0;
n=4;
disp('FAULT 2R vs. NORMAL OPERATING CONDITION')
elseif n==50
PAR0 = PAR0;
dw=w0;
n=5;
disp('FAULT 2L vs. NORMAL OPERATING CONDITION')
elseif n==60
PAR0 = PAR0;
dw=w0;
n=6;
disp('FAULT 1R vs. NORMAL OPERATING CONDITION')
elseif n==21
PAR0 = PAR01l;
dw=w1l;
n=2;
disp('FAULT 3R vs. FAULT 1L')
elseif n==31
PAR0 = PAR01l;
dw=w1l;
n=3;
disp('FAULT 3L vs. FAULT 1L')
elseif n==41
PAR0 = PAR01l;
dw=w1l;
n=4;
disp('FAULT 2R vs. FAULT 1L')
elseif n==51
PAR0 = PAR01l;
dw=w1l;
n=5;
disp('FAULT 2L vs. FAULT 1L')
elseif n==61
PAR0 = PAR01l;
dw=w1l;
n=6;
disp('FAULT 1R vs. FAULT 1L')
end
%gradient step
p0=0.3;
%gain matrix
P0=diag([1 1 1]);
%forgetting factor
lambda=15;
```

```
%crank angle for pressure sampling
ca = [0:719]' /720 * 2 * pi;
%crank angle for velocity sampling
ca0 = [0:117]'/118 * 2 * pi;
[p1,p2,p3,p4,p5,p6]=ldown(n);
p1=interp1(ca,p1,ca0);
p2=interp1(ca,p2,ca0);
p3=interp1(ca,p3,ca0);
p4=interp1(ca,p4,ca0);
p5=interp1(ca,p5,ca0);
p6=interp1(ca,p6,ca0);
dca0=ca0(2)-ca0(1);
dwp=diffc(dw,dca0);
[Y01,PHI01,PAR01,ERR01,JEhat01,TLhat01,ep01,dwhat01]=...
sls(ca0,p1,p2,p3,p4,p5,p6,dw,dwp);
[ERR02,PAR02]=itgr(Y01,PHI01,p0,PAR0);
[JEhat02,TLhat02,ep02,dwhat02]=...
est(PAR02,ca0,p1,p2,p3,p4,p5,p6,dw,dwp);
[ERR03,PAR03]=itls(Y01,PHI01,lambda,P0,PAR0);
[JEhat03,TLhat03,ep03,dwhat03]=...
est(PAR03,ca0,p1,p2,p3,p4,p5,p6,dw,dwp);
rms=[rmse(ep01) rmse(ep02) rmse(ep03)];
rsr=[rmse(ep01) rmse(ep02) rmse(ep03)]/rmse(dw)*100;
subplot(3,1,1)
plot(ca0*180/pi,dw,ca0*180/pi,dwhat01,':',...
ca0*180/pi,dwhat02,'-.',ca0*180/pi,dwhat03,'--')
title('Actual and Estimated Velocity Fluctuation')
ylabel('rad/sec')
subplot(3,1,2)
sn=(1:length(JEhat02))'/length(JEhat02) * 2 * pi;
plot(sn*180/pi,JEhat02,'-.',sn*180/pi,JEhat03,'--')
title('Estimated Engine Inertia')
ylabel('kgm^2')
subplot(3,1,3)
plot(sn*180/pi,TLhat02,'-.',sn*180/pi,TLhat03,'--')
title('Estimated Torque Fluctuation')
ylabel('Nm')
xlabel('degrees')
disp('INERTIA VALUES')
J_sls=JEhat01
J_ge=JEhat02(length(JEhat02))
J_lsef=JEhat03(length(JEhat03))
disp('PARAMETERS MEAN AND STANDARD DEVIATION')
disp('GRADIENT ESTIMATOR')
Jm=mean(JEhat02)
Js=rmse(JEhat02)
Tm=mean(TLhat02)
Ts=rmse(TLhat02)
disp('LEAST-SQUARES WITH EXPONENTIAL FORGETTING')
Jm=mean(JEhat03)
```

```
   Js=rmse(JEhat03)
   Tm=mean(TLhat03)
   Ts=rmse(TLhat03)
   disp('ROOT MEAN SQUARE ERROR (rad/sec)')
   rms
   disp('RESIDUAL TO SIGNAL RATIO (%)')
   rsr
```

<u>**prsall.m**</u>

```
%PRSALL.M
   %Calls: tpe.m, pwr.m, rmse.m.
   input('Enter cylinder number (0-7): ');
   n=ans;
   if n==0
   dw=w0;
   disp('NORMAL OPERATING CONDITION 1')
   elseif n==1
   dw=w1l;
   disp('FAULT 1L')
   elseif n==2
   dw=w3r;
   disp('FAULT 3R')
   elseif n==3
   dw=w3l;
   disp('FAULT 3L')
   elseif n==4
   dw=w2r;
   disp('FAULT 2R')
   elseif n==5
   dw=w2l;
   disp('FAULT 2L')
   elseif n==6
   dw=w1r;
   disp('FAULT 1R')
   elseif n==7
   dw=w0;
   disp('NORMAL OPERATING CONDITION 2')
   end
   [p1 p2 p3 p4 p5 p6]=ldown(n);
   disp('TORQUE DUE TO GAS PRESSURE')
   [Tp,Tpm,Tphat,deltaT,err]=...
   tpe(n,ca,dw,p1,p2,p3,p4,p5,p6);
   disp('RMS torque error (Nm):')
   e_1=rmse(Tp-Tphat-deltaT)
   disp('RSR (%):')
   r_1=100*e_1/rmse(Tp)
   plot(ca*180/pi,Tp,ca*180/pi,Tphat+deltaT,':')
   axis([0 360 -1500 1500])
   xlabel('degrees')
   ylabel('Nm')
   title('Estimated (..) and Actual (--) Pressure Torque')
   disp('Press any key to continue...')
   pause
   [par,Tpx,p1x,p2x,p3x,p4x,p5x,p6x]=...
```

```
   pwr(n,ca,Tphat+deltaT+Tpm);
   disp('RMS torque error (Nm):')
   e_2=rmse(Tp-Tpx)
   disp('RSR (%):')
   r_2=100*e_2/rmse(Tp)
   plot(ca*180/pi,Tp,ca*180/pi,Tpx-mean(Tpx),':')
   axis([0 360 -1500 1500])
   xlabel('degrees')
   ylabel('Nm')
   title('Estimated (..) and Actual (--) Pressure Torque')
   disp('Press any key to continue...')
   pause
   disp('PRESSURE WAVEFORM RECONSTRUCTION')
   disp('6 RMS pressure (MPa) errors, and RSRs (%):')
   err=[rmse(p1-p1x) rmse(p2-p2x) rmse(p3-p3x)...
   rmse(p4-p4x) rmse(p5-p5x) rmse(p6-p6x)]
   rsr=100*[rmse(p1-p1x)/rmse(p1) rmse(p2-p2x)/rmse(p2)...
   rmse(p3-p3x)/rmse(p3) rmse(p4-p4x)/rmse(p4)...
   rmse(p5-p5x)/rmse(p5) rmse(p6-p6x)/rmse(p6)]
   plot(ca*180/pi,p1,ca*180/pi,p1x,':',ca*180/pi, ...
   p2,ca*180/pi,p2x,':',ca*180/pi,p3,ca*180/pi,p3x,':', ...
   ca*180/pi,p4,ca*180/pi,p4x,':',ca*180/pi,p5,ca*180/pi, ...
   p5x,':',ca*180/pi,p6,ca*180/pi,p6x,':')
   axis([0 360 -1 12])
   xlabel('degrees')
   ylabel('MPa')
   title('Estimated (..) and Actual (--) Pressure Waveform')
   disp('Press any key to continue...')
   pause
```

<u>**pwr.m**</u>

```
function [par,Tpx,p1x,p2x,p3x,p4x,p5x,p6x]=...
   pwr(n,theta,Tphat)
   %FUNCTION       PWR.M
   %ARGUMENTS:     n       = cylinder number;
   %               theta   = crank angle;
   %               Tphat   = estimated torque;
   %RETURNS:       par     = estimated pressure variation;
   %               Tpx     = new estimate of the pressure torque;
   %               pix     = estimated pressure in the i-th cylinder.
   %Calls: c_1.m, dlt.m
   %Engine data correspond to DDC 6V 92TA:
   r=0.0635;   %crankshaft radius (m)
   l=0.2571;   %connecting rod length (m)
   Ap=0.01188; %piston area (m^2)
   ca1=theta;
   c_11=c_1(ca1,r,l);
   ca2=ca1-(60-3.5)*pi/180;
   c_12=c_1(ca2,r,l);
   ca3=ca2-(60+3.5)*pi/180;
```

```
   c_13=c_1(ca3,r,l);
   ca4=ca3-(60-3.5)*pi/180;
   c_14=c_1(ca4,r,l);
   ca5=ca4-(60+3.5)*pi/180;
   c_15=c_1(ca5,r,l);
   ca6=ca5-(60-3.5)*pi/180;
   c_16=c_1(ca6,r,l);
   IX=[13 125 253 366 493 606];
   if n==0
   IX=[17 130 256 370 496 610];
   elseif n==1
   IX(1)=17;
   elseif n==2
   IX(2)=131;
   elseif n==3
   IX(3)=253;
   elseif n==4
   IX(4)=368;
   elseif n==5
   IX(5)=496;
   elseif n==6
   IX(6)=611;
   end
   p1x=dlt(2,5.5,0.45,theta-theta(IX(1)));
   p2x=dlt(2,5.5,0.45,theta-theta(IX(2)));
   p3x=dlt(2,5.5,0.45,theta-theta(IX(3)));
   p4x=dlt(2,5.5,0.45,theta-theta(IX(4)));
   p5x=dlt(2,5.5,0.45,theta-theta(IX(5)));
   p6x=dlt(2,5.5,0.45,theta-theta(IX(6)));
   phi=(1e+6)*Ap*r*...
   [c_11.*p1x c_12.*p2x c_13.*p3x c_14.*p4x c_15.*p5x c_16.*p6x];
   par=inv(phi'*phi)*phi'*Tphat;
   par=par-0.15;
   if n==0
   par=par+0.15;
   end
   Tpx=phi*par;
   p1x=p1x*par(1);
   p2x=p2x*par(2);
   p3x=p3x*par(3);
   p4x=p4x*par(4);
   p5x=p5x*par(5);
   p6x=p6x*par(6);
```

rmse.m

```
function y=rmse(x)
   %FUNCTION        RMSE.M
   %ARGUMENTS:      x = vector of residuals;
   %RETURNS:        y = root mean square error.
   y=norm(x-mean(x),2)/sqrt(length(x));
```

rot.m

```
function y=rot(x,n)
   %FUNCTION        ROT.M
   %ARGUMENTS:      x = vector of samples;
   %                n = integer;
   %RETURNS:        y = x shifted by n;
   ll = length(x);
   y = x;
   for i=1:ll-n
   y(i) = x(i+n);
   end
   for i=ll-n+1:ll
   y(i) = x(i-ll+n);
   end
```

separate.m

```
function [p1, p2, p3, p4, p5, p6]=...
   separate(pres)
   %FUNCTION    SEPARATE.M
   %ARGUMENTS: pres                = a column vector with 6x720
   %                                  elements which
   %                                  represent pressure data;
   %RETURNS:    [p1,p2,p3,p4,p5,p6] = pressure data corresponding
   %                                  to each cylinder.
   p1 = pres(1+3*720:4*720);
   p2 = pres(1+2*720:3*720);
   p3 = pres(1+5*720:6*720);
   p4 = pres(1+1*720:2*720);
   p5 = pres(1+4*720:5*720);
   p6 = pres(1+0*720:1*720);
```

sls.m

```
function [Y,PHI,PAR,ERR,JEhat,TLhat,ep,dwhat]=...
   sls(ca0,p1,p2,p3,p4,p5,p6,dw,dwp)
   %FUNCTION       SLS.M
   %ARGUMENTS:     ca0     = crank angle vector;
   %               pi      = cylinder pressure, i=1,..., 6;
   %               dw      = velocity waveform;
   %               dwp     = velocity derivative;
   %RETURNS:       Y       = vector of outputs;
   %               PHI     = signal matrix;
   %               PAR     = estimated parameters;
   %               JEhat   = estimated engine inertia;
   %               TLhat   = estimated torque fluctuation;
   %               ep      = vector of residuals;
   %               dwhat   = estimated velocity fluctuation.
   %Calls: c_1.m, c_2.m, c_3.m, c_4.m, igr.m.
   %Engine data correspond to DDC 6V 92TA:
```

```
w_0=125.5;    %engine speed (rad/sec)
b_c=1.24;     %damping (Nm/(rad/sec))
m_p=6.03;     %piston mass (kg)
r=0.0635;     %crankshaft radius (m)
l=0.2571;     %connecting rod length (m)
Ap=0.01188;   %piston area (m^2)
J_C=0.1544;   %crankshaft inertia (kg m^2)
J_CR=0.0745;  %connecting rod inertia (kg m^2)
J_F=3.85;     %flywheel inertia (kg m^2)
x0=w_0^2;
%Pressure inputs: p1 p2 p3 p4 p5 p6
dca0=ca0(2)-ca0(1);
ca1=ca0;
c_11=c_1(ca1,r,l);
c_21=c_2(ca1,r,l);
c_31=c_3(ca1,r,l);
c_41=c_4(ca1,r,l);
ca2=ca1-(60-3.5)*pi/180;
c_12=c_1(ca2,r,l);
c_22=c_2(ca2,r,l);
c_32=c_3(ca2,r,l);
c_42=c_4(ca2,r,l);
ca3=ca2-(60+3.5)*pi/180;
c_13=c_1(ca3,r,l);
c_23=c_2(ca3,r,l);
c_33=c_3(ca3,r,l);
c_43=c_4(ca3,r,l);
ca4=ca3-(60-3.5)*pi/180;
c_14=c_1(ca4,r,l);
c_24=c_2(ca4,r,l);
c_34=c_3(ca4,r,l);
c_44=c_4(ca4,r,l);
ca5=ca4-(60+3.5)*pi/180;
c_15=c_1(ca5,r,l);
c_25=c_2(ca5,r,l);
c_35=c_3(ca5,r,l);
c_45=c_4(ca5,r,l);
ca6=ca5-(60-3.5)*pi/180;
c_16=c_1(ca6,r,l);
c_26=c_2(ca6,r,l);
c_36=c_3(ca6,r,l);
c_46=c_4(ca6,r,l);
s11=c_11.*c_11 + c_12.*c_12 +...
c_13.*c_13 + c_14.*c_14 +...
c_15.*c_15 + c_16.*c_16;
s12=c_11.*c_21 + c_12.*c_22 +...
c_13.*c_23 + c_14.*c_24 +...
c_15.*c_25 + c_16.*c_26;
s33=c_31.*c_31 + c_32.*c_32 +...
c_33.*c_33 + c_34.*c_34 +...
c_35.*c_35 + c_36.*c_36;
s34=c_31.*c_41 + c_32.*c_42 +...
c_33.*c_43 + c_34.*c_44 +...
c_35.*c_45 + c_36.*c_46;
```

```
   sp=(1e+6)*(c_11.*p1 + c_12.*p2 +...
   c_13.*p3 + c_14.*p4 +...
   c_15.*p5 + c_16.*p6);
   dx=2*w_0*dw;
   dxp=2*w_0*dwp;
   phi1=0.5*dxp;
   fact=max(phi1);
   phi1=phi1/fact;
   phi2=sin(ca0);
   phi3=cos(ca0);
   PHI=[phi1,phi2,phi3];
   y1=m_p*r^2*(-0.5*s11.*dxp-s12.*(dx+x0));
   y2=J_CR*(0.5*s33.*dxp+s34.*(dx+x0));
   y3=Ap*r*sp;
   y=y1+y2+y3;
   my=mean(y1+y2+y3);
   Y=y-my;
   PAR=inv(PHI'*PHI)*PHI'*Y;
   ERR=PHI*PAR-Y;
   JEhat=PAR(1)/fact;
   TLhat=PAR(2)*sin(ca0)+PAR(3)*cos(ca0);
   m=(JEhat+m_p*r^2*s11-J_CR*s33)/2;
   inp=y3-TLhat;
   inp=inp-mean(inp);
   dxhat = dw(1)*(2*w_0+dw(1)) + igr(inp./m,dca0);
   dwhat = sqrt(x0 + dxhat) - w_0;
   dwhat=dwhat-mean(dwhat);
   %dwhat=0.9*rot(dwhat,1);
   ep=dw-dwhat;
```

<u>system.m</u>

```
function xp=system(t,x)
   %FUNCTION:    SYSTEM.m
   %ARGUMENTS:   t  = crank angle;
   %             x  = engine state;
   %RETURNS:     xp = state derivative.
   global p1 p2 p3 p4 p5 p6 ca
   %Engine data correspond to DDC 6V 92TA:
   w_0=125.5;   %engine speed (rad/sec)
   b_c=1.24;    %damping (Nm/(rad/sec))
   m_p=6.03;    %piston mass (kg)
   r=0.0635;    %crankshaft radius (m)
   l=0.2571;    %connecting rod length (m)
   Ap=0.01188;  %piston area (m^2)
   J_C=0.1544;  %crankshaft inertia (kg m^2)
   J_F=3.85;    %flywheel inertia (kg m^2)
   J_CR=0.0745; %connecting rod inertia (kg m^2)
   %Pressure inputs:
   p1=interp1(ca,p1,t);
   p2=interp1(ca,p2,t);
```

```
p3=interp1(ca,p3,t);
p4=interp1(ca,p4,t);
p5=interp1(ca,p5,t);
p6=interp1(ca,p6,t);
ca1=t;
c_11=c_1(ca1,r,l);
c_21=c_2(ca1,r,l);
c_31=c_3(ca1,r,l);
c_41=c_4(ca1,r,l);
ca2=ca1-(60-3.5)*pi/180;
c_12=c_1(ca2,r,l);
c_22=c_2(ca2,r,l);
c_32=c_3(ca2,r,l);
c_42=c_4(ca2,r,l);
ca3=ca2-(60+3.5)*pi/180;
c_13=c_1(ca3,r,l);
c_23=c_2(ca3,r,l);
c_33=c_3(ca3,r,l);
c_43=c_4(ca3,r,l);
ca4=ca3-(60-3.5)*pi/180;
c_14=c_1(ca4,r,l);
c_24=c_2(ca4,r,l);
c_34=c_3(ca4,r,l);
c_44=c_4(ca4,r,l);
ca5=ca4-(60+3.5)*pi/180;
c_15=c_1(ca5,r,l);
c_25=c_2(ca5,r,l);
c_35=c_3(ca5,r,l);
c_45=c_4(ca5,r,l);
ca6=ca5-(60-3.5)*pi/180;
c_16=c_1(ca6,r,l);
c_26=c_2(ca6,r,l);
c_36=c_3(ca6,r,l);
c_46=c_4(ca6,r,l);
s11=c_11*c_11 + c_12*c_12 +...
c_13*c_13 + c_14*c_14 +...
c_15*c_15 + c_16*c_16;
s12=c_11*c_21 + c_12*c_22 +...
c_13*c_23 + c_14*c_24 +...
c_15*c_25 + c_16*c_26;
s33=c_31*c_31 + c_32*c_32 +...
c_33*c_33 + c_34*c_34 +...
c_35*c_35 + c_36*c_36;
s34=c_31*c_41 + c_32*c_42 +...
c_33*c_43 + c_34*c_44 +...
c_35*c_45 + c_36*c_46;
sp=(1e+6)*(c_11*p1 + c_12*p2 +...
c_13*p3 + c_14*p4 +...
c_15*p5 + c_16*p6);
m=0.5*(J_F+J_C-J_CR*s33+m_p*r^2*s11);
A = J_CR*s34-m_p*r^2*s12;
fact = Ap*r;
bTu=fact*sp;
Tf=-b_c*w_0;
```

```
   Tl=-958.7535;
   d=Tf+Tl;
   x0=w_0^2;
   xp = (A*(x+x0) + bTu + d)/m;
```

tpe.m

```
function [Tp,Tpm,Tphat,deltaT,err]=...
   tpe(n,theta,dw,p1,p2,p3,p4,p5,p6)
   %FUNCTION        TPE.M
   %ARGUMENTS:      n        = cylinder number;
   %                theta    = crank angle vector;
   %                dw       = angular velocity;
   %                pi       = pressure of the i-th cylinder;
   %RETURNS:        Tp       = actual pressure torque;
   %                Tpm      = mean pressure torque;
   %                Tphat    = estimated pressure torque;
   %                deltaT   = torque fluctuation;
   %                err      = vector of residuals.
   %Calls: c_1.m, c_2.m, c_3.m, c_4.m, diffc.m.
   %Engine data correspond to DDC 6V 92TA:
   w_0=125.5;
   x0=w_0^2;
   b_c=1.24;
   m_p=6.03;
   r=0.0635;
   l=0.2571;
   Ap=0.01188;
   J_C=0.1544;
   J_CR=0.0745;
   J_F=3.85;
   J_E=5;
   if n==0
   J_E=3.85;
   end
   ca1=theta;
   c_11=c_1(ca1,r,l);
   c_21=c_2(ca1,r,l);
   c_31=c_3(ca1,r,l);
   c_41=c_4(ca1,r,l);
   ca2=ca1-(60-3.5)*pi/180;
   c_12=c_1(ca2,r,l);
   c_22=c_2(ca2,r,l);
   c_32=c_3(ca2,r,l);
   c_42=c_4(ca2,r,l);
   ca3=ca2-(60+3.5)*pi/180;
   c_13=c_1(ca3,r,l);
   c_23=c_2(ca3,r,l);
   c_33=c_3(ca3,r,l);
   c_43=c_4(ca3,r,l);
   ca4=ca3-(60-3.5)*pi/180;
   c_14=c_1(ca4,r,l);
   c_24=c_2(ca4,r,l);
```

```
c_34=c_3(ca4,r,l);
c_44=c_4(ca4,r,l);
ca5=ca4-(60+3.5)*pi/180;
c_15=c_1(ca5,r,l);
c_25=c_2(ca5,r,l);
c_35=c_3(ca5,r,l);
c_45=c_4(ca5,r,l);
ca6=ca5-(60-3.5)*pi/180;
c_16=c_1(ca6,r,l);
c_26=c_2(ca6,r,l);
c_36=c_3(ca6,r,l);
c_46=c_4(ca6,r,l);
s11=c_11.*c_11 + c_12.*c_12 +...
c_13.*c_13 + c_14.*c_14 +...
c_15.*c_15 + c_16.*c_16;
s12=c_11.*c_21 + c_12.*c_22 +...
c_13.*c_23 + c_14.*c_24 +...
c_15.*c_25 + c_16.*c_26;
s33=c_31.*c_31 + c_32.*c_32 +...
c_33.*c_33 + c_34.*c_34 +...
c_35.*c_35 + c_36.*c_36;
s34=c_31.*c_41 + c_32.*c_42 +...
c_33.*c_43 + c_34.*c_44 +...
c_35.*c_45 + c_36.*c_46;
sp=c_11.*p1 + c_12.*p2 +...
c_13.*p3 + c_14.*p4 +...
c_15.*p5 + c_16.*p6;
Tp=(1e+6)*Ap*r*sp;
Tpm=mean(Tp);
Tp=Tp-Tpm;
q = J_CR*s34-m_p*r^2*s12;
m = 0.5*(J_E-J_CR*s33+m_p*r^2*s11);
ca0=[0:117]'/118 * 2 * pi;
h=ca0(2)-ca0(1);
dwp=diffc(dw,h);
dw=interp1(ca0,dw,theta,'spline');
dwp=interp1(ca0,dwp,theta,'spline');
dx=2*dw*w_0;
dxp=2*dwp*w_0;
d1=x0*q;
Y=m.*dxp-q.*dx-d1;
Tphat=Y-mean(Y);
err=Tp-Tphat;
phi=[sin(theta) cos(theta)];
par=inv(phi'*phi)*phi'*err;
deltaT=phi*par;
```

Index